Chapter 9

European slope processes

9.1 Introduction

In this chapter we investigate the ability of the models to reproduce the current pathways and physical processes which have been observed around the European continental shelves and slope regions. Although the models were not designed to necessarily reproduce these processes in a realistic way, being instead mostly concerned with the larger-scale flows across the whole North Atlantic basin, it is nevertheless worthwhile and informative to assess the performance of the models in this respect, particularly since the flows in this region have such a direct impact upon the European nations. We will consider in particular the region from the Iberian shelf (off the Portuguese coast) extending northwards through the Bay of Biscay and into the areas northwest of Ireland and Scotland. The remainder of this section will briefly review the available observations in this area. Thereafter, section 9.2 will describe the upper water circulation patterns in the models, and section 9.3 will consider the deeper flow structure and properties, at depths corresponding to the core of the Mediterranean Water in the Northeast Atlantic.

The region off the Iberian shelf is well known as an area of strong coastal upwelling in the summertime. NYKJAER and VAN CAMP (1994), for instance, using average conditions between 1969–1976, show that the upwelling band is centred between about 37–42°N (covering more or less the complete Iberian shelf area), and that during July–October, near coastal temperatures can be typically 3–4°C cooler than in the deeper ocean. The upwelling band usually extends to about 100–150 km offshore. These authors have shown that the upwelling is most likely to be driven by the surface winds, which in the summer have a strong equatorward component, so that the associated net Ekman drift in the upper layers is almost directly offshore (i.e. to the west). Deeper, cooler water is therefore upwelled to the surface layers to compensate for this net offshore drift. Furthermore, PINGREE (1993) has analysed drifting buoys and shown that the mean surface flows further north are also equatorwards. The buoys have typical record lengths of several hundred days, and show a westward motion off the north Spanish slopes, and a southeastward motion off the Celtic and Armorican shelves. Consequently, it appears that the prevailing surface current pattern, which is particularly prevalent in the summer, is for equatorward flow over a wide area of the shelf margins.

During the winter months, however, there is a change in the general wind direction to westerly and southwesterly, and this is associated with a change in the surface circulation patterns. This is evident in HAYNES and BARTON (1990), who showed that six near-surface drifter tracks indicated a net northward flow off the Iberian shelf during September 1986 to March 1987. Moreover, these authors show evidence from a cruise in September and October 1986 for a tongue of warm water beginning to spread northwards (off the Iberian shelf), just offshore from the region of upwelling (which at this time of year seems to be in decline). Furthermore, the observations of PINGREE and LECANN (1990) clearly show the arrival of warm water during the winter months on the north Spanish slopes. This event has been called the "Navidad" (the Spanish word for "Christmas"). PINGREE and LECANN (1990) present SST satellite images showing warm water extending around the north Spanish slopes and up into the Bay of Biscay in December 1989. The warm water, moving northwards, leaves the near-coastal regions at Cap Ferret Canyon (about 45°N) and thereafter follows the continental shelf-slope contours. These authors also present results from a mooring on the north Spanish slopes (at about 44°N, 7°W) which show that the near surface flow (at 210 m) is on average westward (equatorward) for the summer months, but then reverses to flow polewards (eastwards) during the winter months. Temperatures at this location are typically around 11.5°C, but rise with the onset of the Navidad, reaching about 13.5°C by February, near the end of the poleward phase of the near-surface currents. Furthermore, observations by WHITE and BOWYER (1997) under the OMEX programme (funded by the CEC MAST-II programme) show that the effects of the Navidad may be felt at least as far north as the Malin Shelf, northwest of Ireland, where the presence of a warm, saline tongue of water has been noted in water depths of about 400 m.

Overall, then, the near-surface currents seem to be equatorwards around the European margins, particularly in the summertime, when there is pronounced upwelling off the Iberian shelf. But during the winter, the surface currents reverse and flow polewards, bringing warm (saline) waters northwards in the Navidad. These flows appear to be mostly driven by the winds, and show a corresponding seasonality.

By contrast, there is a deeper, more constant, "poleward undercurrent", which is somewhat pronounced near the depths of the Mediterranean Water (MW) tongue in the North-East Atlantic (near 1000–1200 m depth at the Gibraltar Straits outflow). Although the most obvious extension of the MW is westward across the North Atlantic from its source at the Gibraltar Straits outflow (e.g. as seen in the atlas of LEVITUS, 1982), there is also a northward extension along the coast of Europe. REID (1979) analysed properties (in particular the salinity and silica distribution) on an isopycnal surface that passed through the core of the high salinity MW near its source, and deduced that, although it was hard to be certain, it was at least likely that the MW could spread a considerable distance northwards and provide a major component of the waters passing through the Faeroe- Shetland channel into the Greenland-Iceland-Norwegian (GIN) sea, the so-called "Reid hypothesis". The MW could therefore in this way affect wintertime deep convection and overturning in the GIN sea, an important component in the global thermohaline circulation of the world's oceans.

The poleward undercurrent at depths corresponding to the MW core is also clearly seen in the results of the MORENA project (funded under the CEC MAST-II programme). At 41°N, DIAS et al. (1995) show a pronounced flow polewards (directed towards about North-Northeast, along the shelf-slope topographic contours) at 1200 m at 9°30'W (in 2000 m total water depth) which exists for a complete annual cycle, apart from some brief periods of reversed flow due to eddies. Further into the deep ocean, other moorings show much more variability, so that the poleward undercurrent appears to be confined fairly closely to the shelf slope. Further, ALONSO et al. (1995) show results from three current meter moorings at about 42°20'N. At 9°50'W, there is again a more or less steady poleward flow for most of the year at 1237 m depth (of typically 2–3 cm/s), and salinities of around 36.2 psu (at 840 m depth), which is probably near the core of the undercurrent. At 10°15'W there is also a net poleward flow at 1150 m (and salinities of near 36.2), although there is also a period of equatorward flow. In summary, though, all three moorings, sited between 9°30'W and 10°15'W show net northward flow in the long-term averages, with an identifiable maximum between 800–1200 m of some 2–3 cm/s.

Finally, HUTHNANCE (1984) has shown that the joint effect of baroclinicity and relief (the "JEBAR" effect) provides important local forcing near continental shelves, and could drive a significant poleward current, of order 10 cm/s, at eastern oceanic slope regions. It therefore seems that this could be at least partially responsible for maintaining the persistent poleward undercurrent around the European margins.

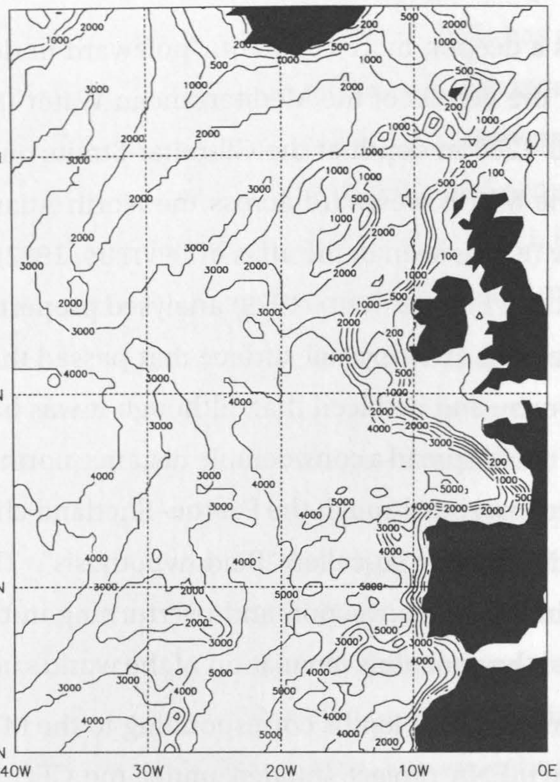
60N
50N
40N
30N
40W
30W
20W
10W
0E

(a) Level

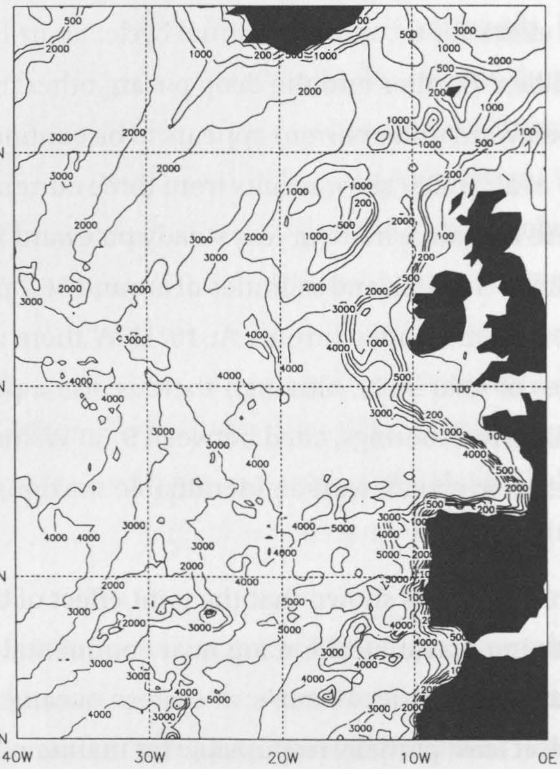
60N
50N
40N
30N
40W
30W
20W
10W
0E

(b) Isopycnic

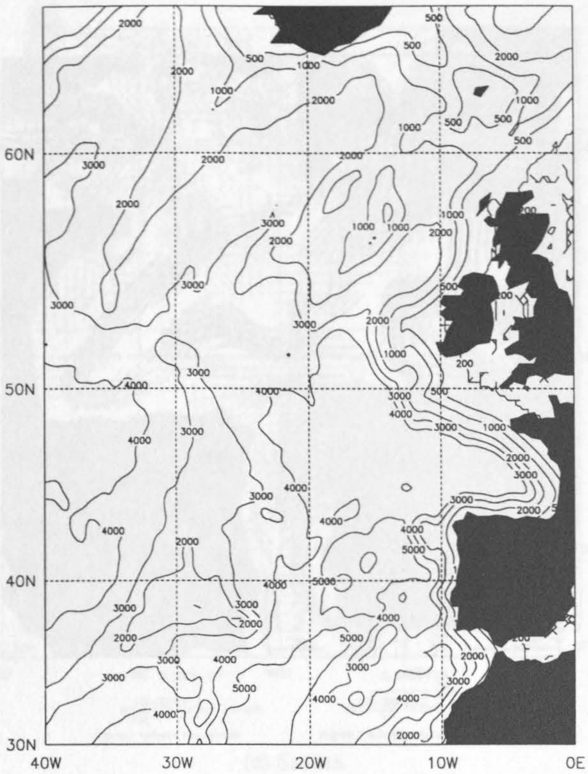

(c) SIGMA

Figure 9.1: Model topographies (m).

9.2 Near-Surface Circulation Patterns

Since we are here discussing the flow around a complex topographic terrain, it is worthwhile to firstly present the bottom topographies from the models, which are all derived from the ETOPO5 (5' resolution) database.

Fig. 9.1 shows the degree of realism achieved in each case. In ISOPYCNIC, the depths at each model gridpoint are simply taken as the median (to eliminate errors from possible outliers) of all the ETOPO5 values within that grid cell. This gives a faithful representation of the bottom topography. In LEVEL, the gridpoint depth values are furthermore taken as the nearest depth level in the model. This also gives a reasonably faithful bottom topography, although there is some noticeable smoothing and broadening of the shelf break areas (e.g. in the Bay of Biscay). For SIGMA, the topography was necessarily smoothed in order to produce suitably accurate horizontal pressure gradient terms, and the effect of this is to produce somewhat overly smooth bathymetry.

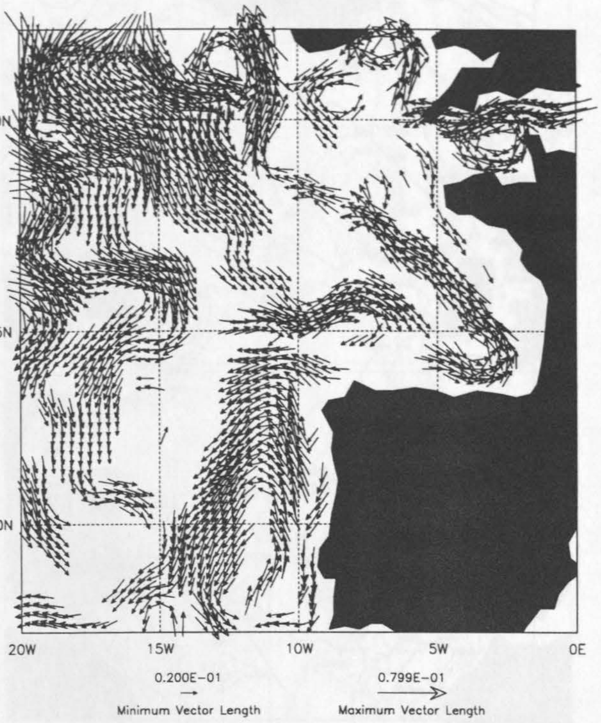
50N
45N
40N
20W
15W
10W
5W
0E
0.200E−01
Minimum Vector Length
0.799E−01
Maximum Vector Length

(a) LEVEL

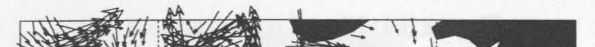
50N
45N
40N
20W
15W
10W
5W
0E
0.200E−01
Minimum Vector Length
0.125E+00
Maximum Vector Length

(b) ISOPYCNIC

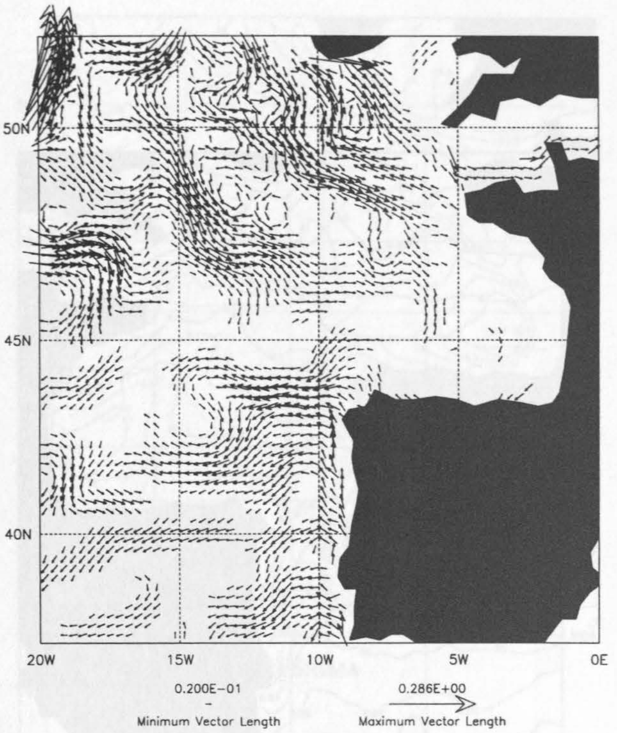

(c) SIGMA

Figure 9.2: Summer climatological surface currents (m/s). Minimum and maximum vector lengths are 0.02 and 0.30 m/s.

We now begin by comparing in Fig. 9.2 the surface circulation patterns from the summer mean climatological state for the three models (averages over every July-September in the last 5 years of the integrations). This is the time of equatorward flows near the continental shelf break, and upwelling off the Iberian coast in the observations. ISOPYCNIC shows an equatorward shelf break flow extending from the Celtic shelf, through the Bay of Biscay along the Armorican shelf, then along the north coast of Spain, and then southwards and westwards off the Iberian shelf (i.e. the Portuguese coast). These flows appear to be in agreement with the observations in this area. Further, the influence of the North Atlantic Current (NAC) is also seen as a strong eastward flow near 50° N, part of which forms up into a poleward surface current northwards of the Celtic shelf. We also note the somewhat spuriously strong westward flow near 35–40° N which results from the model Azores Current reaching the Moroccan coast and turning too strongly to the north and then back to the west.

For LEVEL, the shelf break flow around the Celtic, Armorican and north Spanish shelves is polewards, which seems against the prevailing direction inferred from the observations for

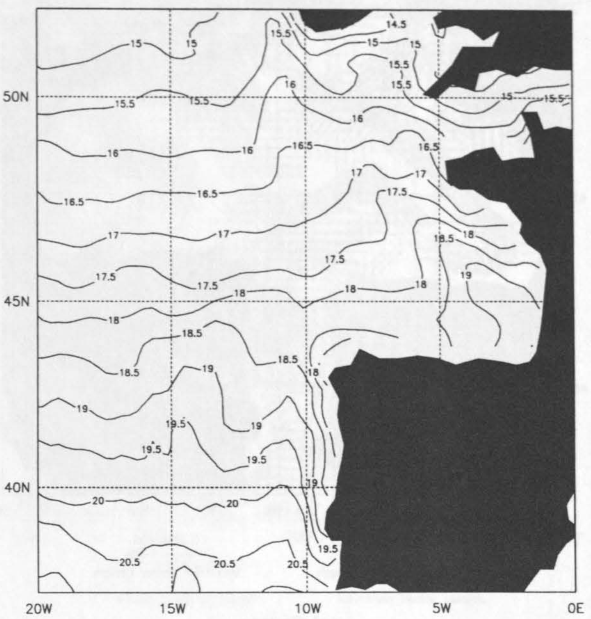
50N
45N
40N
20W
15W
10W
5W
0E

(a) LEVEL

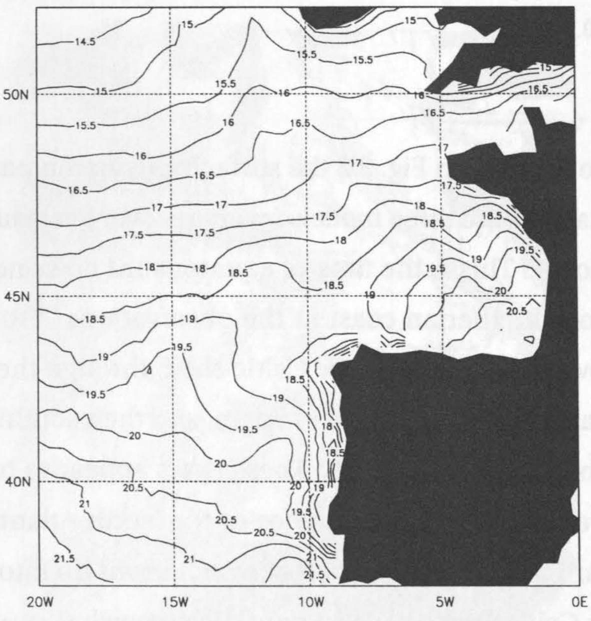
50N
45N
40N
20W
15W
10W
5W
0E

(b) ISOPYCNIC

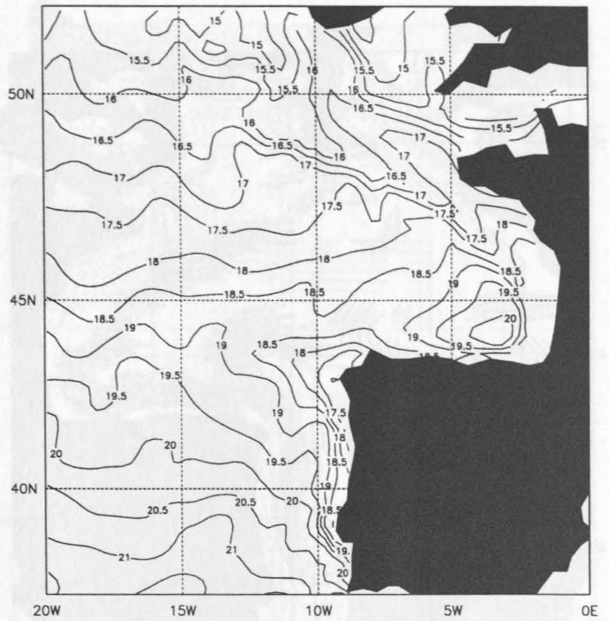

(c) SIGMA

Figure 9.3: Summer climatological surface temperatures (°C).

this time of year (PINGREE and LECANN, 1990; PINGREE, 1993). It seems that this poleward flow could be driven by a branch of the NAC which extends southeastwards towards 45°N, 10°W, and appears to be connected with the near-slope flows. A further branch of the NAC is also supplementing the poleward shelf break flow north of about 50°N, much as for ISOPYCNIC. Further south, however, the flow off the Iberian coast is largely westwards, and rather similar to expectations based upon the observations (i.e. anticipating that this is related to the offshore Ekman drift and upwelling).

In SIGMA, there is an equatorward flow along the slope from south of Ireland and into the Bay of Biscay, but this diminishes over the Armorican shelf and north Spanish slopes. Nonetheless, there is again a clear westward drift off the Iberian slope, much as in the other models.

In Fig. 9.3 we now relate these circulation patterns to the sea-surface temperature (SST) distributions in the summer. For ISOPYCNIC, the SSTs follow expectations from the current patterns. There is a northward drift of warm surface water north of 50°N, and evidence of the southward transport of somewhat cooler water on the Armorican slope (off the French coast). There is also a strong signal of upwelling off the Iberian coast, as evidenced by the region of anomalously cool SSTs there, up to 2.5–3.0°C cooler than the SSTs in the deeper ocean. For

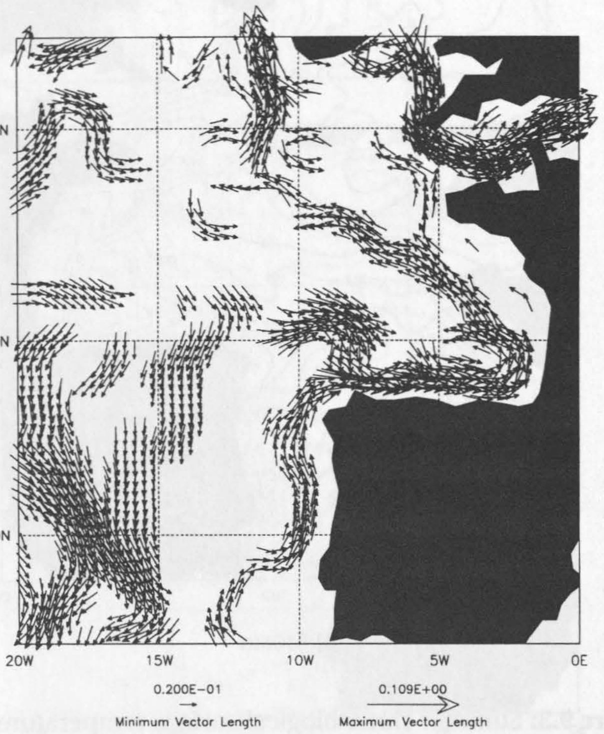
50N
45N
40N
20W
15W
10W
5W
0E
0.200E-01
Minimum Vector Length
0.109E+00
Maximum Vector Length

(a) LEVEL

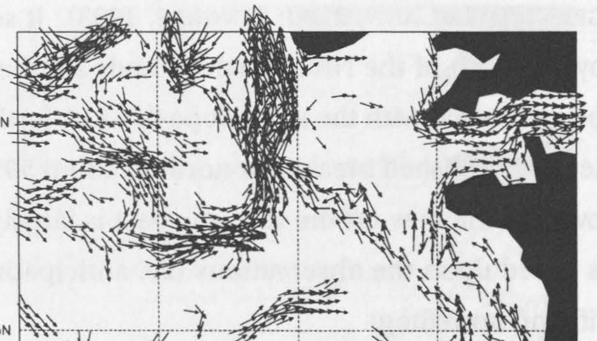
50N
45N
40N
20W
15W
10W
5W
0E
0.200E-01
Minimum Vector Length
0.132E+00
Maximum Vector Length

(b) ISOPYCNIC

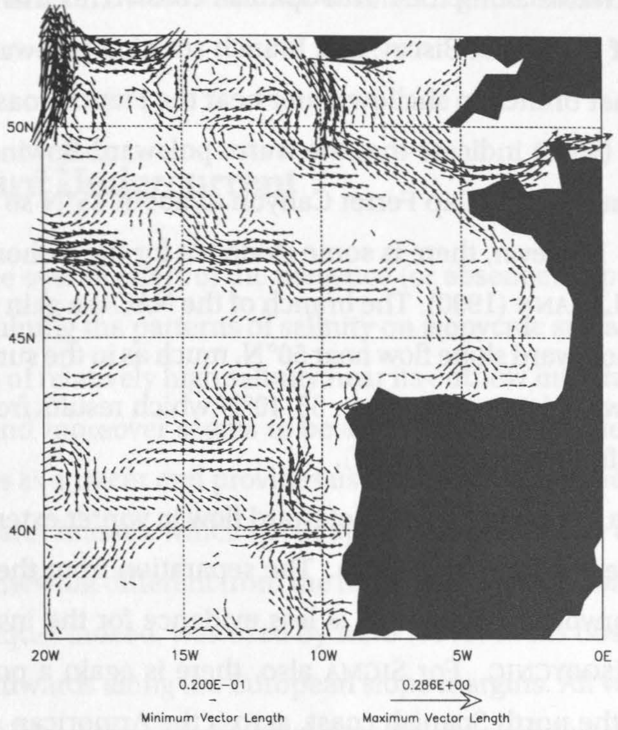

(c) SIGMA

Figure 9.4: Winter climatological surface currents (m/s). Minimum and maximum vector lengths are 0.02 and 0.20 m/s.

LEVEL, there is a clear signature of northward transport of warm SST up the Armorican and Celtic shelves, again as would be expected from the circulation patterns. Further, we note again the presence of cool water off the Iberian coast denoting the upwelling of deeper water, but here the coolest waters are only some 1.5°C cooler than in the deep ocean. For SIGMA, the southward transport of cooler water is evident along the Celtic and Armorican shelves, again in line with expectations from the current structure. Further, we see that SIGMA also predicts upwelling off the Iberian coast, with temperature differences of about 2.0–2.5°C.

These DYNAMO models, even though they were not designed to focus on the shelf break processes, compare favourably with the much finer (1/12°resolution) but limited area (the Iberian shelf-slope region) model constructed under the MORENA programme by STEVENS and JOHNSON (1997), which predicts that the near-coastal waters in summer are about 3.0–3.5°C cooler than in the deeper ocean.

Turning our attention now to the winter situation, Fig. 9.4 shows the surface circulation patterns for the three models. In ISOPYCNIC there is a poleward flow just off the Iberian coast which turns eastwards along the north Spanish coast. This then splits into two in the southeastern corner of the Bay of Biscay, one branch running polewards up the shelf-slope bathymetry, and another branch in shallow water near the French coast. The observations of PINGREE and LECANN (1990) indicate that the warm poleward-flowing waters should really separate from the coastline near Cap Ferret Canyon at about 45°N so that the separation in ISOPYCNIC is too early. However, there is some evidence for the inshore branch of the warm water in PINGREE and LECANN (1990). The branch of the NAC is a gain clearly evident in ISOPYCNIC, and joins the poleward slope flow near 50°N, much as in the summer case. Note again the overly strong westward jet near between 35-40°N which results from the retroflection of the Azores Current (as for the summer case).

For LEVEL, there is a clear and distinct poleward flow in winter extending around the continental slopes over the whole of this region. The separation from the coastline occurs correctly at Cap Ferret Canyon, though there is less evidence for the inshore branch near the French coast than in ISOPYCNIC. For SIGMA also, there is again a poleward flow from the Iberian slope, around the north Spanish coast, across the Armorican and Celtic shelf areas, and further north around the southern Irish shelf. We note here that the flow over the Armorican and Celtic shelves is further inland than in both ISOPYCNIC and LEVEL, and that this is associated with the smoothing of the bathymetry in SIGMA (see Fig. 9.1), which means that (e.g.) the 500 and 1000 m isobaths are closer in to the coastlines in this model.

Moving on now to the SST patterns in the winter, we see in Fig. 9.5 that ISOPYCNIC clearly shows the poleward spreading of warm near-surface waters up around the Iberian shelf, the north Spanish shelf, across the Armorican and Celtic shelves, and up around the southern Irish shelf, much as would be expected from the surface circulation patterns. This situation is more or less reflected in the other models. In LEVEL, the temperature contrast in the Iberian jet is even more marked than in either ISOPYCNIC or SIGMA, which here show a similar behaviour. Also, all models show a similar northward spreading of warm water through the Armorican and Celtic shelf regions, although the warm water jet in SIGMA is again somewhat too far in towards the European coastline, but in line with expectations from the current fields in this model.

Again, the DYNAMO models in winter compare well with the modelling study of STEVENS and JOHNSON (1997) under the MORENA programme. These authors showed that the wintertime surface circulation patterns off the Iberian coast were sensitive to the precise wind forcing used, and were only able to reproduce poleward near-coastal flows with the ECMWF winds (as used in the present study). Furthermore, the strength of these poleward currents is of the order of 5 cm/s in both the DYNAMO models, and in the model of STEVENS and JOHNSON (1997).

9.3 The Poleward Undercurrent

We now investigate the overall effect of the presence (or absence) of poleward undercurrents in the models by examining the patterns of salinity on isopycnic surfaces. Since the Mediterranean Water (MW) is of relatively high salinity near its outflow into the North Atlantic (at the Straits of Gibraltar), and moreover seems to be associated more or less with the core of the undercurrent, this acts as a tracer and provides useful insights into the net Lagrangian movement of the various water masses, which occur approximately on the isopycnic surfaces, and can in principle be somewhat different from the mean Eulerian motion averaged at particular locations. This technique, indeed, was used by REID (1979) in his observational study of the spreading of MW northwards along the European slope margins. All values of density used in the present chapter will be values of potential density referenced to the sea-surface, in units of kg/m^3, with 1000 subtracted for convenience.

REID (1979) defined a surface identified by a potential density value of 27.69 (above 500 m depth, and its extension onto a matching surface below 500 m) to define the core of the MW. Here, we investigate the three surfaces with density values of 27.38, 27.52 and 27.64, which we believe span the core of the undercurrents in the models. These are values of the ISOPYCNIC layer densities, but all model datasets (including those for ISOPYCNIC) were interpolated onto the common A-grid (and the corresponding set of horizontal levels) before properties on isopycnic surfaces were evaluated, in order not to bias the comparison unfairly in favour of any one model. We will present figures showing the climatological mean summer state for all models, when the mixed layer has most retreated, and the density surfaces exist over the largest portion of the study area.

Fig. 9.6 shows the patterns for the 27.38 isopycnal, which is above the MW core at its source. However, Fig. 9.6(a) illustrates the initial conditions used for the models (actually taken from ISOPYCNIC) which was derived from the LEVITUS (1982) dataset, and we see a clearly defined maximum salinity, in excess of 35.8 psu, near the Gibraltar outflow region, indicating the distinct influence of the MW on this layer. The main spreading is clearly to the west and southwest in a tongue of relatively high salinity reaching across the basin near 35°N. But there is also a distinct northward spreading polewards around the European continental slopes. This appears to extend as far north as the Iceland-Scotland (IS) ridge, and possibly

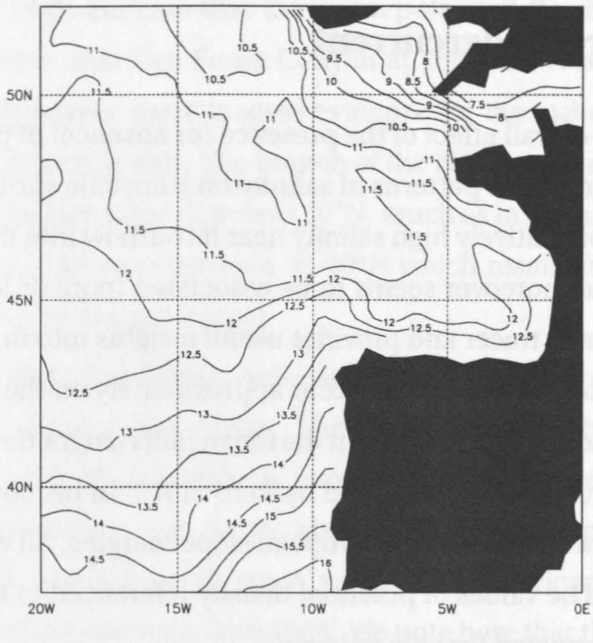
50N
45N
40N
20W
15W
10W
5W
0E
11
11.5
12
12.5
13
13.5
14
14.5
15
15.5
16
10.5
10
9.5
9
8.5
8
7.5

(a) LEVEL

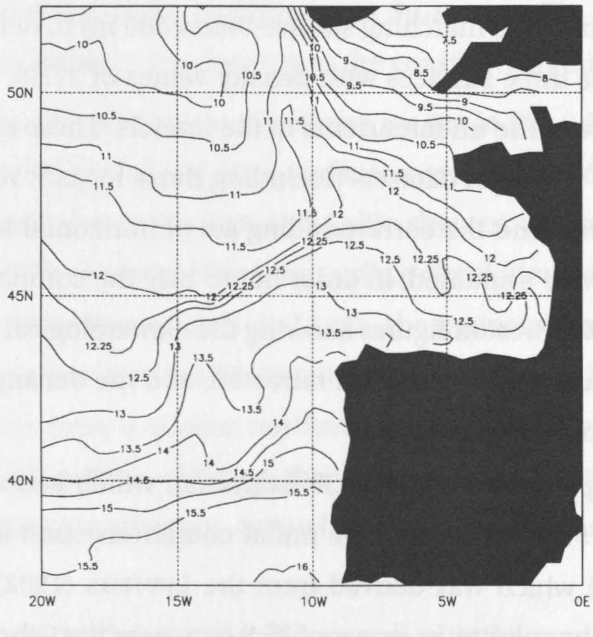
50N
45N
40N
20W
15W
10W
5W
0E
10
10.5
11
11.5
12
12.25
12.5
13
13.5
14
14.5
15
15.5
16
9.5
9
8.5
7.5

(b) ISOPYCNIC

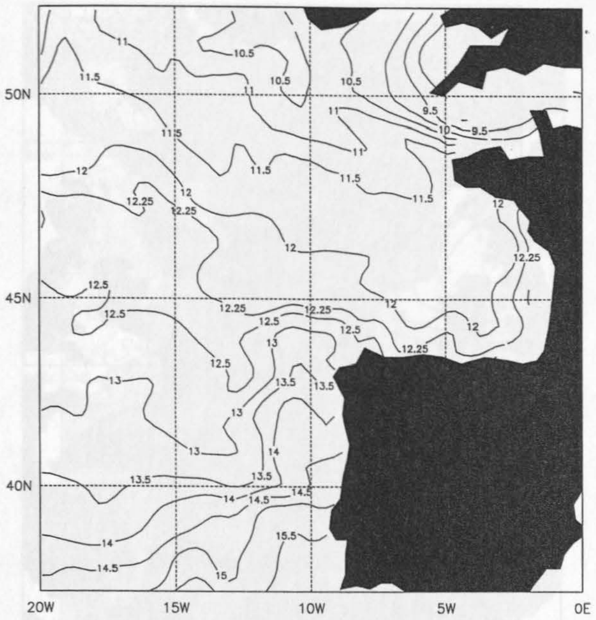
50N
45N
40N
20W
15W
10W
5W
0E
11
10.5
11.5
10.5
10.5
11
11
9.5
10
9.5
11.5
11
12
11.5
11.5
11.5
12.25
12
12.25
12
12
12.25
12.5
12.5
12.25
12.25
12.5
12.5
12
13
12.25
12
12.5
13
13.5
13.5
13
13
14
13.5
13.5
14
14.5
14.5
15.5
14
14.5
15

(c) SIGMA

Figure 9.5: Winter climatological surface temperatures (°C).

beyond into the Norwegian Current, where salinities as high as 35.3–35.35 psu are seen.

For the summer state in ISOPYCNIC, the maximum salinity near the outflow region has reduced slightly to 35.7 psu, and there is clearly a continued spreading westwards, although a sharp gradient now appears near 32°N, which is associated with an overly strong Azores Current (which appears to prevent spreading in a more southerly direction). There is also a tongue of relatively high salinity water (with salinities about 35.35) which stretches polewards around the European continental margins and reaches across the IS ridge, and this seems close to the Levitus observations, although the connection around the Porcupine Bank near 53°N is only marginal. We also see advection of high salinities around the Reykjanes Ridge and further into the Irminger Basin. For LEVEL, maximum salinities remain near 35.8, but the westward spreading is less evident. Instead, high salinity water seems to leak away too strongly to the south (as compared with the observations), and this may result from this model not having an Azores Current-type feature. Although there is again evidence of poleward spreading up as far as the IS ridge and beyond (with salinities of around 35.45 psu), one notable feature for LEVEL is that a large portion of the northeast Atlantic (i.e. the area between the influence of the NAC near 50°N, 30°W and the Bay of Biscay) has become rather homogenised, showing fairly uniform salinities between 35.45–35.5 psu. This seems to suggest

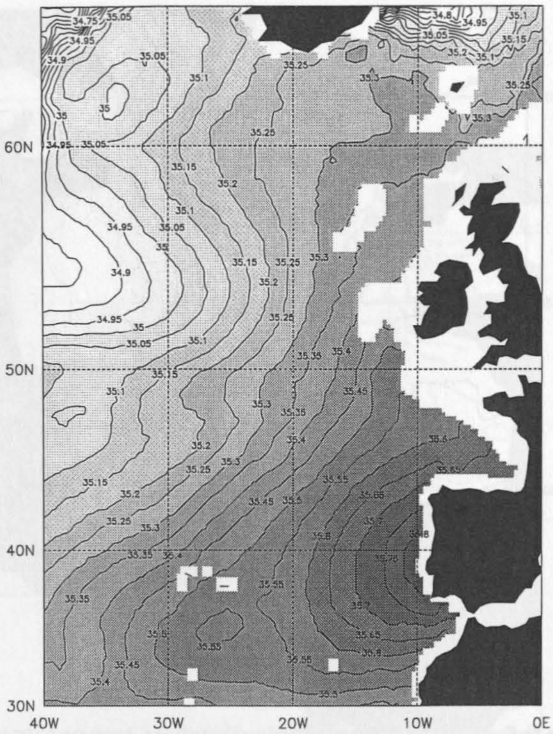
60N
50N
40N
30N
40W
30W
20W
10W
0E

(a) Levitus observations and initial state for models (taken from ISOPYCNIC)

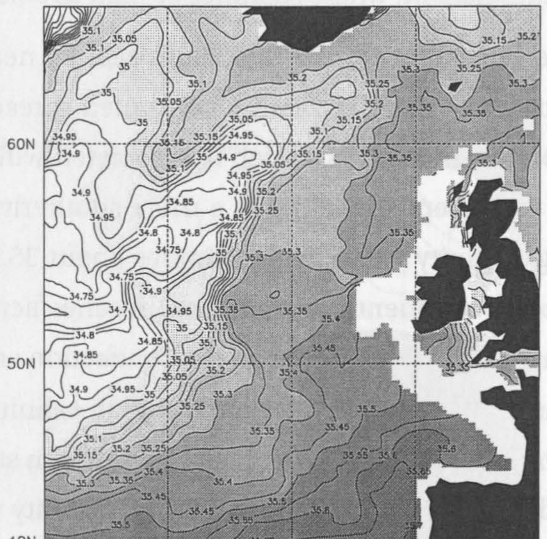
60N
50N
40N
30N
40W
30W
20W
10W
0E

(b) ISOPYCNIC summer mean

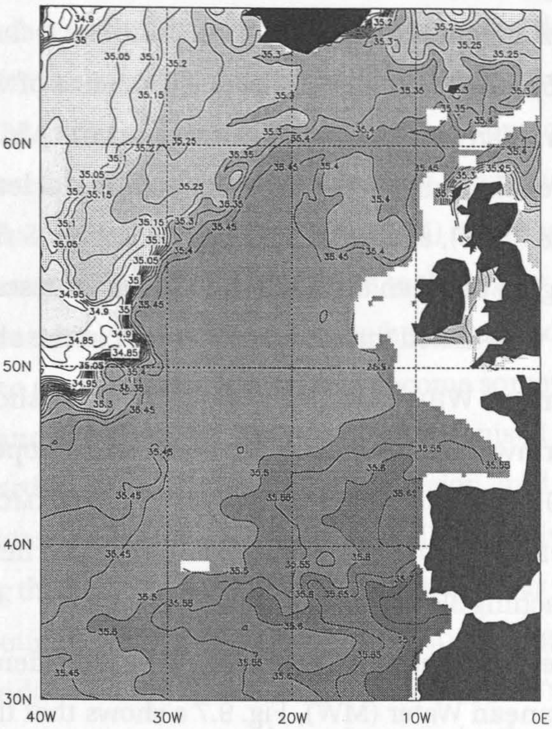
60N
50N
40N
30N
40W
30W
20W
10W
0E

(c) LEVEL summer mean

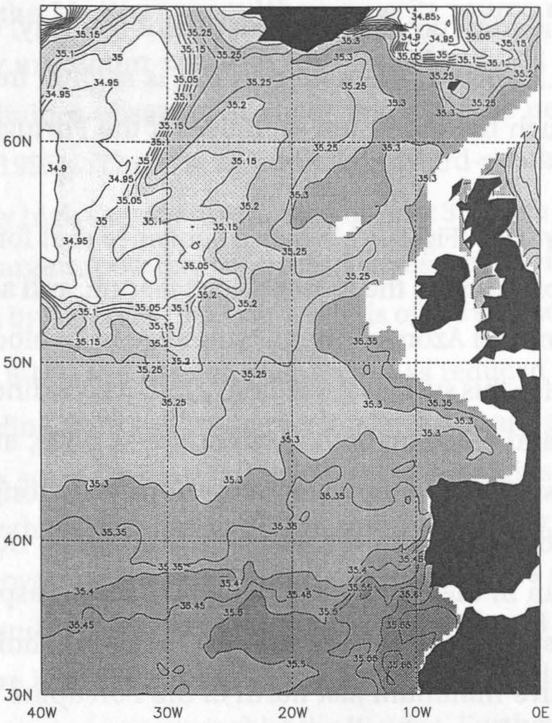
60N
50N
40N
30N
40W
30W
20W
10W
0E

(d) SIGMA summer mean

Figure 9.6: Salinity (psu) on the isopycnal surface 27.38.

the effect of overly-strong mixing (either horizontal or vertical). For SIGMA (Fig. 9.6(d)), which also has no noticeable Azores Current, maximum salinities near the Straits of Gibraltar have dropped to around 35.65, and, as for LEVEL, there is evidence of weak westward spreading and some saline water is clearly escaping southwards near the African coast. There also appears to be poleward spreading around the European margins at least as far as the Porcupine Bank (salinities of around 35.35), and quite possibly across the IS ridge, and also around the Reykjanes Ridge. The region between the NAC and the Bay of Biscay is not so homogenised as for LEVEL, but is more well-mixed than for ISOPYCNIC or in the observations.

In the OMEX experiment, WHITE and BOWYER (1997) have shown that salinities on the 27.38 density surface northwest of Ireland, on the Malin shelf/slope, were about 35.36–35.37 psu in the summer of 1995, in a water depth of 1000 m. The DYNAMO models all compare very favourably with this, ISOPYCNIC showing about 35.35–35.40 psu here, LEVEL attaining about 35.45 psu, and SIGMA reaching 35.30 psu.

Moving on now to the 27.52 isopycnal, which could be considered as representing an upper level in the Mediterranean Water (MW), Fig. 9.7 a shows that the pattern for the Levitus observations (i.e. the initial conditions) is much the same as for the 27.38 surface. We observe both westward/southwestward spreading as the main feature, but also poleward spreading around the eastern boundaries, possibly (but not unambiguously) crossing the IS ridge with salinities of between 35.25–35.30. We note that this is slightly fresher than for the lighter surface above, even though the maximum salinities off the Portuguese coast are noticeably higher, about 36.0.

The pattern for ISOPYCNIC (Fig. 9.7(b)) is also similar to that for the 27.38 surface. There is enhanced westward spreading as the most obvious feature, and also a strong gradient near 32°N resulting from the model Azores Current, which seems to block any southward spreading. There appears to be for this surface spreading of relatively saline water polewards around the European margins, and reaching both north of the IS ridge, and around the Reykjanes Ridge. For instance, the salinities of the water in the northward tongue show a gradual freshening with distance to the north, and the water crossing the IS ridge has salinities of 35.3–35.35, slightly higher than in the initial conditions. These two aspects seem to support the view that the water has spread northwards and that the high salinities derive from the MW. However, there is a relative minimum just north of the Porcupine Bank which is somewhat against this. Also detrainment from the wintertime mixed layer near the IS ridge, which is also of salinity near 35.3, cannot be ruled out either at this stage, as a possible mechanism for injecting saline water into the ocean interior here. The maximum salinity near the source region has dropped to about 35.75 psu.

For LEVEL (Fig. 9.7(c)), the maximum salinity near the source region has also dropped, but not by as much as for ISOPYCNIC, with values of 35.85 psu still observed. Again, comments apply much as for the 27.38 surface. There is some westward spreading, but this seems a little weak and is compensated by the southward spreading down the African coast. There is some evidence of relatively high salinities (in excess of 35.4) reaching polewards up the European margins, but these are not necessarily connected to the higher salinity MW. Also, again, a large area of the northeastern Atlantic has become homogenised near salinities of 35.35. For SIGMA (Fig. 9.7(d)), the northeastern Atlantic has become somewhat more homogenised than in the observations and in ISOPYCNIC, but not so homogenised as for LEVEL. There again seems to be weak westward spreading from the source region, and also some leakage to the south along the African coast, as for the 27.38 isopycnal. There is also clear evidence of poleward boundary spreading through the Bay of Biscay at least as far as the Porcupine Bank (with salinities above 35.2), though whether this is connected to the region of salinities of about these values over the IS ridge and Reykjanes Ridge for now appears to be an open question. The maximum salinities in the source region have decreased rather noticeably to only 35.6.

Finally, Fig. 9.8 shows the situation for the 27.64 isopycnal, which is considered as being close to the core of the Mediterranean Water near its source region. The observations (initial conditions) show maximum salinities of around 36.15 psu off the Portuguese coast, which is close to the salinities observed at about the MW core near 42°N in the MORENA project (ALONSO et al., 1995). There is again the westward-southwestward spreading, but also a tongue of relatively high salinity in excess of or near 35.2 psu which spreads polewards around the European margins, possibly connecting across the IS ridge. This is rather similar to the pattern presented by REID (1979) in his analysis of the spreading of the MW core.

In ISOPYCNIC (Fig. 9.8(b)), the maximum salinity has reduced to 35.85, and again there is clear westward spreading from the source region, and a sharp gradient near 32°N. There is also clearly polewards spreading around the European margins at least as far as the Porcupine Bank at 53°N (with salinities near 35.15), but then further north the salinities again increase to around 35.3 over the IS ridge. These values over the IS ridge are more saline than in the initial condition, and can only have resulted from northward spreading of MW from the original high salinity core in an early stage of the integration, or else from detrainment from the mixed layer somewhere near (presumably) the IS ridge. Further analysis will be needed to resolve this question. For LEVEL, the maximum salinities are near 35.90–35.95, higher than for ISOPYCNIC, although still slightly reduced from the observations. There is again weak west-

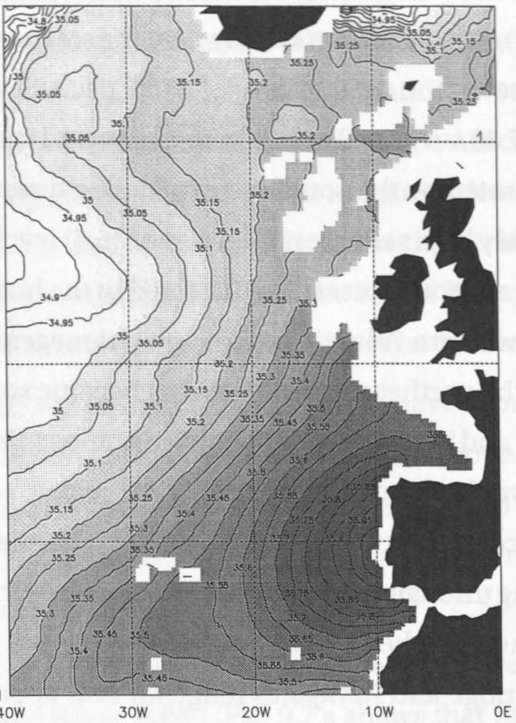
60N
50N
40N
30N
40W
30W
20W
10W
0E

(a) Levitus observations and initial state for models (taken from ISOPYCNIC)

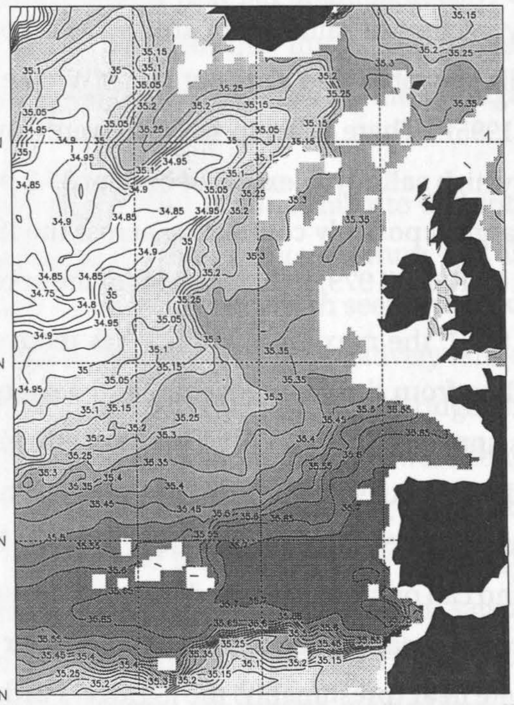
60N
50N
40N
30N
40W
30W
20W
10W
0E

(b) ISOPYCNIC summer mean

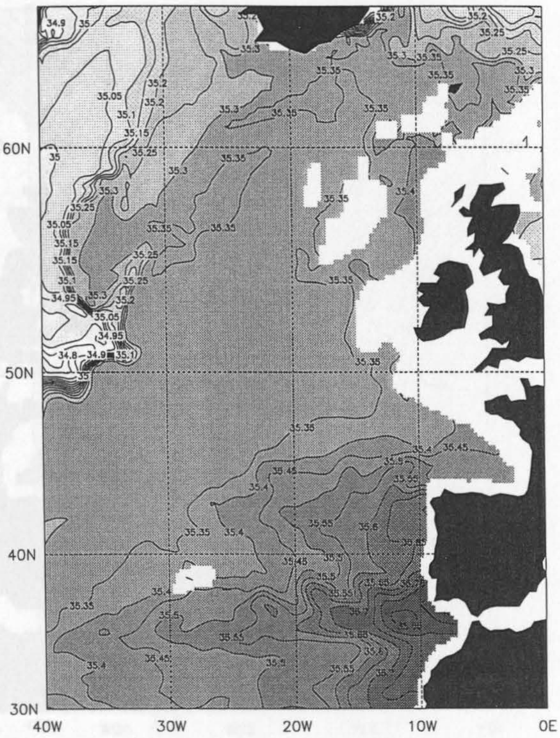
60N
50N
40N
30N
40W
30W
20W
10W
OE

(c) LEVEL summer mean

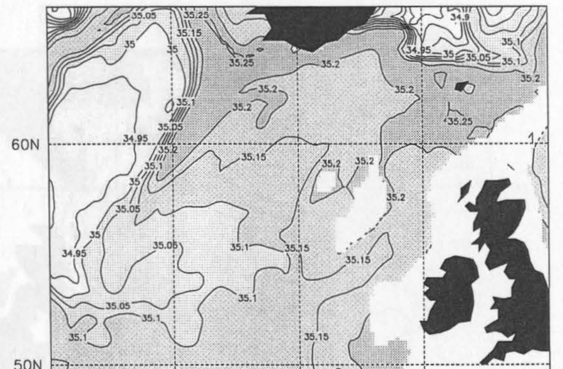
60N
50N
40N
30N
40W
30W
20W
10W
OE

(d) SIGMA summer mean

Figure 9.7: Salinity (psu) on the isopycnal surface 27.52.

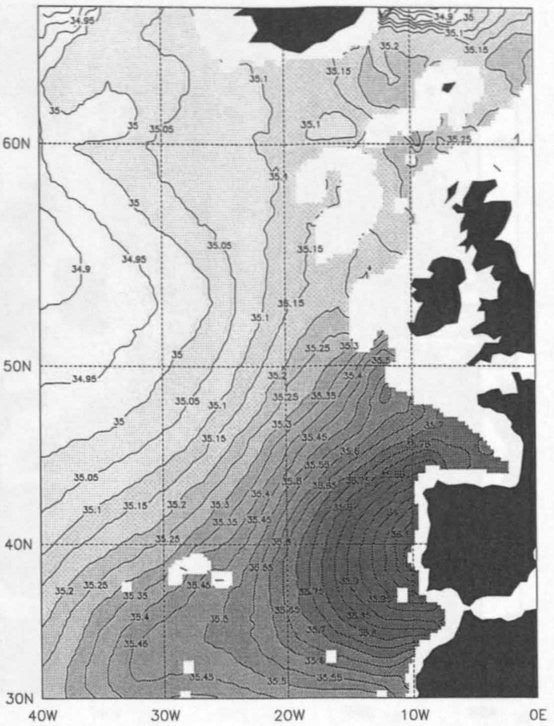
60N
50N
40N
30N
40W
30W
20W
10W
0E

(a) Levitus observations and initial state for models (taken from ISOPYCNIC)

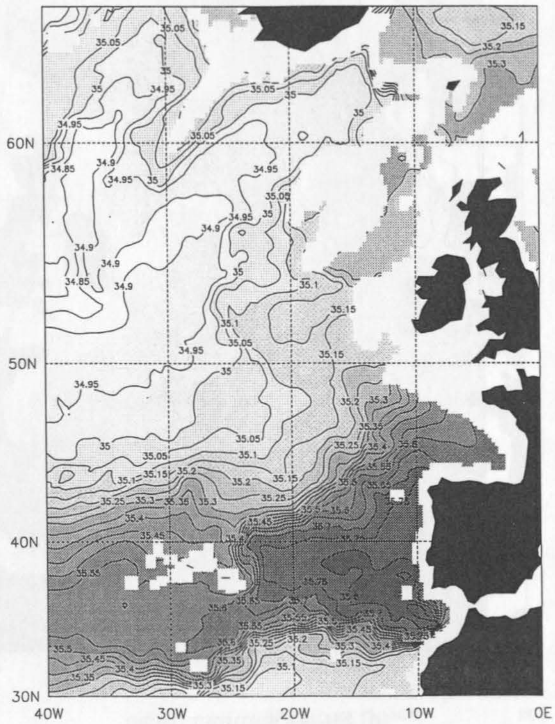
60N
50N
40N
30N
40W
30W
20W
10W
0E

(b) ISOPYCNIC summer mean

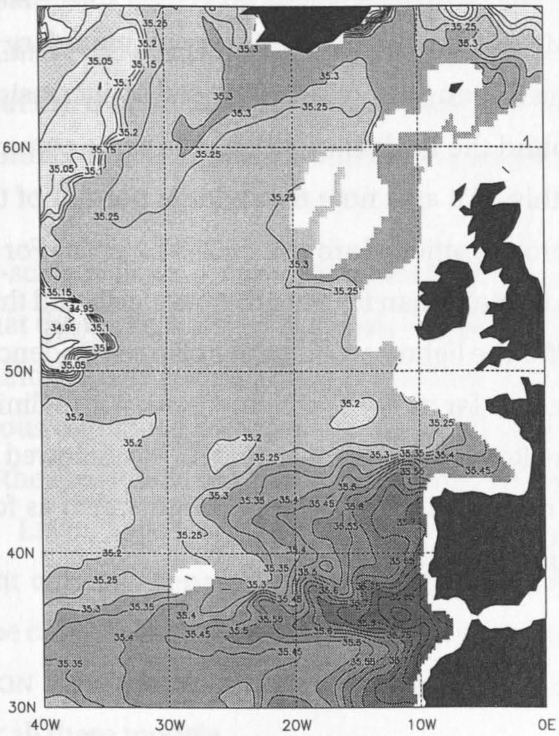
60N
50N
40N
30N
40W
30W
20W
10W
0E

(c) LEVEL summer mean

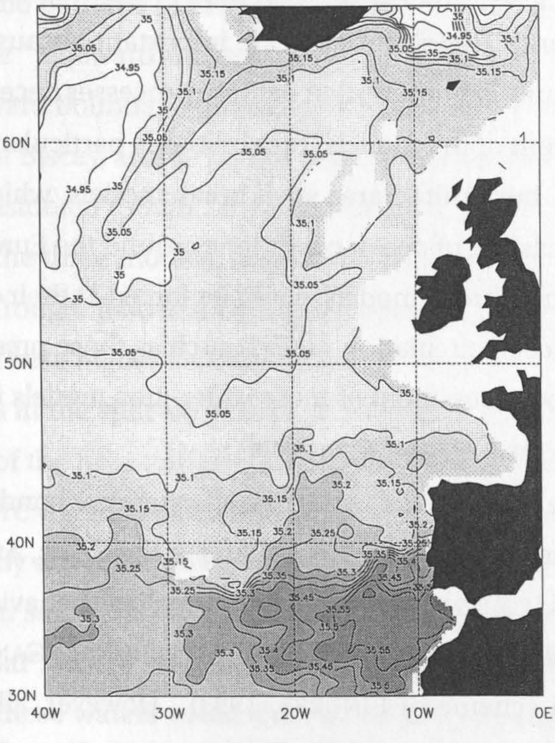
60N
50N
40N
30N
40W
30W
20W
10W
0E

(d) SIGMA summer mean

Figure 9.8: Salinity (psu) on the isopycnal surface 27.64.

ward spreading, and leakage to the south. But there is also clear northward spreading round into the Bay of Biscay. Moving further up the European boundary, there is then a minimum salinity region around the Goban Spur (49°N) followed by increasing salinities, reaching 35.3 over the IS ridge and around the Reykjanes Ridge. The same comments apply as for ISOPYCNIC on the meaning of this. We also note that a large portion of the northeast Atlantic has now been homogenised to salinities of around 35.2–35.25 psu. For SIGMA, salinities near the core have dropped to 35.6 (more than for the other models), and there is again westward and southward spreading as for the lighter surfaces. We also see evidence of spreading around the European margins at least as far as the Porcupine Bank with salinities above 35.1, but there is then a minimum in the Rockall Trough (i.e. near 55°N), followed by increasing salinities to above 35.15 over the IS ridge and the Reykjanes Ridge, much as for the other models. This also will need further work to explain.

9.4 Conclusions

The main goals of this chapter have been to assess the ability of the three state-of-the-art models to represent the processes which occur in the waters around the European continental shelf and slope regions. These processes are important because of their relevance to the European nations. Not only is a description of these processes necessary for the fishing industry, but also an assessment of the models' capabilities is particularly relevant when coupling to very high resolution, but limited area shelf break models, which may soon be in operational use for daily forecasting of ocean conditions around the European seas. It is envisaged that these forecasting shelf-break models would be forced at their open boundaries by wider area, lower resolution ocean circulation models such as those presented here. It is therefore important to have a good assessment of these wider-area models in providing realistic open boundary conditions to the forecasting models.

For the near-surface flows, and considering the summer condition first, we remark that the models predict somewhat different behaviours in the Celtic, Armorican and north Spanish slopes, with perhaps ISOPYCNIC giving the most realistic behaviour (i.e. the westward flow on the north Spanish slopes as observed by PINGREE and LECANN, 1990, and the general anticyclonic circulation scheme of PINGREE, 1993). However, all models correctly predict the upwelling region of cool water off the Iberian coast. Here, LEVEL appears to give the weakest upwelling (SST differences of about 1.5°C), SIGMA is intermediate (SST differences of about 2.0–2.5°C), and ISOPYCNIC is the marginally the strongest (SST differences of about

2.5–3.0°C). These compare with observational SST differences in the summer of 3.5-4.5°C (e.g. NYKJAER and VAN CAMP, 1994). In addition, all the DYNAMO models compare favourably with the very high resolution, limited area, modelling study of STEVENS and JOHNSON (1997) in the MORENA programme, which predicts summertime upwelling SST differences of 3.0–3.5°C.

For the winter near-surface flows on the other hand, all the models show a reasonably realistic "Navidad" in that the warm water of southern origins is clearly advected strongly in a poleward direction around the continental margins between (at least) Portugal and southern Ireland. The most obvious difference between the models is that the Navidad in SIGMA is a little too far in towards the coastlines, but this is due to the topographic smoothing which is required in this model. LEVEL appears to have the best representation over the Armorican slope in that the current correctly separates from near the coastline at Cap Ferret Canyon. Again, for the wintertime case, all the DYNAMO models compare well with the MORENA study of STEVENS and JOHNSON (1997) for the Iberian shelf area in that northward flows of order 5 cm/s are predicted by all these models.

We have also studied the northward spreading of high salinity water of Mediterranean origin by investigating the patterns of salinity on various isopycnic surfaces, chosen to span the probable core of the "poleward undercurrent". Overall, the three models all agree and seem to show the poleward boundary spreading of high salinity waters from the Portuguese slopes around the Bay of Biscay, and as far north as at least the Porcupine Bank (53°N) on all the density surfaces considered (potential density values of 27.38, 27.52 and 27.64). On most density surfaces for all the three models, there often then appears to be a minimum salinity in or near the Rockall Trough, followed by higher salinities over the Iceland-Scotland ridge and Reykjanes Ridge. These higher salinities could have resulted from the northward flow of higher salinity waters in the spin-up phases of the model integrations, or by detrainment and downward mixing of the near-surface waters in the wintertime. However, a preliminary investigation with ISOPYCNIC shows that the latter mechanism is more likely: high salinity surface waters are clearly advected polewards around the European margins in the wintertime in this model, from southern origins (south of 40°N) to the Iceland-Scotland (IS) area, probably in the "Navidad", where salinities of 35.35 psu are achieved. It seems quite plausible at this stage that these waters could then be subducted and give rise to the relatively high salinities, also near 35.35 psu, seen on all the layers in this region of this model. It may be that the Mediterranean Water (MW) could be spreading all the way north to the IS area, but its salinity is being masked by the slightly higher salinity detrained from the mixed layer.

This could explain why it is difficult to deduce unambiguously from the observations of, for instance, salinity on isopycnals, that the MW does indeed spread as far north as the IS ridge. Clearly, much more work is needed to clarify this issue, but in principle we see that models such as those used in the DYNAMO project can give very significant insights into processes such as these, and can resolve the issues in the "Reid hypothesis". At this stage, though, the models are all in agreement that the high salinity water spreads polewards at least as far as the Porcupine Bank or thereabouts.

There are also some areas of discrepancies between the models which are worth summarising. Firstly, the maximum salinities near the Portuguese coast are reduced from those in the initial state in all models, indicating a somewhat inadequate relaxation scheme near the Straits of Gibraltar (which should instead have perhaps been centred further north, off the Portuguese coast). However, these high salinities are eroded the least in LEVEL and the most in SIGMA, on all density surfaces investigated. In this context, we note that the boundary current systems in SIGMA are generally stronger than in the other models, so that water would advect more quickly through the relaxation zone near the Gibraltar outflow, and have correspondingly less time to adjust to the relaxation conditions there. This could explain why the maximum salinities near the Gibraltar outflow region are lower in SIGMA than in the other models.

There are also marked differences south of about 40°N due to the presence of a strong Azores Current-type feature in ISOPYCNIC, and its absence in the other models. This seems to give strong westward spreading in ISOPYCNIC, and no spreading southwards (the Azores Current and its retroflection back to the west, see other chapters of this report, seeming to act as a boundary in this respect), whereas both LEVEL and SIGMA show only weak westward spreading, and noticeable southward spreading down the African coast. The real world (as evidenced by the observations of LEVITUS, 1982, shown in the initial model state, and also by REID, 1979) seems to fall somewhere between these two extremes. In the real world, there does appear to be an Azores Current almost all the way to the Moroccan coast near 32–35°N, but we conjecture that mixing by eddies (not adequately resolved in ISOPYCNIC) allows some southward as well as westward spreading across this current feature.

In addition, we remark that there are considerable differences between the models in maintaining the salinity gradients on the isopycnic surfaces in a wide region of the north-east Atlantic, between the influence of the North Atlantic Current near 50°N, 30°W, and the higher salinities around the European margins. Here, LEVEL has the most homogenised salinity fields, there typically being no more than 0.05 psu salinity difference across this whole region on any of the density surfaces considered. SIGMA shows patterns which are less well mixed, but still significantly more mixed than in the observations. ISOPYCNIC, on the other hand, seems to do a reasonably good job of maintaining the salinity contrast in the northeastern Atlantic. At this stage, it seems most plausible that these homogenised regions may be due to enhanced mixing by eddies in the Gulf Stream system. These would tend to mix properties on isopycnic surfaces which would then advect (and spread) with the North Atlantic Current, so filling approximately the areas shown. We note that the eddy field in ISOPYCNIC is much weaker (unrealistically so) than in the other models, so this could explain why there is no homogenisation in this model. However, this does not explain why there are strong salinity gradients in the real world in this area (given that there is a strong eddy field in the Gulf Stream of the real world), and more work is needed to elucidate this.

In summary, we have shown that the three DYNAMO models are suprisingly successful in representing the flows and processes around the European margins. They compare well with the much finer (1/12° resolution) MORENA model of STEVENS and JOHNSON (1997), and also show the flow patterns over a much wider area. In due course, by investigating the flow patterns on either levels or isopycnic surfaces in the DYNAMO models, we will be able to reveal for the first time (i.e. this has not been done before in models of this resolution) the "connectivity" of the poleward slope current, that is, whether the current exists as a continuous feature from the Iberian shelf up to the Iceland-Scotland area (for instance), something which has not so far been possible either with the limited area models such as STEVENS and JOHNSON (1997), or from observations, which are too sparsely spaced at any particular period in time. The DYNAMO models will also be able to give significant physical insight into whether or not Mediterranean Water spreads north of the Iceland-Scotland ridge as conjectured by REID (1979).

Chapter 10

Assimilation

10.1 Introduction

A satellite altimeter yields observations of the ocean surface only. The sea surface topography, however, consists of the geoid and the dynamic topography due to ocean currents. Since present geoids are not accurate enough to determine the absolute dynamic topography except at very long wavelengths of some thousand kilometres, oceanographers interested in mesoscale processes can only extract the time-varying part of the dynamic topography from the altimeter signal and use independent measurements to estimate the time mean.

Much work has been dedicated to the use of altimeter data for analyzing the mesoscale variability at the ocean surface (e.g., LE TRAON et al., 1990; STAMMER, 1992). Global statistical descriptions were obtained ranging from maps of the rms surface height variability to regional spectral analysis and characterization of typical space and time scales of mesoscale variability. These statistical descriptions have in common that they are essentially restricted to the ocean surface. It is only the use of our knowledge of ocean dynamics that may enable us to infer subsurface information from the altimetric data set.

It is evident that a single observation of the sea surface topography alone will not allow a unique determination of the deep ocean's state. One can immediately imagine very different states of the ocean which produce the same instantaneous surface elevation. However, different states will in general evolve differently in time, eventually leading to distinct dynamic topographies. Hence, a second measurement taken by the satellite after some time restricts the number of possible states consistent with both observations. It is then legitimate to expect that a long time series of surface observations combined with some understanding of ocean dynamics should gradually reveal more and more about the deep ocean.

Combining ocean dynamics and large amounts of data is usually best organized around a numerical circulation model including much of what today is known about the dynamical behaviour of the ocean. By assimilating the data into a numerical model, a huge number of observations can be dynamically extra- and interpolated both in space and in time. In particular, the model's ability to dynamically constrain the ocean interior given a time series of surface measurements gives a very tempting prospect to globally monitor the state and, of course, also the potential changes, of today's ocean. In this regard it seems appropriate to use one of the most realistic ocean circulation models available. For the DYNAMO project, restricted to the study of the North Atlantic Ocean, after careful discussion, we concluded that the KMD model was well suited for this task. However, a major subtask of the DYNAMO project was to develop and establish an assimilation scheme best adapted to this model.

In this part of the final report we first discuss what flow properties would be altered and improved by assimilation; we then briefly review existing methods; discuss methods investigated for use in the DYNAMO assimilation; and then give details of the method chosen, based on work by OSCHLIES and WILLEBRAND (1996). We then discuss the effects of assimilating TOPEX/Poseidon data into the LEVEL model using this method.

10.2 What can we expect assimilation to achieve?

We here examine what assimilation can and cannot be expected to achieve. For the near future, the data used for assimilation will need to be global in nature. This is likely, therefore, to involve only the sea surface height since this is the only field readily available from satellites (sea-surface temperature is discussed later). Since the ocean geoid is not known to sufficient accuracy, assimilation can only involve the time-varying part of the sea surface height.

We can anticipate therefore that variability of the flow will be improved by assimilating the time-varying sea surface height. But no aspects of the *mean flow* will be assimilated. This means that any changes to the mean flow induced by assimilation will have to occur through *nonlinear interaction terms.* These are of two kinds. In the tracer (heat, salt, etc.) equations there are *advection* terms $\mathbf{u} \cdot \nabla \mathrm{T}$. In the momentum equations there are Reynolds' stress terms such as $\mathbf{u} \cdot \nabla \mathbf{u}$. These two sets of terms play quite different roles, so that the changes in these terms from assimilating data will modify the mean flow in different ways.

The advection terms, following assimilation, will contain terms such as $\overline{\mathbf{u}' \cdot \nabla \mathrm{T}'}$, or, equivalently, $\nabla \cdot \overline{\mathbf{u}'T'}$, where the prime here refers to deviations from the mean. This divergence of fluxes has an effect on the mean density field (which will itself modify the mean circulation).

Furthermore, the divergence terms in the tracer equations are the only terms modifying the tracer and so are of direct importance. The size and effect of the divergence terms depend on how far from observations the model ocean lies. If the model is close to reality, the flux divergence will be naturally small, and will have little effect. If the model is far from reality, the divergence term will be strong, but may have an effect counter to what is needed to bring the flow closer to reality.

The Reynolds' stress terms, in contrast, are not the largest terms in the momentum equations except in certain locations. Over most of the ocean, the predominant balance is geostrophic. Thus if there is little change to the mean water mass structure, thermal wind implies that there will be little direct change to the momentum structure. The Reynolds' stress terms, however, have a secondary effect through the vorticity budget, obtained from the curl of the momentum equations. In regions of strong current, the stress terms can be of similar order to the beta-spiral terms, so that assimilation can be expected to modify the *mean path* of western boundary currents, for example.

Nonetheless, the key fact remains that if the model trajectory lies naturally far from observations, the act of assimilating data will invoke strong changes to the model. These will manifest themselves in the nonlinear terms, and the changes may not be as required. It is important, therefore, to make every effort to ensure that the model runs close to reality naturally (see the pre-assimilation method below). Assimilating data strongly into a poor model will never give as acceptable results as assimilating data weakly into a good model.

10.3 Assimilation methods

10.3.1 Principal existing methods

For the problem of assimilating observations into numerical ocean circulation models a variety of different methods already exists, most of them originally developed in meteorology. An extensive review can be found in GHIL and MALANOTTE-RIZZOLI (1991). However, there are major differences in the use of data in oceanography and meteorology. First, data coverage in meteorology is far more uniform and complete than in oceanography, which has no observations at all for large regions of the deep ocean. Second, the motivation for data assimilation differs from the pressing need for accurate weather forecasts to the objective of better understanding the ocean circulation. Third, there are differences in the properties of the two fluids and also in the geometry and nature of the boundaries. Finally, numerical models of the atmosphere are rather more mature than present ocean circulation models. Taking into account the above mentioned points, we shall briefly discuss the most common assimilation techniques with respect to the objective of this study.

Adjoint method

Based on the calculus of variations, the adjoint method determines the one model trajectory that fits the sequence of observations best. Depending on the norm defined to measure the quality of the fit, one constructs a penalty or cost function which is minimized with respect to some control variables, usually the initial conditions of the model (LE DIMET and TALAGRAND, 1986). It is important to emphasize that adjusting only the initial conditions to find the best fit implicitly assumes that the model is perfect (LEWIS and DERBER, 1985), which may cause problems especially when applied to present ocean models. The minimization is efficiently carried out by essentially integrating the model forward and backward in time to compute gradients of the cost function. However, storage of the forcing terms as well as of non-linear effects is required over the full length of the time series of observations used. At least for basin-wide eddy-resolving circulation models this clearly goes beyond the storage capabilities of present computing systems. A further disadvantage of applying the adjoint method to non-linear systems is that increasing the assimilation period will rapidly increase the complexity of the shape of the cost function, making it virtually impossible to determine its global minimum. In this respect the introduction of more data will not always result in the "optimized" state being closer to reality (STENSRUD and BAO, 1992).

Kalman filter

In contrast to the adjoint method the Kalman filter represents a sequential assimilation procedure (e.g., GHIL et al., 1981). It is based on the statistical concept of optimal interpolation: At each observation time the Kalman filter optimally interpolates between the model forecast and the observations to obtain a new state vector with reduced error covariance. This state is subsequently used as initial state for the model to compute a forecast for the next observation time. By repeating this assimilation cycle and keeping track of the error covariance of the model state, the model step by step absorbs the information of the sequence of observations. The crucial point is that for this technique to be optimal one has to compute the time evolution of the covariance matrix of the model errors. It is again the corresponding computational burden which for our purpose clearly rules out the use of the Kalman filter.

Suboptimal methods

Both methods mentioned above are statistically optimal in the sense that they minimize the covariance of the estimated errors. Furthermore, for linear models it can be shown that given the same information both the adjoint method and the Kalman filter finally yield the same state estimate (THACKER, 1986). We note that the idea of minimizing the error covariance is not always adequate for present ocean models. If the probability distribution of the errors is not Gaussian – which in particular is the case for systematic model errors – the optimized state will in general not be one of maximum likelihood. In any case, the huge computational cost immediately prohibits the application of these techniques to non-linear models with high-dimensional phase spaces. No simple statistically optimal method is available, and for our objective we therefore have to resort to suboptimal methods.

A large number of suboptimal methods has been used in oceanography. Not all of these are equally well adapted to assimilation. So far, most studies directed at the assimilation of satellite altimeter data have employed the conceptually (and also computationally) simple nudging technique, which is basically a relaxation of prognostic model variables towards the observations. Due to the presence of an additional relaxation (or nudging) term the model physics with assimilation differs from that without. WOODGATE and KILLWORTH (1997) show that these differences can be important, with radical changes to natural frequencies of the ocean system when nudging is employed. This in turn can change length scales within the system, thus altering eddy behaviour and boundary layer structure. Thus the very act of nudging can in some circumstances prevent the movement of the solution towards that required.

Nevertheless, quite a number of studies have successfully employed the nudging technique to combine numerical models and observations. The success of this suboptimal approach is closely related to its property of passively conserving subsurface potential vorticity, which is appropriate for models with a single ventilated layer like QG models (see below). As the vertical resolution of the ocean model is increased, this property eventually becomes an adverse effect, and some active extrapolation of the surface information into the ocean interior is required. Within the present study, this is accounted for by new assimilation methods based on the re-initialization concept. Like the Kalman filter, these methods sequentially update successive model forecasts. However, in contrast to the Kalman filter none of them is optimal in a purely statistical sense.

10.3.2 Approaches due to Haines

An alternative assimilation scheme for assimilating altimeter data into eddy-resolving primitive equation models has been proposed by COOPER and HAINES (1996). It is based on the concept of conserving potential vorticity (PV) in the assimilation step, which was first applied to a quasi-geostrophic model by HAINES (1991) and subsequently extended to a 3-layer shallow water model. Both of these latter models were layer models in which subsurface PV tends to be almost uniform in regions of strong eddy activity. This can be explained as PV homogenization due to mixing by eddies (RHINES and YOUNG, 1982). HAINES (1991) pointed out that this corresponds to only weak vertical correlations between PV in different model layers, associated with strong vertical correlations in the streamfunction or current fields.

Both in the real ocean and also in more realistic models that allow for isopycnal outcropping the picture is less simple. Atmospheric conditions act to reset PV on surfacing isopycnals, thereby introducing sources or sinks of PV for individual isopycnic layers. As noted by COOPER and HAINES (1996), the vertical PV correlations may nevertheless be weak. They claim that there is hence no reason to change interior PV and consequently impose the constraint of PV conservation at assimilation times.

Any surface height misfit between model forecast and altimetric observations produces hydrostatic subsurface pressure increments:

$$\Delta p(z) = \rho g \, \Delta\eta + g \int_z^0 \Delta\rho \, dz \, .$$

with density increments $\Delta\rho$. Neglecting contributions due to relative vorticity, they use the linearized form $\mathrm{PV}(\rho) = -(f/\rho_0)\partial\rho/\partial z$. Conservation of PV then becomes equivalent to lifting or lowering all isopycnals in the water column by the same amount Δh. To find this, they introduced the additional constraint of no pressure change at the bottom (and hence no change in the bottom currents) so that the change in weight of the entire water column compensates for the change in surface pressure due to $\Delta\eta$.

The associated changes in the temperature and salinity fields are determined by conserving these tracers on isopycnals, while the corresponding increments of the velocity field are obtained from the geostrophic balance condition followed by a small adjustment to achieve mass continuity.

This assimilation method is attractive in the sense that it avoids the use of uncertain model statistics. However, from the identical twin experiments discussed by COOPER and HAINES (1996) and also from experiments with Geosat data performed at IfM Kiel it is clear that the method does not work well in weakly stratified regions where the method requires artificially large water excursions. The CME model test experiments showed that this problem is not restricted to high latitude convection regions, but does in fact occur as far south as the Gulf of Mexico. Problems also arise in the presence of topography.

These considerations led DRAKOPOULOS et al. (1996) to suggest a generalisation of the approach to include – perhaps arbitrarily – the barotropic relative vorticity. They argue that the relative vorticity of the water column is related to the vertical displacement Δh by

$$\Delta\bar{\zeta} = \frac{f}{H}\Delta h\,.$$

They further relate this vorticity change geostrophically to the *deep* pressure change (rather than the vertically integrated pressure change), to give

$$\Delta\bar{\zeta} = \frac{1}{\rho_0 f}\nabla^2\Delta p_b$$

where the suffix b denotes a bottom value. Solving for Δp_b then yields a Helmholtz equation:

$$\frac{gH(\rho_b - \bar{\rho}_s)}{\rho_0 f^2}\nabla^2\Delta p_b - \Delta p_b = -\Delta p_s\,.$$

In regions of shallow water, weak stratification, or when the applied pressure change is large-scale compared with the deformation radius, the first term on the l.h.s. is small and the solution reduces to the barotropic change $\Delta p_b \sim \Delta p_s$. When the applied change has length scales of order the deformation radius, the change is spread over a deformation radius in a manner similar to geostrophic adjustment.

This approach, too, is attractive, but appeared too late in the project for consideration.

10.3.3 Minimum energy approaches

Minimum energy

HAINES' ideas are attractive – in that he seeks to maintain conservation of certain properties – but suffer from some difficulties. The obvious difficulty is that an assimilation which begins from a state too far from reality (e.g., with incorrect water mass structure) can never attain the correct structure since water temperature and salinity are being 'conserved' in some sense. The second difficulty is more profound. In adjusting a water column upwards or downwards, some method must be used to specify the degree of movement; Haines has employed two different methods, discussed above.

We have investigated another approach, based on energetics. Consider a geostrophic adjustment problem. If this were created by some injection of information into a system, then the adjusted state would be one of *minimum energy* compared with the original, unadjusted state. Suppose we apply the same concept to HAINES' method. Consider a free-surface model whose surface elevation η has been directly inserted from data (ignoring for simplicity, as does HAINES, the possibility of nudging here). Each fluid column is raised or lowered by an unknown amount , maintaining water mass structure, so that the change in energy between the initial configuration and the resulting one is minimised. We shall assume that the velocity changes are geostrophic to leading order.

Let the applied change in surface pressure ($\rho_0 g\eta$) be $\hat{p}(x,y)$. The change in density is $\Delta\rho = \hat{z}\rho_z + \frac{1}{2}\hat{z}^2\rho_{zz}$ to second order in $\hat{z}$. It is necessary to work to this order as the resulting expression for kinetic energy changes would be second order automatically. The change in pressure at some depth is, from the hydrostatic relationship,

$$\Delta p = \hat{p}/\rho_0 + (g/\rho_0)\left\{\hat{z}(\rho_s - \rho) + \frac{1}{2}\hat{z}^2(\rho_{sz} - \rho_z)\right\}$$

where suffices s, b denotes surface and bottom values respectively, and small changes $\hat{z}$ are assumed. The changes in velocity $\Delta u, \Delta v$ are quadratic in $\hat{z}$ so that the change in kinetic energy is given by (dA denotes an element of horizontal area)

$$\Delta KE = \int dA\,\rho_0 \int_{-H(x,y)}^{0} \frac{1}{2}\left\{(u+\Delta u)^2 - u^2 + (v+\Delta v)^2 - v^{2)}\right\} dz$$

$$= \int dA\left\{A + \mathbf{B}\cdot\nabla\hat{z} + C\hat{z} + D(\hat{z}_x^2 + \hat{z}_y^2) + F\hat{z}\hat{z}_x + G\hat{z}\hat{z}_y + K\hat{z}^2\right\} + \text{higher order terms}$$

after some algebra, where A, etc., are known functions of horizontal position, involving integrals of properties w.r.t. z and need not concern us here.

Similarly, the change in potential energy is

$$\Delta PE = \int dA\,(M\hat{z} + N\hat{z}^2)$$

where M, N are again functions of horizontal position.

The energy minimisation requires a Lagrange multiplier, to ensure no net mass change, and thus gives a Poisson-like system for $\hat{z}$, and is soluble numerically by iteration together with an equation for no net mass change providing the system is diagonally dominant.

The method, like that of DRAKOPOULOS et al., reacts differently to different scales of motion. The change in potential energy per unit area is

$$\Delta PE = O(\hat{z})gH\Delta\rho$$

where $\Delta\rho$ is a typical top-to-bottom density variation. Similarly,

$$\Delta KE = O(uH\rho_0\Delta u) = O(\hat{z})\cdot\frac{H^2g^2\Delta\rho^2}{f^2L^2\rho_0}$$

where L is a typical horizontal scale for the motion, so that

$$\frac{\Delta KE}{\Delta PE} = \frac{gH\Delta\rho}{f^2L^2\rho_0}$$

independent of the magnitude of $\hat{z}$. For gyre-scale motions, as is well known, available potential energy dominates kinetic: if L=1000 km, the above ratio is of order 1.6×10^2. In other words, in the equation for $\hat{z}$ above, the term M dominates the rest of the l.h.s. However, in more realistic conditions such as eddy-resolving problems, L=100 km and the ratio is unity. So for large-scale problems one might be better to minimise kinetic energy only, but for the normal case of an ocean containing eddies this method should yield a sensible solution. In addition, the method has the attractive property that the change in column depth is not determined locally, but depends on the global distribution of properties. The velocity changes are (as in the DYNAMO assimilation) not divergence-free, and a small velocity correction must be made to ensure zero divergence.

Tests of this approach were made during the DYNAMO project, using a three-layer, flat-bottomed ocean model and identical twin data. It was found that even for no applied surface height change, there was a large change to the gyral circulation following one assimilation step (for this problem, the optimal response would be one of no change, clearly). In other words, the ocean is not naturally near a state of minimum energy, and requiring it to move into such a state forces it away from reality.

Minimum energy change

Another approach would be to require that the *change* in energy is minimised by the act of assimilation, rather than the resulting energy itself. This would produce no change in circulation if no surface pressure change is applied, which is an attractive feature, while maintaining water mass and potential vorticity structures.

The change in formalism is straightforward: instead of minimising $\Delta(KE+PE)$, we minimise $(E_{assim}-E_{model})^2$. To do this, perturbation quantities above quadratic can be neglected. The formalism is not here reproduced, save for the resulting equation for $\hat{z}$, which can be written schematically:

$$A\,\hat{z}_{xx} + 2B\,\hat{z}_{xy} + C\,\hat{z}_{yy} + \text{lower terms} = \text{forcing.}$$

This is apparently a Helmholtz equation of similar form to that above, which can be solved with suitable boundary conditions. However, it can be shown that the discriminant of the second order terms, $D = AC - B^2$, has a value identically equal to zero. This means that the system is spatially parabolic and not elliptic. This change is fundamental, and means that the system is only well-posed following timelike characteristics across the ocean. Certainly the boundary conditions relevant to – for example – no normal flow into the basin are now overspecified for the problem.

This finding is surprising, and it is unclear how to proceed. The requirement of a flow after assimilation which is as close to the original as possible in an energetic sense is appealing physically, and intuitively should be well-posed (certainly it is difficult to see how more than one solution could exist). Yet the analysis shows this not to be the case. We have been unable to overcome this difficulty, and so have not proceeded further with this line of work.

10.3.4 Pre-assimilation

To assimilate SSH into ocean models, we often take the mean flow from either the numerical model itself or the climatologies. In the first approach, one has to assume that model has correct physics as well as correct forcings. In general, this must be false. This means that the model will naturally lie further from observations than we would prefer, so that the act of assimilation will involve the model being 'pulled' harder towards observations; such a strong pull may well modify the ocean in a nonlinear fashion. Now the missing physics can be seen as an extra forcing function in the model which is necessary to make it run in a similar way to observations. Thus the question we would like to address is: can we extract information about this extra forcing function from the time varying quantities?

We propose a method as the following. The continuity equation in isopycnal co-ordinates is

$$\frac{\partial h}{\partial t} + \nabla \cdot (h\mathbf{u}) = B,$$

where h is an isopycnal layer thickness and B is an effective buoyancy forcing (we assume, as do most parameterisations, that the majority of errors occur in the thermohaline component of the system. Separating the time-mean part and time-varying part we have

$$\frac{\partial \bar{h}}{\partial t} + \nabla \cdot (\bar{h}\bar{\mathbf{u}}) + \nabla \cdot (\overline{h'\mathbf{u}'}) = \bar{B}.$$

The first term on the l.h.s. is small by definition. Assuming the mean-flow is zonal and geostrophic, the second term on the l.h.s. is also small. We are now left with

$$\nabla \cdot (\overline{h'\mathbf{u}'}) = \bar{B}.$$

Therefore the divergence of eddy volume fluxes equals to the mean forcing. A twin experiment was carried out to test this idea of using eddy fluxes as a forcing function.

We use a three-layer MICOM channel model in two configurations. One run is forced by B and the other is forced by the eddy volume fluxes from the first run. The result is very satisfactory, in that there is almost no difference in the mean-flows in the region where eddies are strong. However there is about 30 m difference in depth outside the eddying region, which could be due to the long term drift of the mean-flow and therefore eddy fluxes no longer balance forcing.

10.3.5 The 'cascade' method

In the 'pre-assimilation' approach, we take eddy fluxes from the control run. In practice, we would like to use eddy fluxes from observations. Unfortunately, the only reliable eddy field is probably the geostrophic surface velocity induced by SSH variations. The key question is how to obtain h' for the surface layer and also $\mathbf{u}'$, h' at all the layers below. (This can be seen both as a way of evaluating the pre-assimilation forcing, and as a way of assimilating itself.) We propose a method as the following. Rewrite the continuity equation as

$$\frac{\partial h'}{\partial t} + \nabla \cdot (h'\mathbf{u}) = -\nabla \cdot (\bar{h}\mathbf{u}') + \nabla \cdot (\overline{h'\mathbf{u}'}).$$

Note that we have not made any assumption so all the terms are still included. The l.h.s. is the advection of h' by the total velocity field $\mathbf{u}$, the first term on the r.h.s. is the eddy transport of mean volume and the second term on the r.h.s. is the divergence of eddy volume fluxes. Assume the mean-flow is known for all layers. Hence $\mathbf{u}_1$ (the flow in the top layer) is known since $\mathbf{u}_1'$ is known, and the second term on the r.h.s. is also known. The third term on the r.h.s. is generally unknown but can be parameterised. We can integrate h' in the surface layer, which will be advected by $\mathbf{u}$ and forced by $-\nabla \cdot (\bar{h}\mathbf{u}') + \nabla \cdot (\overline{h'\mathbf{u}'})$. Once we calculate h_1', the velocity at the layer below can be obtained from the hydrostatic equation, namely,

$$\mathbf{u}_2' = \mathbf{u}_1' + \frac{\Delta\rho}{f}\mathbf{k} \times \nabla h_1'.$$

We can continue this 'cascade' to the bottom layer, where one must ensure that $\sum h' = SSH'$. A twin experiment has been carried out which also shows a satisfactory result of this approach.

10.4 The DYNAMO assimilation

10.4.1 The altimetric data set

In the frame of the DYNAMO project, data from GEOSAT were first considered, as when the project was launched, no other altimetric data were available. But things have changed: at the present time, two satellites (ERS-1 and TOPEX/Poseidon (T/P)) are producing very high quality altimetric data. A third satellite (ERS-2) was launched in April 1995, but the data are not yet available for our purpose. For T/P, the sea level anomaly can be determined with a precision better than 5 cm rms, especially because of the outstanding quality of the orbit determination (error about 2 cm rms; NOUEL et al., 1994). For ERS-1, the radar altimeter has about the same accuracy than for T/P, but the orbit determination is not so good (≈15 cm rms; MASSMANN et al., 1993, SCHARROO et al., 1993). From October 1992 to December 1993, the two spacecraft were operating simultaneously with suitable orbit characteristics for mesoscale studies (10 days repeat orbit and about 315 km equator inter-track for T/P; 35 days repeat orbit and about 80 km equator inter-track for ERS-1), and the high orbit quality of T/P was used to reduce the orbit errors of ERS-1 by minimizing the differences at ERS-T/P cross-over points (LE TRAON et al., 1995). It is the resulting high quality combined T/P and ERS-1 data set (SLA error ≈5 cm rms) that has been used for assimilation into the Kiel DYNAMO Model.

An objective analysis routine was used to interpolate the altimetric data onto the model grid. We used the algorithm of DE MEY and MENARD (1989), which is an adaptation of the general objective analysis algorithm of BRETHERTON et al. (1976), where the number of data points is greatly reduced by considering only statistically independent data within a chosen influence radius (typically 400 km and 30 days). The correlation radius was chosen to vary with latitude, following OSCHLIES and WILLEBRAND (1996). Five-daily maps of the altimetric signal as well as of the expected error variance were produced for the one-year period October 15, 1992 to October 15, 1993.

10.4.2 The method of OSCHLIES and WILLEBRAND

In this section we briefly describe the scheme for assimilating altimeter data developed by OSCHLIES and WILLEBRAND (1996), which has been used to carry out the assimilation here. Although it can by no means be considered as being perfect, it remains – to our knowledge – the only scheme that so far has been successfully applied to the assimilation of real altimeter data into a basin-scale, eddy-permitting primitive-equation model[1]. It is this point that made us choose the method for the DYNAMO assimilation over other possible candidates. Initial tests of the method are reported by OSCHLIES and WILLEBRAND (1996).

The basic concept of essentially all sequential data assimilation methods can be expressed as

$$\mathbf{x}^a = \mathbf{x}^f + \mathbf{K}(\mathbf{y}^{obs} - \mathbf{H}\mathbf{x}^f) \tag{10.1}$$

where $\mathbf{x}$ is the state vector of the numerical ocean circulation model, with indices f and a referring to forecast and analysis respectively. The operator $\mathbf{K}$, which in general will be neither linear nor constant in time, projects (or inverts) the difference between measured variables $\mathbf{y}^{obs}$ and their model forecast counterpart $\mathbf{y}^f \equiv \mathbf{H}\mathbf{x}^f$ onto the model state space. An assimilation cycle then consists of: (a) halting the model integration at observation time to obtain a model forecast $\mathbf{x}^f$ and associated $\mathbf{y}^f$; (b) computing the correction $\mathbf{K}(\mathbf{y}^{obs} - \mathbf{H}\mathbf{x}^f)$ required to adjust the model state to the observations; and (c) restarting the model integration from the updated, or analyzed, state $\mathbf{x}^a$.

The method decomposes $\mathbf{K}$ into three distinct operations to be applied successively. A first operator, $\mathbf{A}$, is used to project the observed model-data SSH misfit onto dynamically consistent corrections to the velocity and density fields (i.e., the fields observable by altimetry) of the model forecast. Here, geostrophy will serve as an appropriate dynamical consistency criterion, that keeps the analyzed model state close to the slow (quasi-geostrophic) manifold and avoids strong excitation of gravity waves. The second operator, $\mathbf{B}$, is a weighting matrix that accounts for the relative accuracies of observations, model forecast and approximations introduced by the operator $\mathbf{A}$. To complete the projection of the observed model-data misfit onto state space, one element of the nullspace must be determined. The function of operator $\mathbf{C}$ is to partition the weighted density increments computed by $\mathbf{B} \cdot \mathbf{A}$ into increments of temperature and salinity. Equation 10.1 may then be rewritten as

$$\mathbf{x}^a = \mathbf{x}^f + \mathbf{C} \cdot \mathbf{B} \cdot \mathbf{A}(\mathbf{y}^{obs} - \mathbf{H}\mathbf{x}^f) \tag{10.2}$$

The operations denoted by $\mathbf{A}, \mathbf{B}, \mathbf{C}$ will be described separately in the following three subsections.

Due to uncertainties in present geoid models, altimetry cannot yet be used to extract the temporal mean SSH on the mesoscale. Only observations $\mathbf{y}^{obs}$ of temporal anomalies of the sea surface elevation, $\delta\eta^{obs}$, can be deduced from the data with sufficient accuracy. Accordingly, the operator $\mathbf{H}$ maps the state vector of the model forecast, $\mathbf{x}^f$, onto a corresponding map of SSH anomalies, $\delta\eta^f$, defined relative to the climatological mean sea surface that, because of a lack of alternatives, is presently taken from the model.

---

[1] HAINES (pers. comm.) is assimilating altimeter data in the global OCCAM model as part of a MAST project.

Finding a dynamically consistent set of correction terms

In order to reduce the computational load we separate horizontal, temporal, and vertical correlations in the ocean. Horizontal and temporal correlations are exploited prior to the assimilation itself by a mapping algorithm applied to the tracked altimeter data which produces objectively interpolated maps of $\delta\eta^{obs}$ (and also of the expected error variance to be taken into account by operator **B**) on the model grid. All that is left to the actual assimilation routine is to extrapolate the information provided by the SSH maps in the vertical.

Given maps of the altimetric SSH residuals, it is then straightforward to compute the model-data misfit in the geostrophic surface velocities,

$$\Delta\mathbf{u}_g = \frac{g}{f}\hat{\mathbf{z}} \times \nabla(\delta\eta^{obs} - \delta\eta^f) \tag{10.3}$$

where $\hat{\mathbf{z}}$ is a unit vector pointing upward, f is the Coriolis parameter, and g the acceleration due to gravity. This misfit can immediately be used to update the surface velocity of the model forecast. Note that the ageostrophic Ekman part of the surface currents, which cannot be observed by altimetry (but is well simulated by the model), will not be affected by the update. On the other hand, the above relation neglects ageostrophic gradient wind contributions to the model-data misfit, which can for example be important in intense Gulf Stream rings that are, however, not properly resolved in the present KMD model resolution. After all, equation 10.3 will not allow application of our assimilation method close to the equator.

As pointed out above, it is reasonable to look for some vertical projection of the surface velocity misfit, $\Delta\mathbf{u}_g$, into the ocean interior and to adjust the deeper model levels as well. One simple way to relate velocities, $\mathbf{u}$, at given depth z to the geostrophic part of the surface currents, $\mathbf{u}_g$, is a statistical linear regression method. For each individual column of model grid points we define the vertical regression coefficients for the zonal and meridional velocity components, u and v, respectively by

$$R_u = \frac{\langle \delta u\, \delta u_g \rangle}{\langle (\delta u_g)^2 \rangle};\ R_v = \frac{\langle \delta v\, \delta v_g \rangle}{\langle (\delta v_g)^2 \rangle} \tag{10.4}$$

where $\delta u = u - \langle u \rangle$ denotes the actual deviation of the zonal velocity component u from its climatological mean $\langle u \rangle$ which, again, is provided by the model. Assuming that any deviation of the model from the observations has on average the same vertical profile as typical fluctuations in the model's velocity field, one can then also estimate a pseudo velocity misfit $\Delta\mathbf{u} \equiv \Delta(u, v)$ at any depth level by the linear regression

$$\Delta u = R_u \, \Delta u_g ; \; \Delta v = R_v \, \Delta v_g \, . \tag{10.5}$$

In this way any observed model-data misfit in the geostrophic surface velocity, $\Delta\mathbf{u}_g$, is projected onto a complete three-dimensional field of estimated pseudo velocity misfits $\Delta\mathbf{u}$.

The theory of geostrophic adjustment implies that a corresponding correction $\Delta\rho$ that dynamically balances the above estimated velocity corrections $\Delta\mathbf{u}$, should be applied to the model's density field as well.Such a $\Delta\rho$ is found by combining the two thermal wind equations for the single unknown $\Delta\rho$,

$$\frac{g}{f\rho_0}\frac{\partial\Delta\rho}{\partial y} = \frac{\partial\Delta u}{\partial z} ; \; \frac{g}{f\rho_0}\frac{\partial\Delta\rho}{\partial x} = -\frac{\partial\Delta v}{\partial z} , \tag{10.6}$$

where ρ_0 refers to the mean ocean density. Substituting for the velocity increments, one obtains

$$\frac{\partial\Delta\rho}{\partial y} = -\rho_0 \frac{\partial R_u}{\partial z}\frac{\partial}{\partial y}\left[\delta\eta^{obs} - \delta\eta^{f}\right] ; \; \frac{\partial\Delta\rho}{\partial x} = -\rho_0 \frac{\partial R_v}{\partial z}\frac{\partial}{\partial x}\left[\delta\eta^{obs} - \delta\eta^{f}\right] . \tag{10.7}$$

Because the z-derivatives of the statistically derived regression coefficients are neither the same for R_u and R_v, nor are they horizontally homogeneous, there is no consistent solution for $\Delta\rho$. Only approximate solutions can be determined.

OSCHLIES and WILLEBRAND (1996) proceeded by assuming the vertical regression coefficients R_u and R_v to be horizontally homogeneous – at least on the scale of individual eddies. Moreover, it is likely that the errors due to imperfect model statistics are more critical than neglecting small horizontal variations in these still uncertain coefficients. Giving both of the above relations the same weight, then in a least square sense the optimal $\Delta\rho$ then becomes

$$\Delta\rho = -\rho_0 \frac{\partial}{\partial z}\left(\frac{R_u + R_v}{2}\right) \cdot \left[\delta\eta^{obs} - \delta\eta^{f}\right] . \tag{10.8}$$

The integration constants are set to zero because for a perfect forecast of the sea surface elevation (i.e., $\delta\eta^{obs} = \delta\eta^{f}$) the density field should not be changed. The relationship 10.8 is *local*, which results in a great saving in computation time.

Operator B: Applying weighting coefficients

Together with the statistically estimated velocity deviations Δu and Δv, the density increment $\Delta\rho$ provides an approximately balanced (and hence dynamically self-consistent) estimate for the correction to the forecast state $\mathbf{x}^{f}$. In order to use these estimated correction terms to update the model forecast (Eq. 10.2), their reliability relative to that of the model forecast should be taken into account in form of the weighting matrix **B**.

To cope with limited computer resources we choose a diagonal matrix **B**, its elements being weighting coefficients μ_u, μ_v, and μ_ρ (to be defined at each grid point). Beginning with the zonal velocity field and inserting the corrections Δu into 10.2, we then obtain a scalar equation for each component of the updated velocity field

$$u^a = u^f + \mu_u \, \Delta u = u^f + \mu_u \, R_u (u_g^{obs} - u_g^f)$$

with $u_g^{obs} - u_g^f = \Delta u_g$ given by 10.3.

Neglecting any correlations between errors of different quantities, one can then derive a set of weighting coefficients μ_u (one for each velocity variable of the model) that minimize the expected error variance of the updated velocity components u^a. The resulting expression for μ_u is a function of the relative errors of model forecast and observations, and also of the error introduced by the simple vertical projection scheme represented by the linear regression coefficient R_u. While one can readily obtain reasonable estimates for the expected errors of the (mapped) altimeter data, as well as for the error introduced by the vertical extrapolation scheme, the major difficulty is to determine the forecast error of the assimilation model. Clearly, the forecast error depends on the length of the forecast period. Although the time interval between successive assimilation steps is only 5 days, the frequency with which relevant information is mapped onto a particular grid point will still be governed by the satellite's repeat period.

For simplicity, we followed OSCHLIES and WILLEBRAND (1996) by approximating the forecast error variance of any model variable (of the assimilation run) as a time-independent constant, set equal to the process variance of the respective variable (of the model with no data assimilated).

Employing these simplifying assumptions one can then derive the following expression for the weighting coefficients used to update the velocity components:

$$\mu_u = C_{u,u_g}^2 (1 - r_\eta)^2$$

where the squared correlation coefficient

$$C_{u,u_g}^2 = \frac{\langle \delta u \, \delta u_g \rangle^2}{\langle (\delta u_g)^2 \rangle \, \langle (\delta u)^2 \rangle} = R_u^2 \frac{\langle (\delta u_g)^2 \rangle}{\langle (\delta u)^2 \rangle}$$

accounts for the accuracy of the linear regression scheme used for vertical extrapolation, and r_η is the expected error variance of the local surface height value, normalized by the variance of the SSH field. Like the regression coefficients R_u, the correlation coefficients are taken from the model climatology, while r_η is provided by the SSH mapping routine. Note that both inaccurate surface height observations (i.e., $r_\eta > 0$) as well as imperfect vertical correlations (i.e., $C^2_{u,u_g} < 1$) will reduce the weight of the estimated velocity correction Δu. If on the other hand observations and vertical projection were perfect (i.e., $\mu_u = 0$) the model forecast, u^f would be completely discarded giving $u^a = R_u u^{obs}$.

To give an analogous expression for the remaining weighting coefficient μ_ρ, we note that via Eq. 10.8 the density increment is directly coupled to the vertical derivative of the regression coefficients. For this reason, the relative error in the vertical shear of these regression profiles has been set to the minimum accuracy of the coefficients that contribute to the (discrete) derivative. The explicit form for the weighting parameters μ_ρ then becomes

$$\mu_\rho = \min_{\mathrm{u}_{up},\, \mathrm{u}_{low}} (C^2_{\ldots,u_g})(1 - r_\eta)^2$$

where the subscripts up and low denote the vertical levels used for computing the individual vertical derivative in Eq. 10.8.

Operator C: Partitioning density into temperature and salinity increments

It is evident that for a particular density there is no unique solution to this inverse problem as long as temperature and salinity are treated as independent variables. However, in the ocean these quantities are not really independent, but are closely tied to individual water masses. Once a water mass has been formed and the water is no longer in direct contact with the atmosphere, its potential temperature and salinity, and hence potential density, can for many purposes be considered as fixed. Ocean eddies can to a good approximation be regarded as adiabatic features. In this respect it is only the action of the surface conditions in the water mass formation area that simultaneously determine – and thereby interrelate – temperature and salinity.

This underlines our previous conclusion that there is no reason to change the distribution of (potential) temperature and salinity on isopycnal surfaces when assimilating altimeter data. It is the conservative aspect of water mass properties which immediately provides us with the additional constraint required for a unique inversion of $\mu(\rho)\,\Delta\rho$ for changes of the temperature and salinity forecast fields.

For a level model, as considered in this study, the suggested algorithm first computes the analyzed (*in situ*) density $\rho^a_k = \rho^f_k + \mu(\rho_k)\Delta\rho_k$ at each depth level k. Subsequently it searches in the local water column of the forecast state for a water parcel (defined by a $\theta - S$ point) that, when moved adiabatically to the depth level under consideration, produces the new density ρ_k^a. In case of a potentially unstable stratification, there may be more than one $\theta - S$ point that satisfies this criterion, whereupon the algorithm always selects the water that requires the minimum vertical displacement. As long as the density change does not lead to the introduction of new potential densities (with the reference pressure of depth level k) not already present in the original water column, this procedure uniquely determines the analyzed temperature and salinity fields. When, on the other hand, the analyzed density exceeds the range of potential densities of the model forecast, no vertically displaced water parcel of the forecast state can acquire the density ρ_k^a. In such cases, most likely to occur when light water is introduced at the top, some extrapolation of the original $\theta - S$ relation towards lower (or greater) densities has to be provided. A simple linear extrapolation of the temperature and salinity differences between adjacent depth levels is not always well behaved when large vertical gradients in temperature and salinity counteract, which turns out to be a particular problem in the seasonal thermocline. Therefore, temperature and salinity are additionally constrained to remain within 3° and 0.5 psu of the model forecast values.

10.4.3 Details of assimilation

In contrast to the main LEVEL run which was run with climatological forcing from the 1986 to 1988 ECMWF analysis, the assimilation experiment was forced with daily ECMWF wind stresses for the actual October 1992 to October 1993 period of the altimetric data set. This was preceded by a six-year "spin-up" run forced with daily ECMWF wind stresses beginning in autumn 1986, which was also planned to serve as a sensitivity experiment in comparison to the standard run with climatological forcing. Heat fluxes and the surface restoring for salinity were kept unchanged. Unfortunately, the barotropic part of the meridional flow through the open southern boundary had a wrong sign in all the experiments using daily winds, an error which was detected too late to be corrected before the end of the DYNAMO project.

The intention of using a different wind forcing in the assimilation experiment (as well as in the companion control, or reference[2], experiment without assimilation) was to have both the pre-assimilation state as well as the forcing during the assimilation run as consistent with the data – with reality – as possible.

Since the assimilation scheme is built around the concept of introducing geostrophically balanced corrections, it will not work near the equator. It was therefore decided to switch off the assimilation between 8°N and 8°S with a one-degree transition zone. Similarly, no data were assimilated in regions with poor tidal corrections, chosen on visual inspection of the mapped data. The latter regions include the European shelf, the Faeroes and Iceland shelves as well as on the Abrolhos Bank off South America.

---

[2] We shall use the two terms interchangeably.

Technical detail: divergence

The velocity corrections added at each step are geostrophically balanced. Since the Coriolis parameter varies spatially, the velocity corrections are horizontally divergent:

$$\Delta u_x + \Delta v_y = -\frac{\beta}{f}\Delta v\,.$$

This, in turn, implies that vertical velocity corrections have been created, since

$$\Delta w_z = -(\Delta u_x + \Delta v_y) = \frac{\beta}{f}\Delta v = \frac{\beta \Delta p_x}{f^2 \rho_0}\,.$$

Since the LEVEL model only computes vertical velocity when it is required, this does not formally present a problem. However, w is computed by integrating horizontal divergence downwards from the surface. The nondivergence in the fluid column will imply that w at the base of the fluid (evaluated at a temperature point) is nonzero; yet the code assumes it to be zero for numerical reasons. Since Δp is related, with a uniform sign, to its surface value, the vertical integration contains no cancelling.

Thus the advection of heat and salt in the lowest fluid layer is formally incorrect by this method, since the lowest box has a divergent flow. A solution would be, following COOPER and HAINES (1996), to remove the smallest barotropic flow field which made the fluid column nondivergent (i.e., solving for an effective barotropic streamfunction). This was not done in the assimilation reported here.

The size of the effect can be estimated from the heat budget of the lowest grid box: the error in this box is of form

$$\frac{\partial}{\partial t}\int_{grid\,box} T\,dz = T\Delta w \sim T\frac{\beta}{f}\Delta v D$$

where D is the scale depth for the correlation coefficients. Taking Δv=0.01 m s^{-1} and D=1000 m, we find $\Delta w = 10^{-6}$ m s^{-1} With $T = 3$°C, this gives a column-integrated error in heat flux of

$$\frac{\partial}{\partial t}\rho_0 c_P \int_{-H}^{0} T\,dz \sim \rho_0 c_P \Delta w T \sim 12\,\mathrm{W m^{-2}}$$

and an error in the local temperature derivative of

$$T_t \sim \frac{\Delta w}{\Delta z} T \sim 1.5\,\times 10^{-8}\,{}^{\circ}\mathrm{C\,s^{-1}}$$

Such values occur on one (half-hour) time step every assimilation cycle (every 5 days) so that these errors are decreased by 1 / (5 × 24) = 1/120. In addition, the applied forcing will change sign as surface lows and highs pass the area of concern, so that large cancellation will occur. An estimate of the overestimation can be seen from the observation that bottom layer temperatures vary by only of order 0.01°C during the calculation. Thus, the neglect of the divergence is only a small effect, provided that assimilation occurs only rarely in the time evolution of the model.

10.4.4 Simultaneous Assimilation of SSH and SST

The assimilation of altimeter SSH residuals can well lead to a more realistic representation of individual eddies, and also of frontal positions, which are often associated with isopycnal outcropping. By moving outcropping positions into regions with distinct atmospheric forcing, water mass characteristics may change during the assimilation. Due to the property of all assimilation schemes presented above to conserve temperature and salinity on isopycnal surfaces, any newly formed water mass characteristics will be preserved after subduction.

Changes in the model hydrography have indeed been observed in test assimilation experiments performed at IfM Kiel. However, to what extent these changes are due to changes in the thermocline ventilation, or to subsurface water mass rearrangement generated by changes in the eddy field, has not yet been examined in detail. The latter process is expected to be essentially adiabatic, while the former will lead to non-adiabatic changes in the $T - S$ relation.

In the CME model, and also in the DYNAMO assimilation experiment, thermohaline surface forcing is derived from climatological data. To possibly improve the T-S characteristics of newly subducted water masses, it seemed worthwhile to investigate the feasibility of supporting altimetric data assimilation by simultaneously assimilating synoptic SSTs. Such surface temperatures are now readily available.

Tests of simultaneous assimilation of SSH and SST were made during the DYNAMO project, and reported in the 1995 annual report. Major problems arose because the model climatology is not fully consistent with real observations of absolute SST.

From the results of these experiments, we concluded that simple local SST assimilation schemes are unlikely to lead to a more realistic (and self-consistent!) description of the North Atlantic Ocean as long as major model deficiencies like a wrong Gulf Stream separation coincide with large "clouded" regions. On the other hand, assimilating SST anomalies, e.g. relative to the seasonal cycle, may have some potential once improved declouding algorithms which retain a larger portion of surface temperature fluctuations are formulated.

10.5 The effect of the assimilation: intercomparisons

10.5.1 Sea surface height

Sea surface variability is directly assimilated by the DYNAMO North Atlantic run, so that the location and magnitude of SSH variation should be much better reproduced following assimilation. There is little effect, of course, on the mean SSH (not shown), since the mean is taken, by necessity, from the unassimilated model; the changes induced are small, and occur mainly in the western boundary current system and in coastal regions.

Fig. 10.1 shows the rms sea surface variability from altimetry, the assimilation, and the control run. The overall levels of both assimilation and control are similar, with high values in the Gulf Stream, the North Atlantic Current, the North Sea (an area of no altimetric information), the Gulf of Mexico, and at about 8°N, 45°W. (This distribution is qualitatively similar to that found for the coarser CME run by OSCHLIES and WILLEBRAND, 1996). Maximum values in mid-ocean are less than 25 cm. The difference between the two fields lies mainly in the positioning of the North Atlantic Current. In the control run, the variability associated with the Gulf Stream extension lies on an ENE line until 30°W, before turning northwards. The assimilation, however, has removed the latter high area of variability, replacing it with a northwards extension at around 30°W.

The altimetric variability differs substantially from the control run. The rms SSH variability from TOPEX/Poseidon is similar to that from Geosat (cf., e.g, STAMMER and BÖNING, 1992). The largest variability is in the Gulf Stream extension between around 65° and 45°W; at the latter longitude the area of strong variability becomes oriented N–S. Other areas of the ocean demonstrate, in the main, higher levels of variability than either computer run. The area of strong variability at 8°N, 45°W in the computer simulations is 33% weaker in the data.

The act of assimilating has achieved the strong reduction in (erroneous) SSH variability at 30°W, and also off Newfoundland. There is evidence of increased background levels of SSH variability in the assimilated run, although levels stay much below those observed. These latter statements apply, of course, to almost all assimilation efforts to date. Thus the assimilation experiment has achieved some success in adjusting erroneous surface variability towards observations.

10.5.2 Eddy Kinetic Energy

Eddy-permitting models are known to possess levels of eddy kinetic energy (EKE) which are too low compared with observations, and it is believed that assimilation of surface features

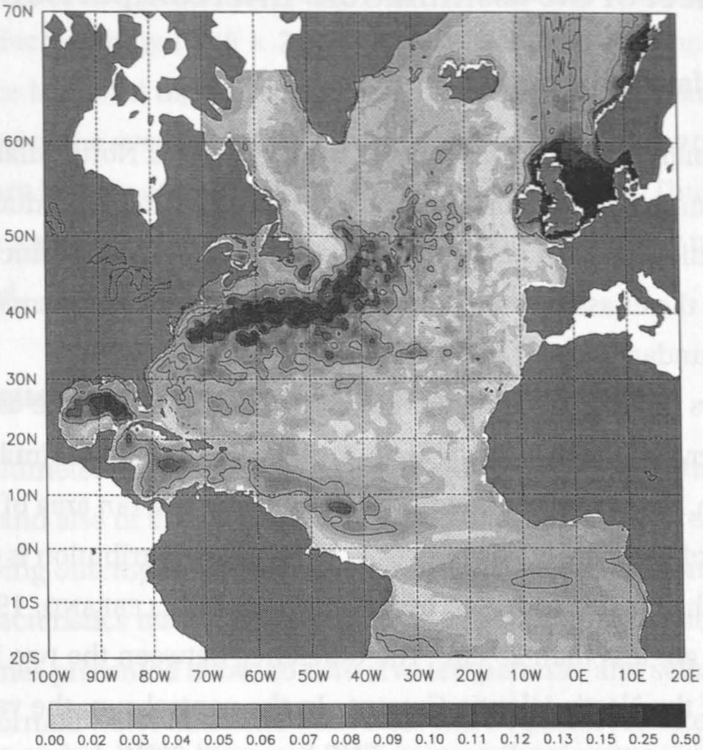
70N
60N
50N
40N
30N
20N
10N
0N
10S
20S
100W 90W 80W 70W 60W 50W 40W 30W 20W 10W 0E 10E 20E
0.00 0.02 0.03 0.04 0.05 0.06 0.07 0.08 0.09 0.10 0.11 0.12 0.13 0.15 0.25 0.50

(a) Assimilation run

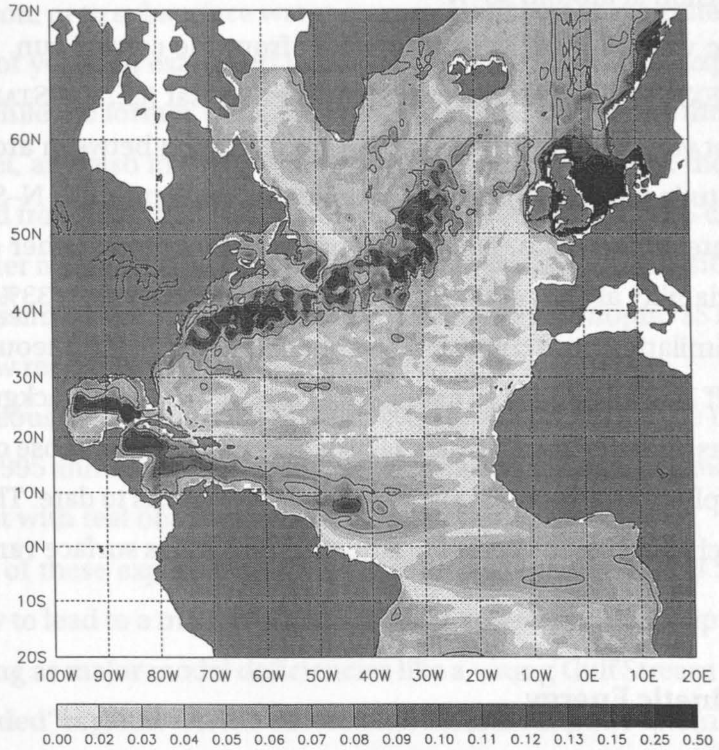
70N
60N
50N
40N
30N
20N
10N
0N
10S
20S
100W 90W 80W 70W 60W 50W 40W 30W 20W 10W 0E 10E 20E
0.00 0.02 0.03 0.04 0.05 0.06 0.07 0.08 0.09 0.10 0.11 0.12 0.13 0.15 0.25 0.50

(b) Reference run

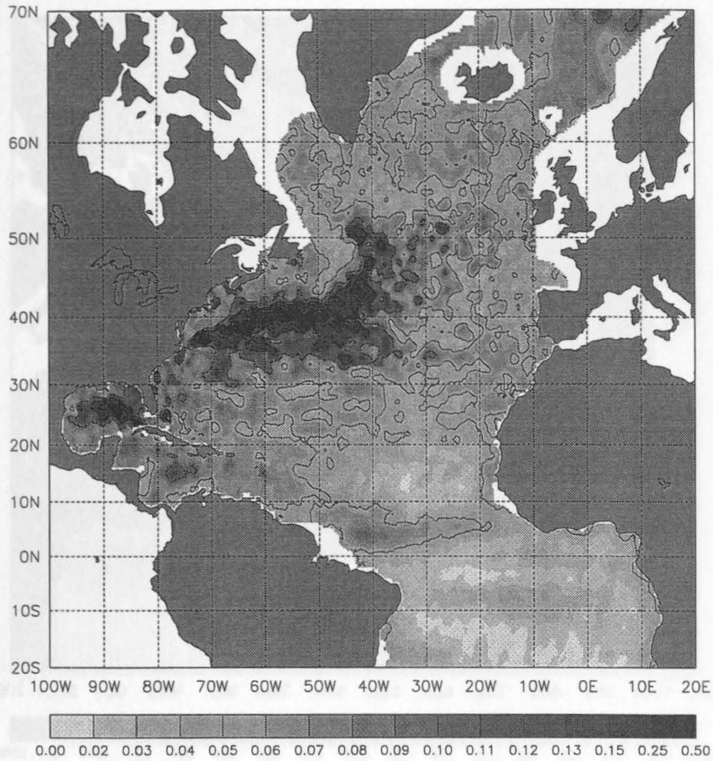

(c) Mapped ERS-1–TOPEX/Poseidon data

Figure 10.1: Annual rms surface height variability in m.

will increase the energy levels in the simulation. Very few direct observations exist to evaluate this belief; these will be used below.

Fig. 10.2 shows the EKE of the assimilated and control runs at 92 m, and estimates of surface geostrophic EKE from TOPEX/Poseidon. The pictures are qualitatively similar to those for rms sea-surface variability (suggesting a preferred geostrophic length scale for the mesoscale features). The control shows similar features to those discussed for the mean circulation. The only areas of high eddy energy are the Gulf Stream, and its extension (which reaches to 30°W), the Denmark Strait overflow, the equatorial current system, and the western boundary flow at low latitudes up to, and including, the Gulf of Mexico – although, interestingly, eddy levels are reduced in the latter region in the assimilation compared with the control run. Elsewhere values of EKE remain uniformly low. Although differing in detail, this picture is qualitatively similar to the results of OSCHLIES and WILLEBRAND (1996) with slightly coarser resolution. The areas of strong and weak EKE in the control agree with the equivalent TOPEX/Poseidon computation. However, the EKE remains underestimated by the control

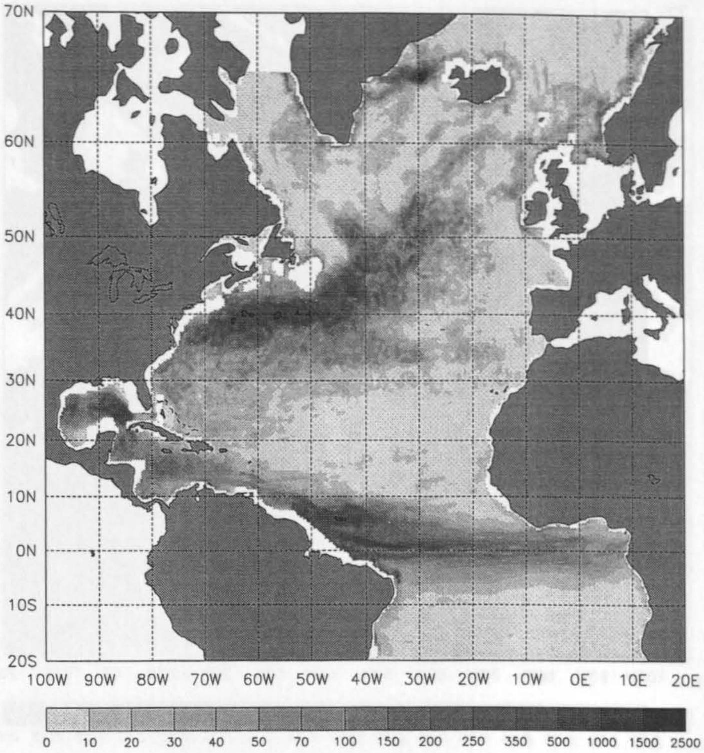
70N
60N
50N
40N
30N
20N
10N
0N
10S
20S
100W 90W 80W 70W 60W 50W 40W 30W 20W 10W 0E 10E 20E
0 10 20 30 40 50 70 100 150 200 250 350 500 1000 1500 2500

(a) EKE for the assimilation run

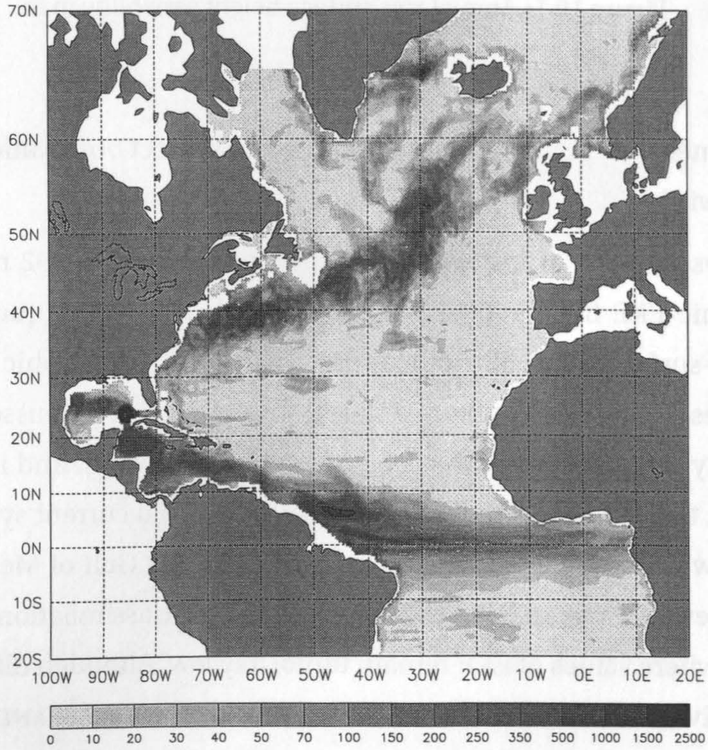
70N
60N
50N
40N
30N
20N
10N
0N
10S
20S
100W 90W 80W 70W 60W 50W 40W 30W 20W 10W 0E 10E 20E
0 10 20 30 40 50 70 100 150 200 250 350 500 1000 1500 2500

(b) EKE for the reference run

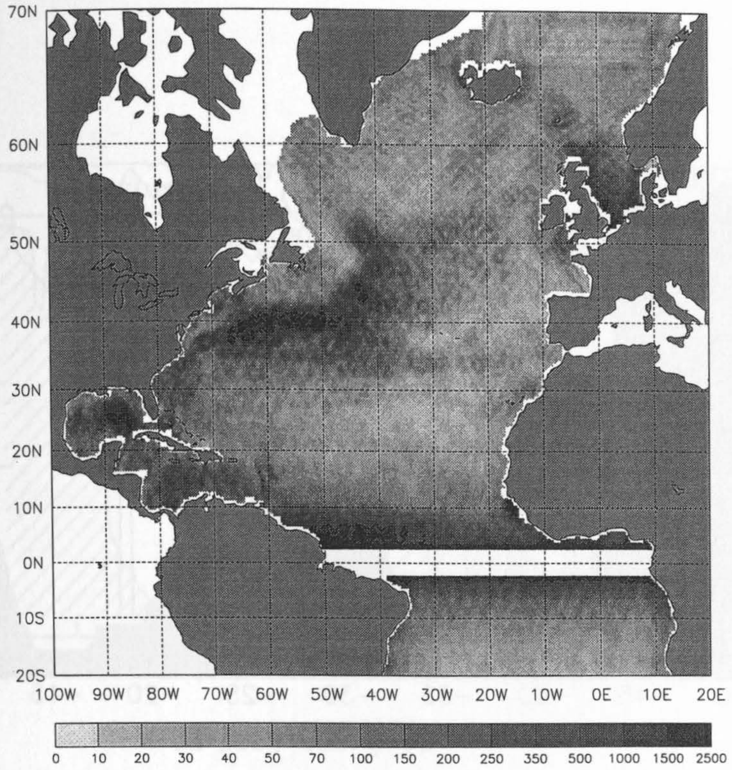
70N
60N
50N
40N
30N
20N
10N
0N
10S
20S
100W
90W
80W
70W
60W
50W
40W
30W
20W
10W
0E
10E
20E
0
10
20
30
40
50
70
100
150
200
250
350
500
1000
1500
2500

(c) Geostrophic EKE of the mapped ERS-1–TOPEX/Poseidon

Figure 10.2: Eddy kinetic energy at 92m in cm^2/s^2 for the assimilation run and the reference run, and the geostrophically derived EKE of the mapped ERS-1–Topex/Poseidon data.

run in both strong EKE regions and, more importantly, in the weak EKE regions.

Assimilation has two main effects on the simulation. First, it *removes* EKE in the Gulf Stream extension east of 40°W, in agreement with observations. Instead, the area of high EKE becomes more diffuse beyond this point, and develops a northward extension. However, the increase by a factor of 5 in the EKE near Europe demonstrates that assimilation can improve aspects of variability away from active eddy regions such as the Gulf Stream. Second, it *increases* eddy activity in regions south and east of the Gulf Stream, towards observed levels of energy. In addition, EKE levels are strongly reduced along the north coast of S. America, which may be produced by a mismatch of phase speeds between observed and modelled eddies in this region.

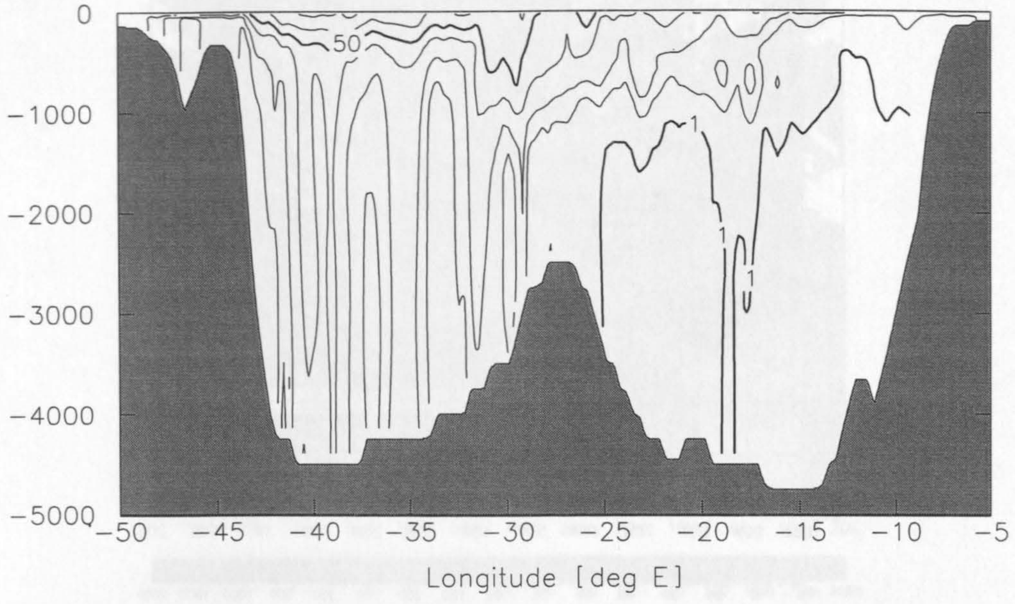

(a) Assimilation run

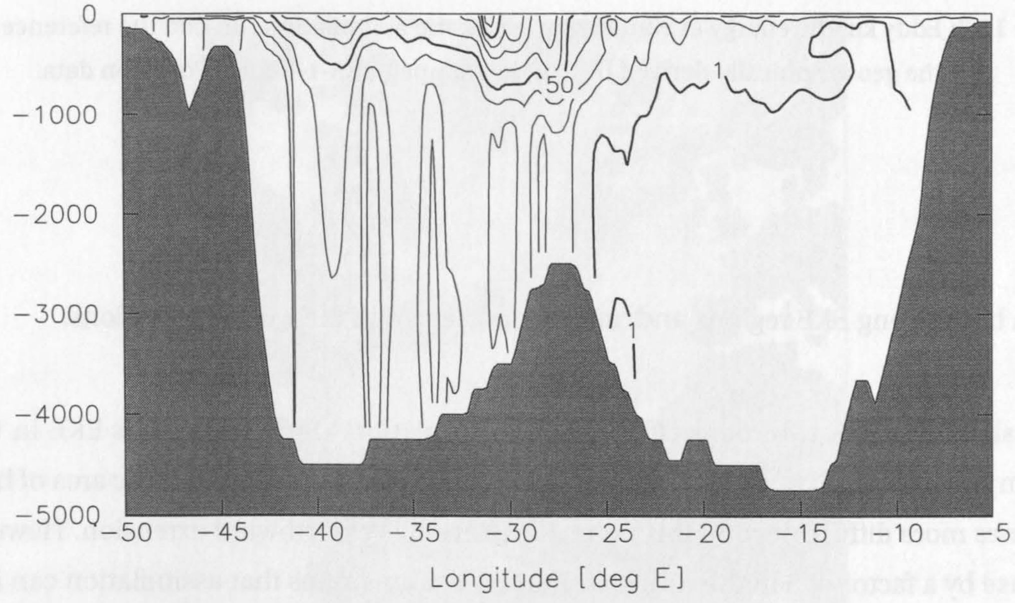

(b) Reference run

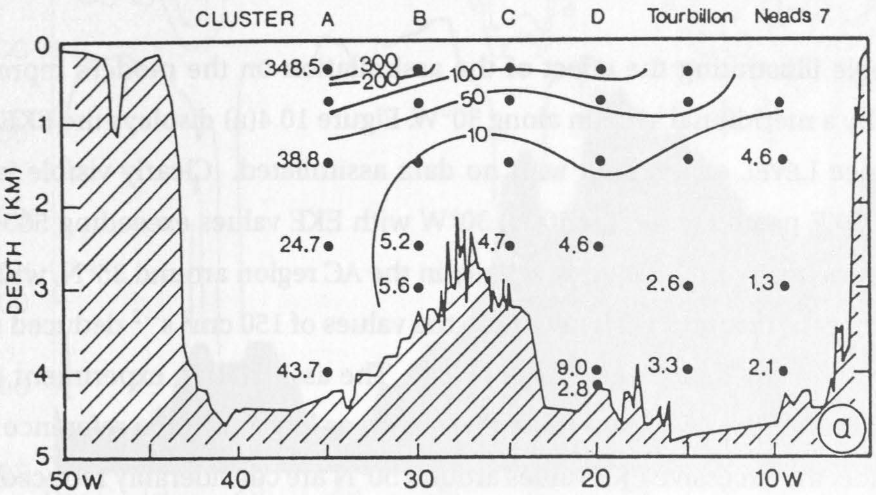

(c) TOURBILLON section

Figure 10.3: Zonal section of eddy kinetic energy (in cm^2/s^2) along 48°N for the assimilation run, the reference experiment and the TOURBILLON section, from DE VERDIÈRE et al. (1989).

Tourbillon

Having so far concentrated on eddy variability at the ocean surface, we now examine to what extent the assimilated surface information can penetrate into the ocean interior. As an example, a zonal section of EKE at 48°N is presented in Figure 10.3, together with the TOURBILLON and TOPOGULF mooring results of COLIN DE VERDIÉRE et al. (1989).

The reference experiment without assimilation of altimetric data (Fig. 10.3(a)) shows a maximum of EKE right over the Mid-Atlantic Ridge (MAR) extending down from the surface to about 1000 m depth. Such a maximum is not present in the Tourbillon data (Fig. 10.3) which show a steady eastward decline of EKE. As discussed above, the assimilation of altimeter data can efficiently reduce the model's overestimated surface EKE in this region. Figure 10.3(b) shows that this reduction of EKE also affects the entire water column above the MAR. The assimilation further leads to a general increase of EKE in the near-Europe basin, yielding a picture much more consistent with the observed EKE distribution. A noteworthy feature of the EKE distribution of both the assimilation as well as of the control experiment is that steps in the topography are often associated with local EKE minima in the entire water column. In the LEVEL model topographic slopes seem to suppress eddy variability.

30°W section

A final example illustrating the effect of the assimilation on the model's representation of EKE is given by a meridional section along 30°W. Figure 10.4(a) displays the EKE distribution of the reference LEVEL experiment with no data assimilated. Clearly visible is the unrealistically high EKE patch centred at 50°N, 30°W with EKE values exceeding 500 $cm^2\ s^{-2}$. In contrast, there is much too little eddy activity in the AC region around 35°N, with EKE values of about an order of magnitude smaller than the values of 150 $cm^2\ s^{-2}$ deduced from surface drifter observations by KRAUSS and KÄSE (1984). The assimilation experiment (Fig. 10.4(b)) shows EKE values in the AC region more than twice as large as in the reference run. On the other hand side, the excessive EKE values around 50°N are considerably reduced, to less than 200 $cm^2\ s^{-2}$. This is, however, on the low side of EKE values reported by KRAUSS and KÄSE (1984) for this region where the NAC crosses the Mid-Atlantic Ridge.

Both reference experiment and assimilation experiment show multiple EKE maxima in the NAC region about 50°N. This is consistent with the findings of SY et al. (1992) who analysed a number of hydrographic sections and concluded that the NAC crosses the MAR in a number of individual current branches. Only the northernmost branch, associated with the subarctic front, was found to be topographically fixed at the Gibbs Fracture Zone at 52°N, while the remaining current bands varied in number, location, and intensity.

10.5.3 Overall North Atlantic comparison

Water mass distribution

Many aspects of the predicted circulation of the North Atlantic remain almost unaffected by the assimilation process, at least on the large scale, as argued above. The deep temperature and salinity fields are almost identical to their control equivalents. Near-surface temperature fields are also very similar: small areas of change are in the eastern basin, near the African coast, where the wind-induced upwelling has been reduced by assimilation, resulting in slightly higher temperatures. There is a small cooling in some midlatitude areas. Despite changes in path and character of the Gulf Stream, no change is visible in the annual average temperature field along the stream.

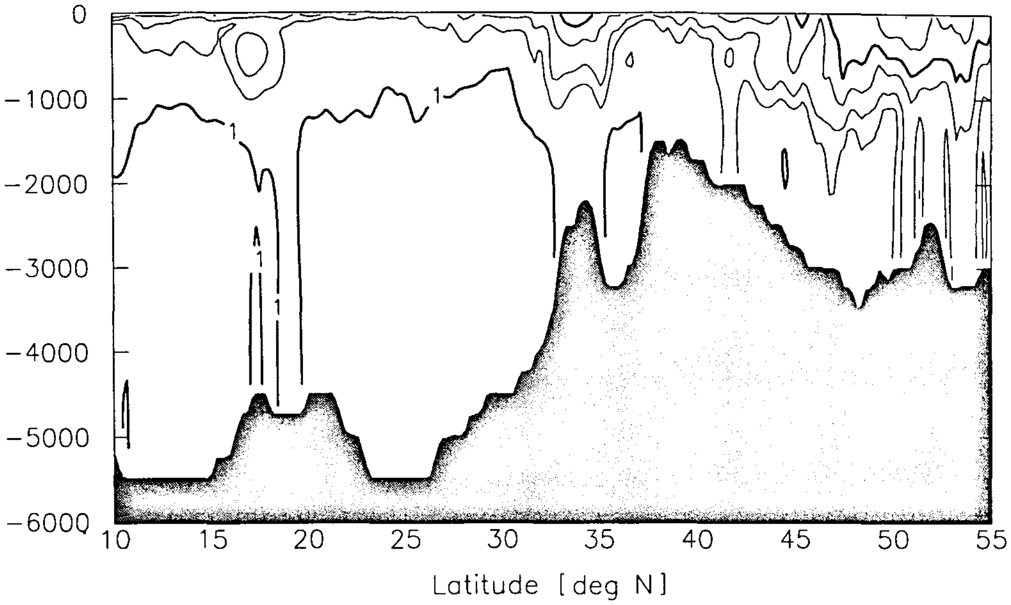

(a) Assimilation run

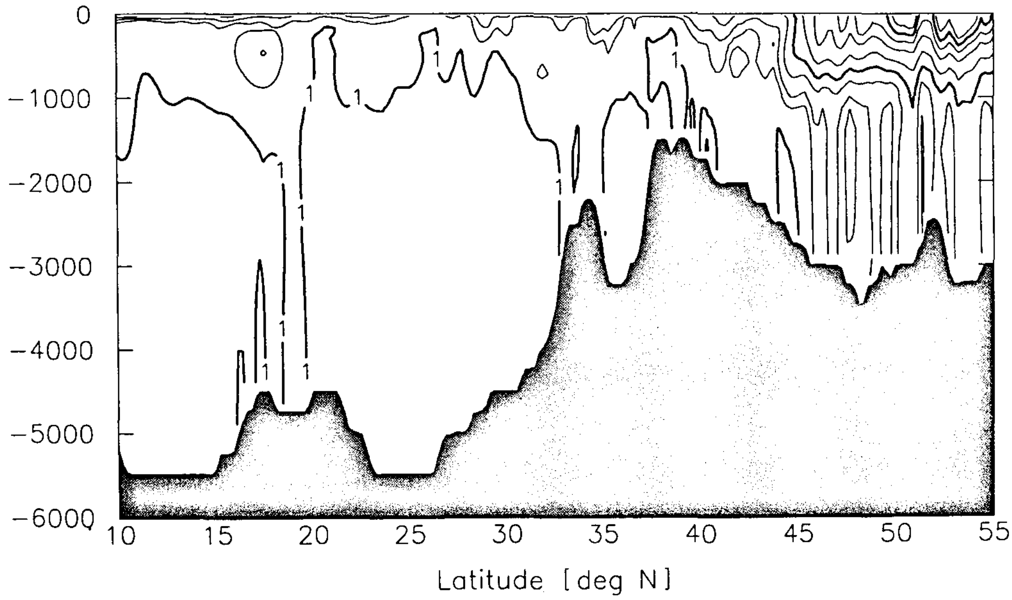

(b) Reference run

Figure 10.4: Meridional section of eddy kinetic energy (in cm^2/s^2) along 30°W.

Salinity, too, remains extremely similar between assimilation and control. There are increases of up to 0.5 psu around 60°W north of the S. American coast, and increases of similar size north of the Gulf Stream (probably reflecting a shift in position, although this is not evident in the temperature field). The assimilated salinity is slightly smaller in the upwelling zone off Africa.

Thus assimilation does not, at first sight, appear to have had a strong effect on the tracer fields during one year of the process, suggesting that a longer period of assimilation will be necessary to modify the water mass structure. We will see below, however, that assimilation has caused a strong reduction in variability of heat and salt in the subtropical gyre compared with the control run.

Mixed layer depth

The mixed layer depth is also largely unchanged. The spatial pattern of this field after assimilation is quantitatively unchanged, with low values (50–100 m) in the subtropics and north of the Gulf Stream surrounding a SW-NE oriented tongue of deeper mixing, between 250 and 500 m, approximately coinciding with the recirculation region west of 30°W. The changes are mostly small, less than 50 m: to the south of this tongue, mixing reaches deeper depths after assimilation. The largest changes are found, predictably, in the Labrador Sea, where the (already incorrect) convective area is modified by the assimilation, with changes in mixed layer depth of around 400 m.

Horizontal temperature-salinity fields

Most changes in near-surface temperature are less than 0.25°C, with larger (warming) changes in the Gulf Stream and cooling in the Iceland-Faeroes area, both by about 1°C. The effect is more marked at 92 m – although the control and assimilation fields remain visually very similar – with the assimilation 1.5 C cooler in the subtropics, up to 2°C cooler in the Iceland-Faeroes area, and warmer only along the Gulf Stream. The reason for the larger changes at depth are unclear.

Salinity resembles Levitus near-surface, with changes between control and assimilation very small save in the Gulf Stream, where the assimilation is up to 0.5 psu saltier than the control. The distribution of changes is almost identical at 92 m. Thus the temperature field responds slightly more strongly to assimilation than does salinity.

Velocity field

The time mean velocity fields, also, are not strongly modified by assimilation. Both vertically-averaged streamfunction and horizontal vector plots are almost indistinguishable between assimilation and control runs; the latter are shown elsewhere in this report and are not repeated here. In particular, all show the Gulf Stream extension reaching 30°W before turning north. Thus assimilation has correctly reduced eddy activity in this region, but has adjusted the *mean flow* rather less (although the intensity of the strong flow in the Gulf Stream extension is lessened at 45°N, 45°W, by the assimilation). The mean path of the Gulf Stream shows essentially no change (so that assimilation has not adjusted the path after separation), and the structure in the Loop Current and other regions remains unchanged also.

This is not surprising, even there are large-scale changes in the momentum flux divergence terms. At 40°W, for example, in the control run the meridional divergence was concentrated around 47°N, extending to depths of 300 m, with values of order 10^{-5} cm s^{-2}. The SSH at this longitude is highly variable, of course, so that the assimilated divergence had noticeable values between 40 and 50°N of the same order. Such values are orders of magnitude smaller than the Coriolis term fu. Thus direct modification to geostrophy will be small, even in the Gulf Stream extension. (Changes to the potential vorticity budget have not been computed.)

Overturning streamfunction

Assimilation has little effect, as we might expect, on the gyre-scale thermohaline circulation, as shown by the overturning streamfunction. This takes almost identical values for the assimilated case and the control case, with maximum changes of 2 Sv at 36°N and 65°N. There is an overall (small) change in that the assimilation run has a larger streamfunction in the top 1000 m south of 40°N, and smaller below; north of 40°N the position is reversed. The main differences are a larger cell of 18 Sv circulation (the largest value of streamfunction, at 40–50°N), and that the return cell has streamlines approximately 100 m deeper in the assimilated case. This again suggests that assimilation on a one-year time scale is too short to modify water mass characteristics widely.

Horizontal streamfunction

The depth-integrated streamfunction changes by assimilation only as indicated above: the path of the Gulf Stream extension is altered towards the west. Otherwise, changes remain less than 5 Sv everywhere.

10.5.4 Surface heating and freshening

Assimilation makes changes to temperature and salinity (but not water mass structure) in the top 1000 m. These changes can potentially modify the net surface heat and salt flux; thus a good test of whether the assimilation is performing well is to examine annual surface fluxes. Those for the control run are similar to those elsewhere in the report, and will not be repeated here. Fig. 10.5 shows the difference in annual surface heating between assimilation and control runs. Heat flux changes are less than 10° W m^{-2} everywhere save three regions. In the Gulf Stream and its extension, and in the Labrador Sea, the surface heat flux is *less* in the assimilation than in the control by as much as 200 W m^{-2}. In the Caribbean, the surface heat flux in the assimilation is larger than in the control by more than 25 W m^{-2}

A fairly similar picture holds for freshwater flux (not shown). Both control and assimilation runs possess ranges of at least 3 m/y Their difference is somewhat noisy – rather more so than for temperature – but the majority of the North Atlantic has differences under 10 cm/y. Up to 0.5 m/y is visible in a band at 30°N, and in the Caribbean and Gulf of Mexico. Again, the largest differences (negative) of at least 3 m/y are found in the area of adjustment of the Gulf Stream and extension positions.

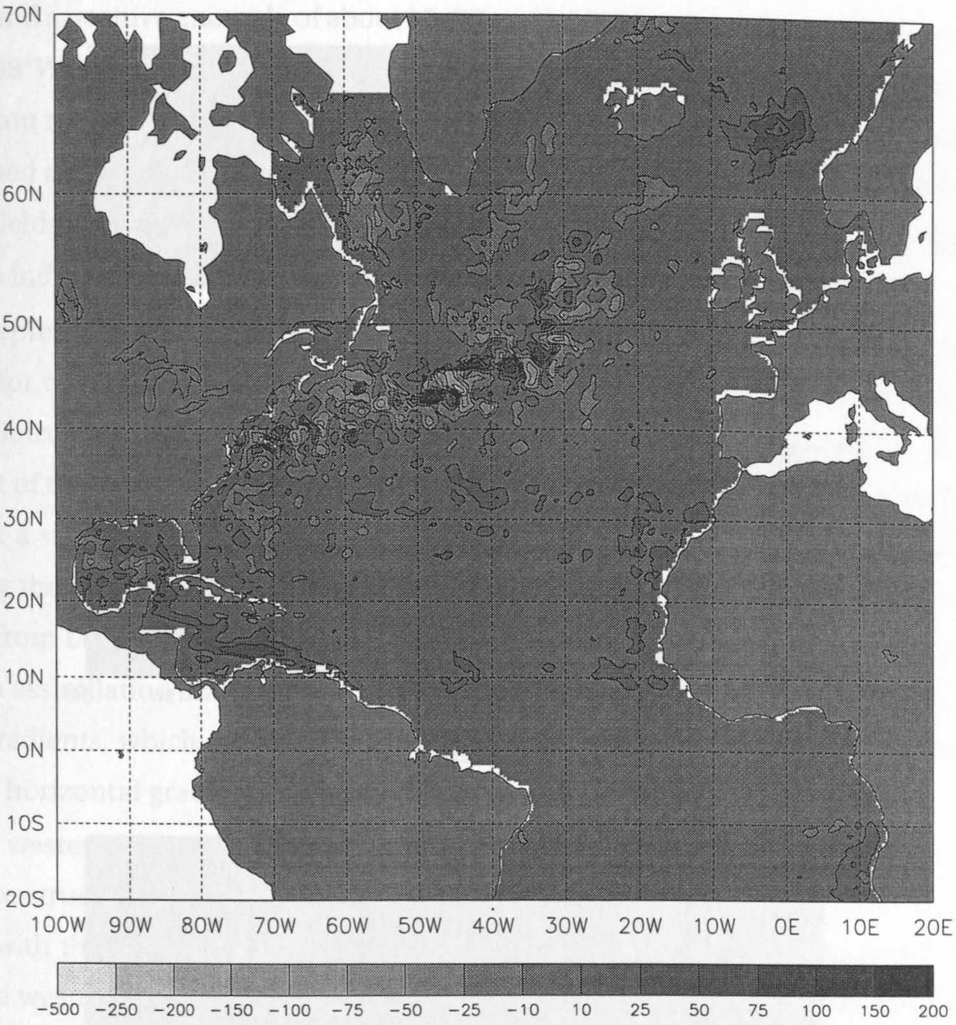
70N
60N
50N
40N
30N
20N
10N
0N
10S
20S
100W
90W
80W
70W
60W
50W
40W
30W
20W
10W
0E
10E
20E
-500
-250
-200
-150
-100
-75
-50
-25
-10
10
25
50
75
100
150
200

Figure 10.5: Changes in the surface heat flux (in W/m^2) due to the assimilation: assimilation minus reference run.

10.5.5 Comparison with observed section

The object of assimilation is to improve the representation of the entire ocean state, not just the sea surface. Accordingly, it is important to analyse the response of the models in the ocean interior, and to compare where possible with observations. We here discuss the comparison with a WOCE North Atlantic cruise.

In July, 1993, the FS Gauss occupied a section between 42 and 49°N, 50 and 10°W between July 7 and July 25, 1993. The section was oriented approximately SE between 50 and 45°W, then NE east of 45°W. During the survey, several surface features crossed the track of the section. The most intense were a negative anomaly of about 20 cm, approximately stationary

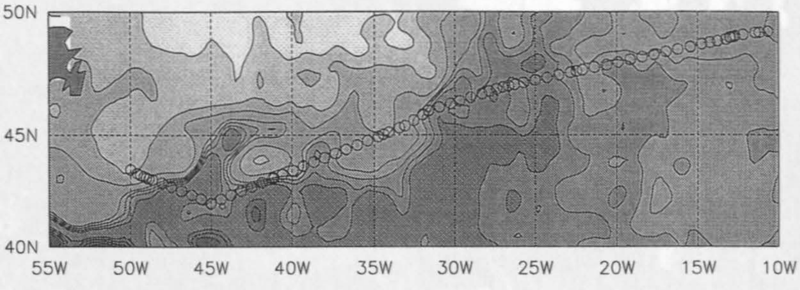
50N
45N
40N
55W
50W
45W
40W
35W
30W
25W
20W
15W
10W

(a) Assimilation run

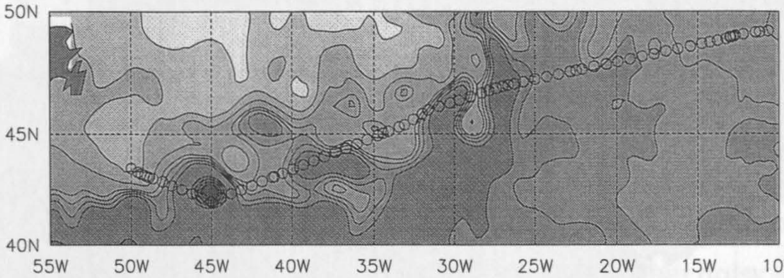
50N
45N
40N
55W
50W
45W
40W
35W
30W
25W
20W
15W
10W

(b) Reference run

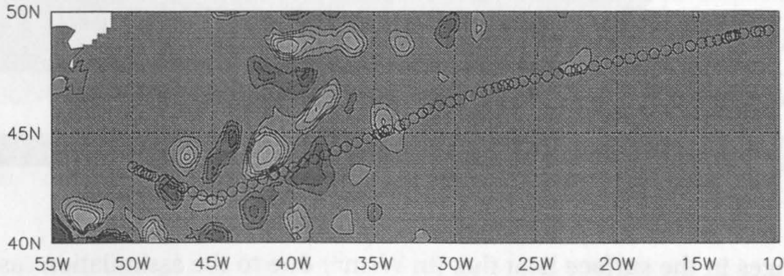
50N
45N
40N
55W
50W
45W
40W
35W
30W
25W
20W
15W
10W

(c) SSH anomaly as observed by ERS-1–TOPEX/Poseidon

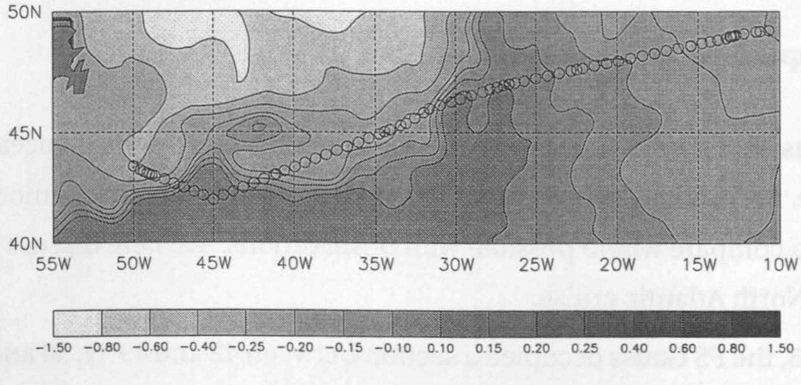
50N
45N
40N
55W
50W
45W
40W
35W
30W
25W
20W
15W
10W
-1.50
-0.80
-0.60
-0.40
-0.25
-0.20
-0.15
-0.10
0.10
0.15
0.20
0.25
0.40
0.60
0.80
1.50

(d) Model climatological mean SSH

Figure 10.6: Sea surface height (in cm) over the region extending from 55°W to 10°W and 40°N to 50°N . The hydrographic stations occupied by FS Gauss are indicated by circles.

at 34°W, and a positive anomaly of about 15–20 cm, which moved northwards across the track at about 39°W during the month. The control run showed no such specific features, while the assimilation run reproduced the features well. This is illustrated in Figure 10.6 which shows the mapped altimetric signal together with the (model) climatological mean SSH, as well as the SSH fields of control and assimilation experiment, respectively. Stations occupied by FS Gauss are indicated by circles.

The representation of thermal and salinity structure along these sections is shown in Fig. 10.7 for observations, control, assimilation, together with (observations – control) and (observations – assimilation). (Note the much larger east-west distance scale in the right-hand part of the section.) Observations and both models possess the same overall T-S structure, with a strong thermocline between 500 and 1000 m, and a lens of warm saline water occupying the top 500 m between 40 and 48°W[3]. This is to be expected, since the models are initiated from Levitus data which represents the large-scale water mass structure well. However, both assimilation and control runs do not possess sufficiently sharp thermal and haline vertical gradients, which are very sensitive to details of vertical mixing. Nor do they possess the sharp horizontal gradients associated with frontal features.

In the western part of the section, there is little evidence that assimilation has modified subsurface structure at all. Subsurface temperature errors are as much as 8°C too warm, associated with the large-scale misplacement of the Gulf Stream extension. At 45°W (eastern end of the western part) temperatures at 500–750 m are over 2° too cold in the assimilation run, compared with 2° too warm in the control run. Similarly, the salinities are up to 0.4 psu too saline (western side) or too fresh (eastern side). The general upward shift of the thermocline at the eastern side in the assimilation run is associated with the negative altimetric SSH anomaly (Fig. 10.6) and the disappearance of the strong cyclonic feature at 42°N, 45°W of the control experiment.

In the eastern part of the section, the observations show evidence of multiple eddy structure, with a cold eddy at 35°W, a warm eddy at about 32°W, and more cold features at 30°, 27° and 23°W. The control run possesses similar features, but much weaker and in different locations. The effects of assimilation are quite strong in this region. The assimilated water mass structure has a strong cold feature at 42°W which is not evident in the data, a correctly placed cold feature at 35°W, and another – correctly sited, but of the wrong strength – at 30°W. Examination of the temperature and salinity differences between observations and simulations shows that assimilation has improved the temperature structure somewhat, especially in the

---

[3] Although the lens extends much too far eastward in the simulations.

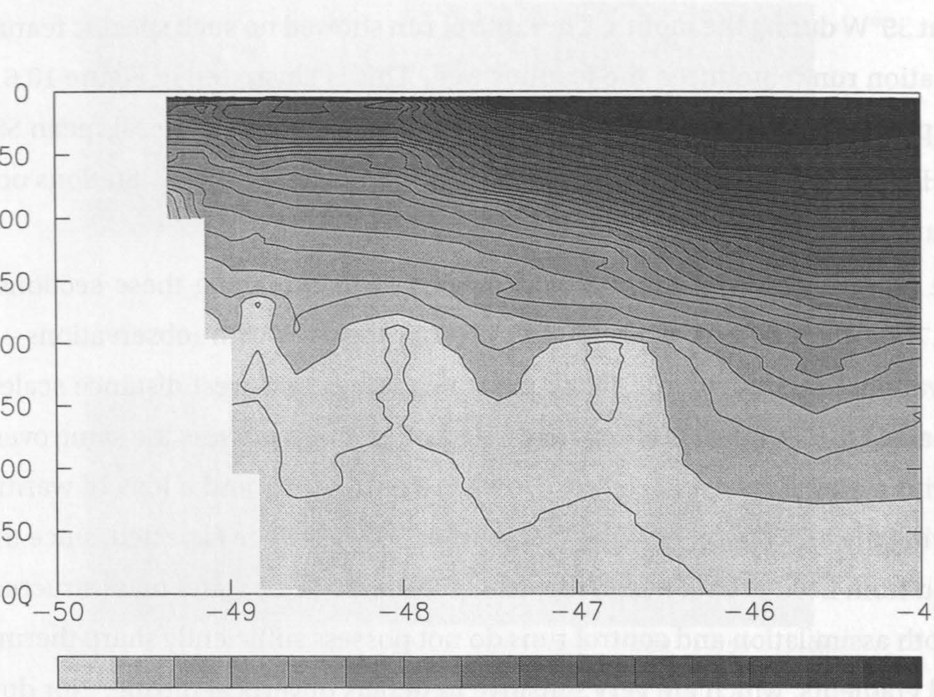

(a) WOCE section: potential temperature (western part)

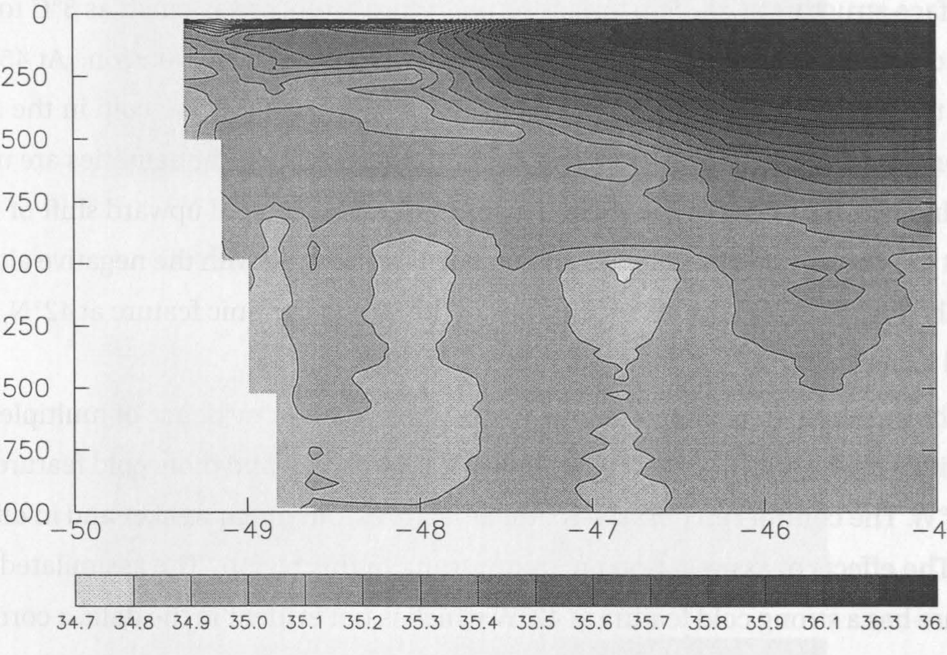

(b) WOCE section: salinity (western part)

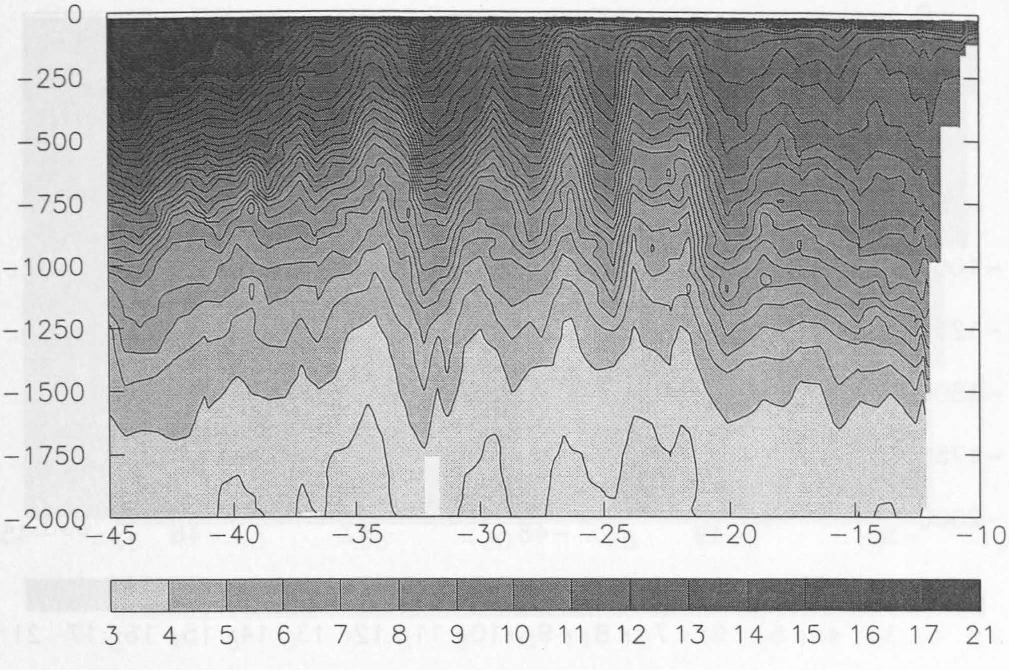

(c) WOCE section: potential temperature (eastern part)

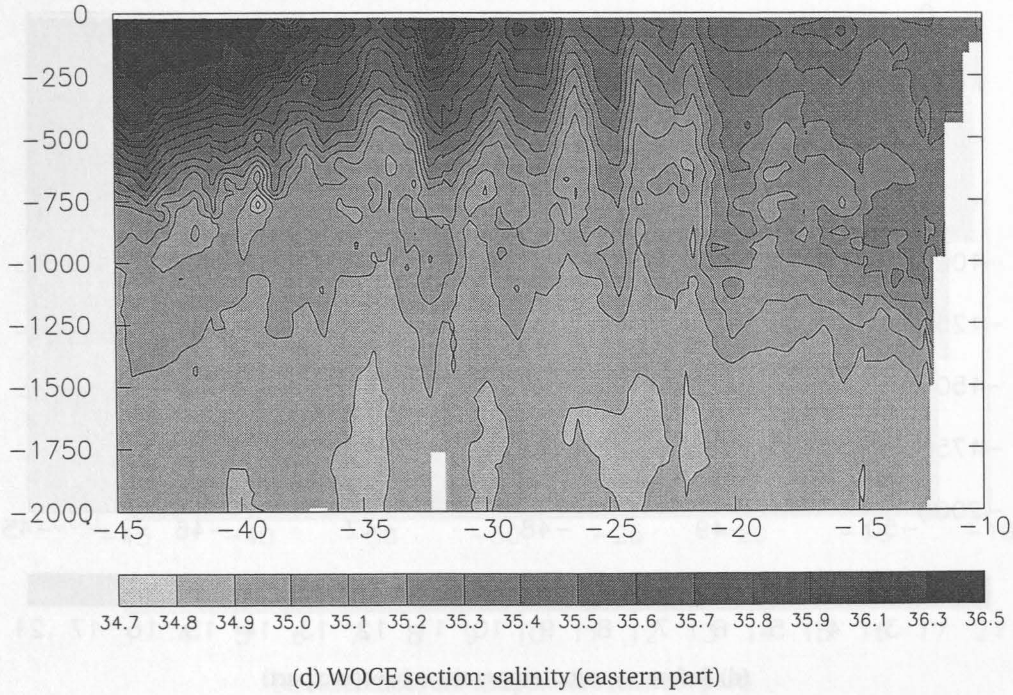

(d) WOCE section: salinity (eastern part)

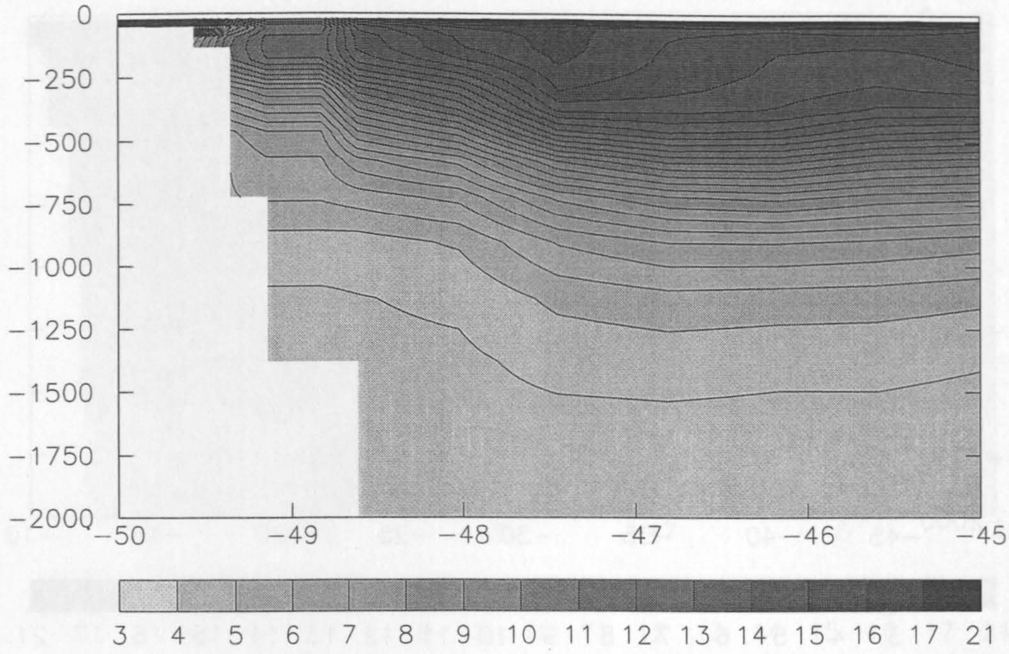

(c) Assimilation run: temperature (western part)

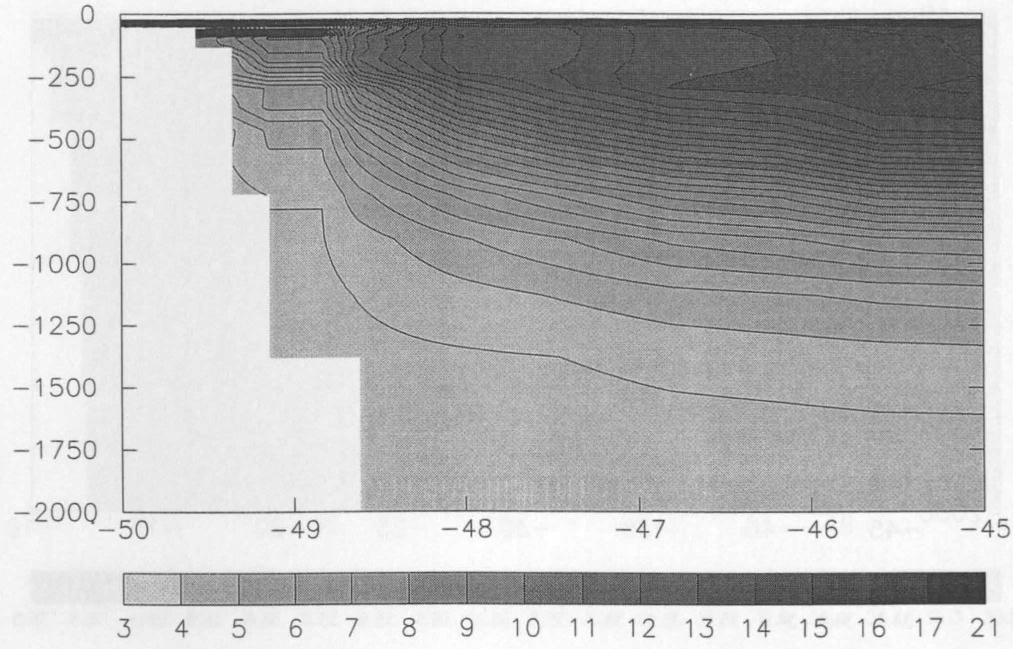

(d) Reference run: temperature (western part)

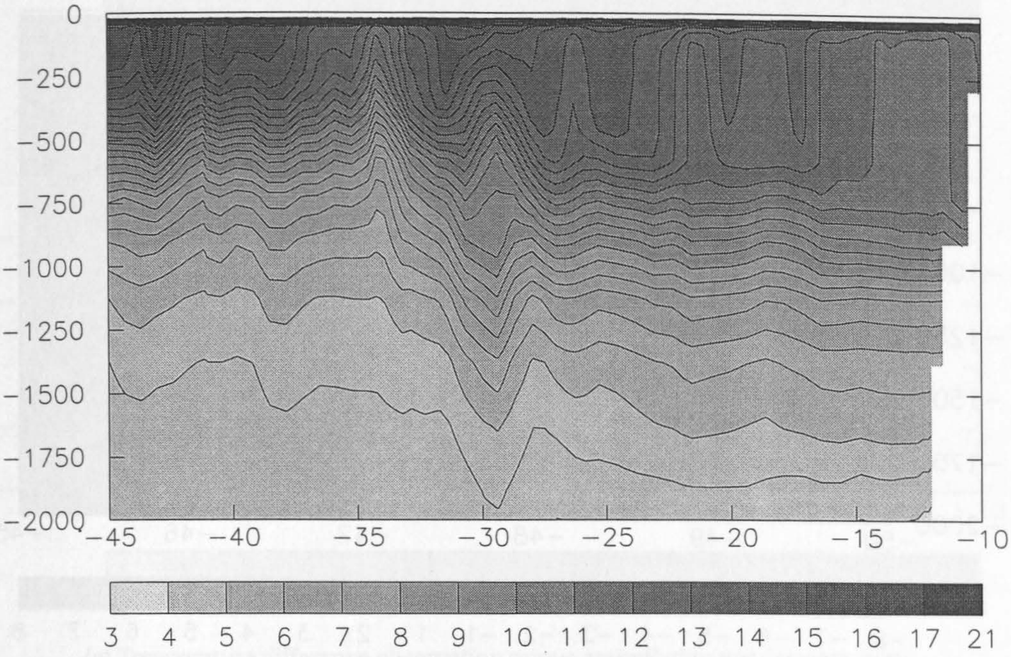

(c) Assimilation run: temperature (eastern part)

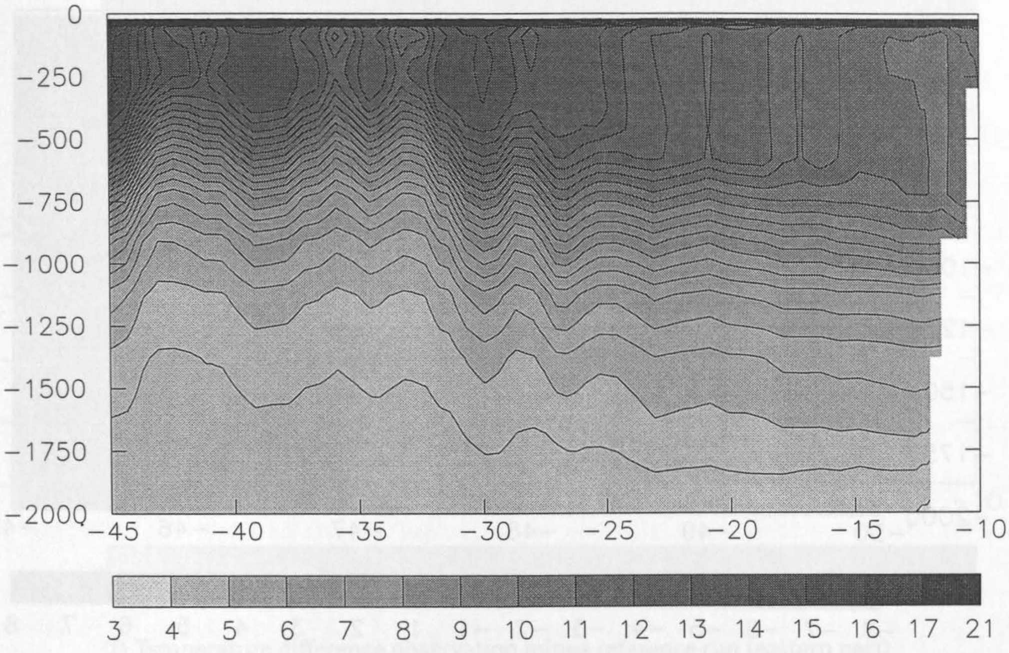

(d) Reference run: temperature (eastern part)

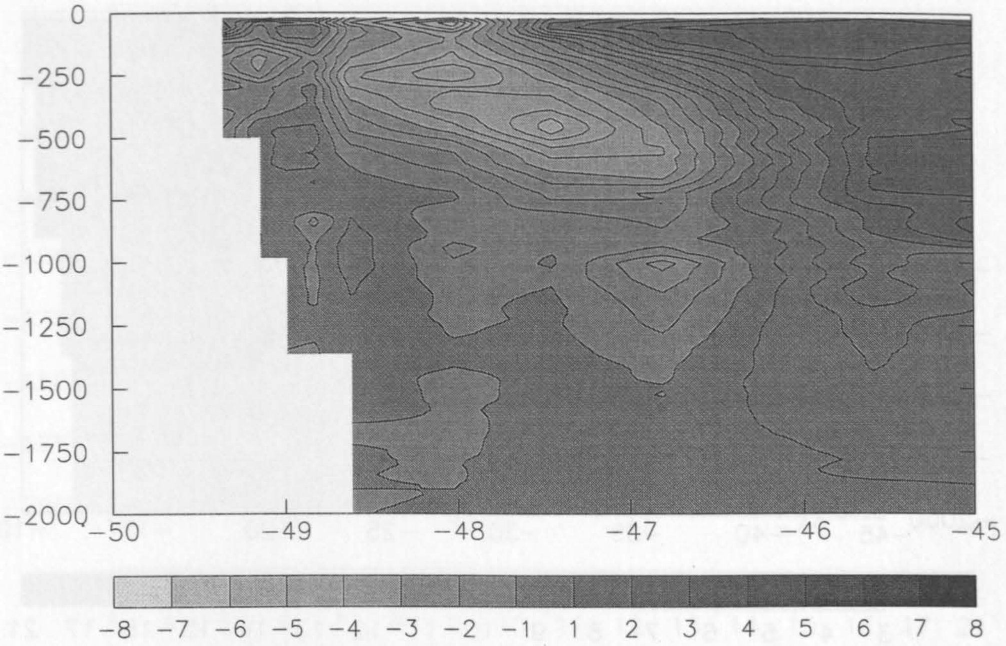

(e) Temperature difference observation minus assimilation run (western part)

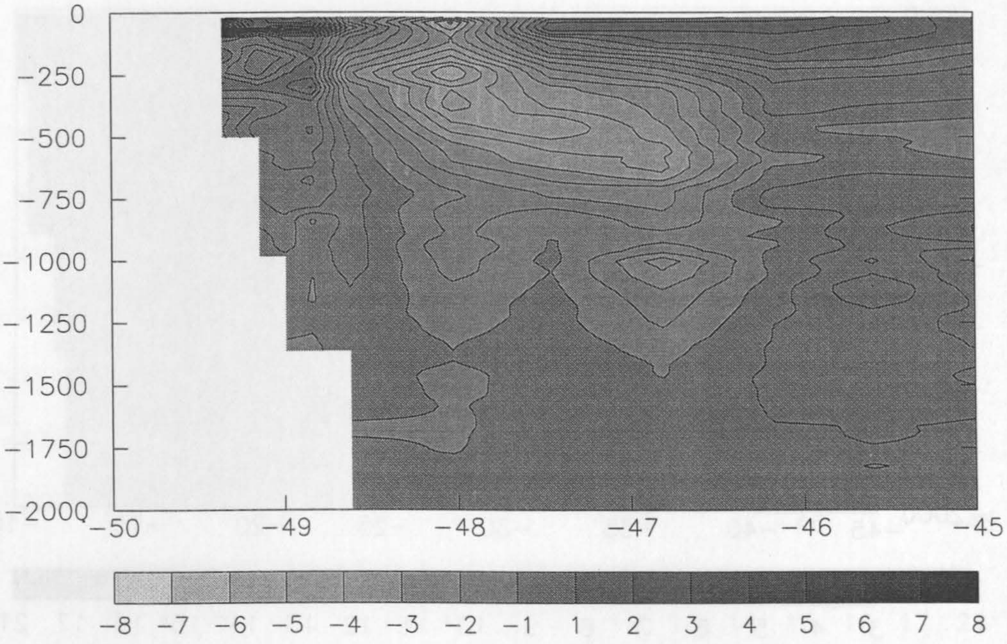

(f) Temperature difference observation minus reference run (western part)

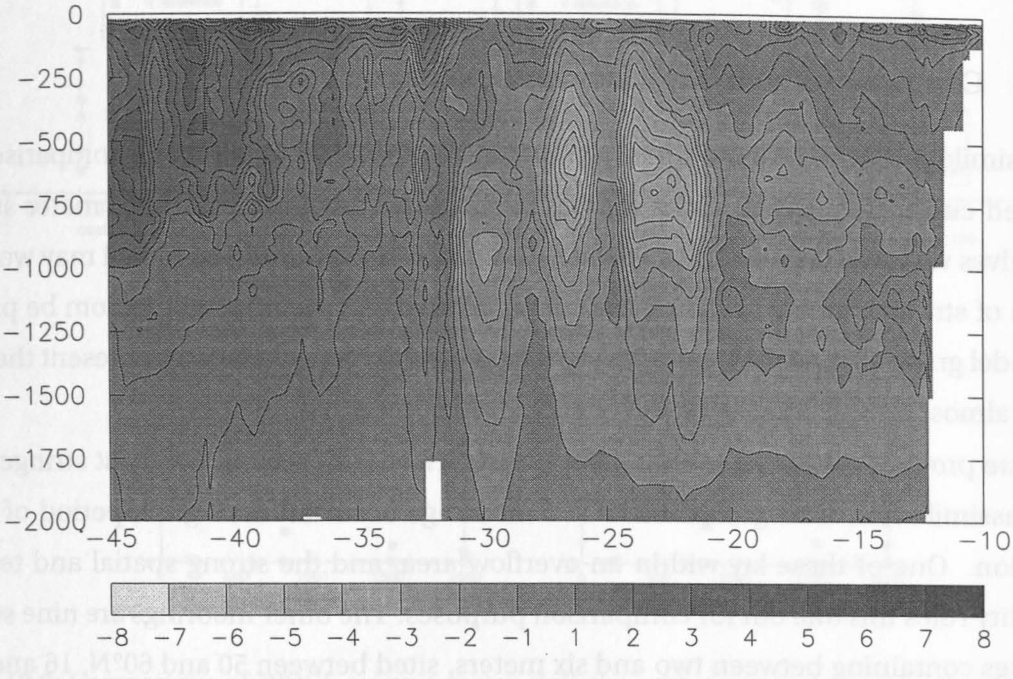

(e) Temperature difference observation minus assimilation run (eastern part)

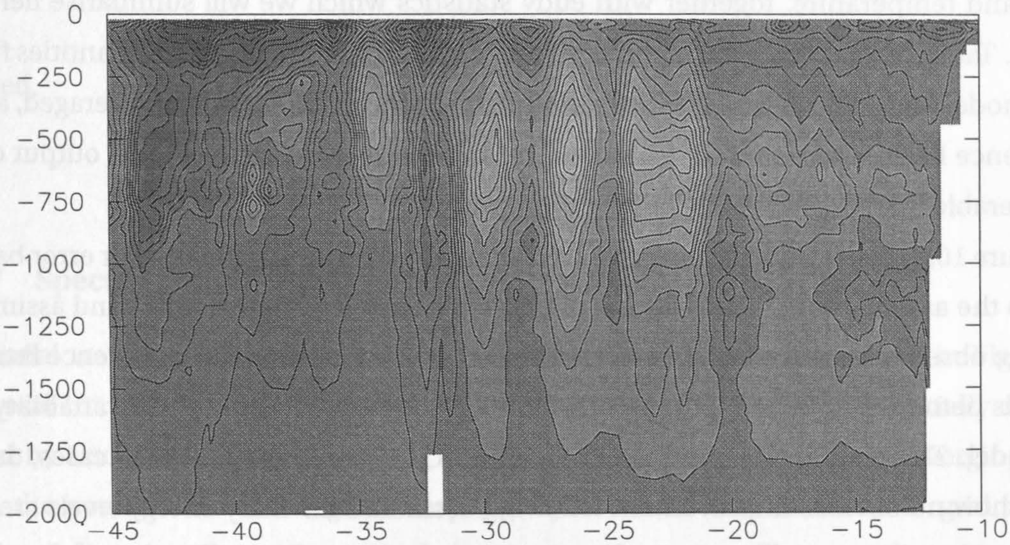

(f) Temperature difference observation minus reference run (eastern part)

Figure 10.7: Hydrographic sections occupied by FS Gauss between July 7 and July 25, 1993.

locations mentioned above, but that severe errors (up to 8°C) remain. The saline structure is represented equally poorly in both control and assimilation, with errors of ±0.4 psu.

10.5.6 Comparison with WOCE current meter statistics

The assimilation primarily modifies currents in the top 1000 m, so that a comparison with observed currents is useful. Such a comparison is far from easy. Current meter statistics themselves vary spatially, so that a specific grid point in the numerical model may well 'miss' an area of strong eddying in the observations. Similarly, a mooring will seldom be precisely at a model grid point, so that averaging within the model is necessary to represent the observation, almost always decreasing the energy level represented.

These provisos notwithstanding, direct comparisons are among the most stringent tests of the assimilation. Two groups of WOCE moorings occurred during the period of the assimilation. One of these lay within an overflow area, and the strong spatial and temporal variability rules this one out for comparison purposes. The other moorings are nine separate moorings containing between two and six meters, sited between 50 and 60°N, 16 and 34°W, at depths ranging from 200 to 3500 m. Inter alia, the summary information provided the time mean and temperature, together with eddy statistics which we will summarise here by $\overline{u'^2}$ and $\overline{v'^2}$. Table 10.1 provides the summary information. Data on the above quantities from the eight model gridpoints forming a 'box' around the observation point were averaged, and 95% confidence limits computed (this process was necessary because the model output displays considerable internal variability between gridpoints).

Figure 10.8 shows a typical example (including the 95% limits; the smaller error bar wings refer to the assimilation). The field u is poorly represented by both control and assimilation, with the observations from the upper two moorings lying outside the confidence limits. The v field is better represented, although this is partly due to the wide spatial variability within the model. The temperature field is as much as 2°C in error at depth. In all cases, the mean fields show no obvious improvement following assimilation. Eddy energy levels are grossly underestimated, especially near-surface; again, assimilation has not improved the situation here.

Table 10.1 shows that these are typical findings. On the whole, mean velocities from the assimilation are closer to observations than in the control run, but not everywhere. Mean temperatures are little changed by the assimilation, and errors are up to 4°C in magnitude. Eddy energies are almost everywhere far too small in both assimilation and control runs, with a tendency towards lower values in assimilation – the opposite tendency to what would be

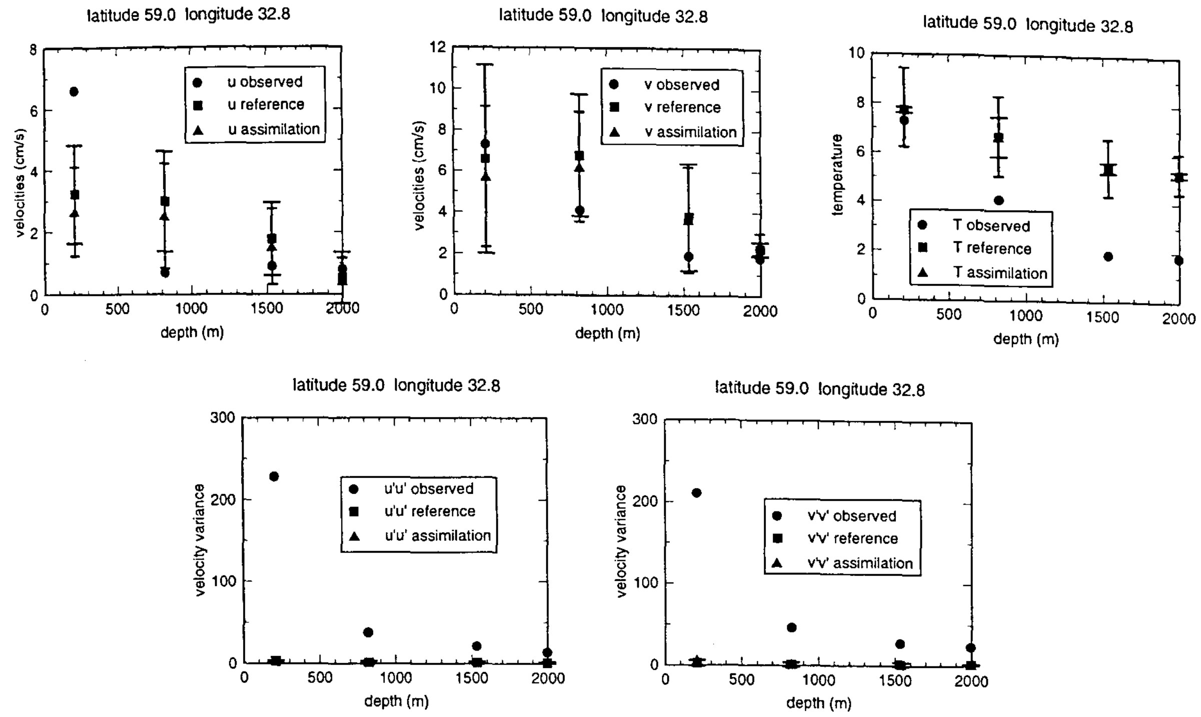

Figure 10.8: Comparison of WOCE current meter statistics with assimilation and reference experiment, respectively.

expected.

10.5.7 Spectra

Meridional wavenumber spectra of the surface height variability are shown in Figure 10.9 for several 10°×10° regions. To ease comparability, these regions were essentially the same as used by OSCHLIES and WILLEBRAND (1996). Due to the meridionally converging grid of LEVEL, the nominal 10°×10° regions vary slightly in size to accommodate 2^n grid points in meridional direction. For each region the spectra were computed by approximating the converging grid with a locally (over the 10°×10° box) equidistant grid.

For all of the four boxes we find that the energy of the mapped ERS-1–TOPEX/Poseidon data for large wavelengths is not significantly different from the older and less accurate GEOSAT data used by OSCHLIES and WILLEBRAND (1996). However, on scales smaller than about 100 km the spectral energy of the mapped ERS-1–TOPEX/Poseidon data exceeds the Geosat data by a factor of about two. With the accuracy of both altimetric data sets being

Position		Bathym.	Depth	u-velocity			v-velocity			Temperature			u'u'			v'v'		
Lat	Long			obs.	cont.	ass.	obs.	cont.	ass.	obs.	cont.	ass.	obs.	cont.	ass.	obs.	cont.	ass.
52.3	-16.3	3510	210	-2.9	-0.62	1.52	-1.3	-2.25	-0.30	10.6	11.38	11.40	313.47	4.12	4.77	176.97	6.88	7.81
52.3	-16.3	3510	510	—	0.55	2.29	—	-0.85	0.92	9.0	11.35	11.22	—	3.54	4.76	—	9.13	7.90
52.3	-16.3	3510	810	—	0.05	1.06	—	-1.49	-0.60	7.4	9.12	8.95	—	2.41	2.81	—	6.24	4.88
52.3	-16.3	3510	2010	—	-2.40	-1.88	—	-4.63	-4.42	3.6	4.34	4.31	—	0.23	0.75	—	0.80	0.74
52.3	-16.3	3510	3010	-.3	-0.03	-0.01	-.2	-0.54	-0.54	2.8	2.90	2.89	19.37	0.06	0.20	36.91	0.26	0.42
52.3	-16.3	3510	3460	-.5	0.15	0.05	-.6	0.13	0.05	2.5	2.67	2.67	38.26	0.06	0.20	12.86	0.16	0.36
59.0	-32.8	2110	209	6.6	3.23	2.66	7.3	6.57	5.71	5.7	7.72	7.83	228.28	2.63	2.95	210.54	2.62	6.56
59.0	-32.8	2110	822	0.7	3.00	2.53	4.1	6.78	6.22	4.0	6.67	6.68	37.69	1.58	1.19	46.50	1.34	2.11
59.0	-32.8	2110	1534	0.9	1.77	1.53	1.9	3.78	3.65	3.5	5.45	5.46	21.26	1.32	1.27	27.15	1.45	1.81
59.0	-32.8	2110	1996	0.8	0.53	0.44	1.8	2.24	2.46	3.3	5.21	5.25	13.77	1.20	1.17	23.69	1.95	2.20
59.1	-34.0	2855	263	-1.7	-4.14	-2.99	10.9	7.32	8.28	7.7	6.75	7.00	214.49	22.79	9.12	253.52	12.49	8.32
59.1	-34.0	2855	876	-.5	-2.30	-1.86	4.7	0.45	1.27	3.6	5.51	5.64	46.86	4.08	2.29	50.89	2.56	3.01
59.1	-34.0	2855	2088	-.6	-0.75	-0.39	2.3	-3.00	-2.38	3.3	4.25	4.28	14.91	2.10	1.96	24.14	1.90	1.64
59.1	-34.0	2855	2551	-.2	0.28	0.54	0.5	-2.20	-1.55	3.0	4.00	4.01	6.70	2.41	2.19	25.15	2.33	1.98
52.4	-16.4	3481	181	-2.5	0.69	2.93	-1.4	-3.26	-2.54	24.9	11.38	11.40	114.83	3.68	5.83	108.79	5.97	12.14
52.4	-16.4	3481	481	—	0.75	3.03	—	-3.59	-2.43	10.3	11.35	11.22	—	3.86	5.55	—	7.61	12.52
52.4	-16.4	3481	781	-1.2	0.01	1.73	-1.1	-3.51	-2.69	8.9	9.12	8.95	65.12	1.79	2.53	63.85	3.76	5.84
52.4	-16.4	3481	1981	-2.2	-1.40	-0.71	-.2	-2.85	-2.58	3.4	4.34	4.31	28.50	0.34	0.95	23.64	0.18	0.30
52.4	-16.4	3481	2981	-.2	-0.18	-0.01	-.8	-0.18	-0.14	2.8	2.90	2.89	17.03	0.10	0.24	22.22	0.14	0.34
52.4	-16.4	3481	3431	-.7	0.17	0.14	-.5	0.00	0.02	2.4	2.67	2.67	35.03	0.09	0.22	39.70	0.19	0.46
54.3	-25.9	3030	175	—	-4.14	1.28	—	1.32	0.25	7.6	11.11	11.35	—	145.38	35.64	—	118.00	19.39
54.3	-25.9	3030	2825	-1.1	1.19	1.17	-2.2	-4.46	-4.75	2.8	3.83	3.80	27.26	4.30	2.24	41.47	6.74	2.96
59.1	-34.1	2630	861	-1.5	-2.30	-1.86	-.9	0.45	1.27	3.2	5.51	5.64	44.88	4.08	2.29	53.91	2.56	3.01
59.1	-34.1	2630	2063	-1.2	-0.75	-0.39	-2.9	-3.00	-2.38	—	4.25	4.28	19.09	2.10	1.96	37.43	1.90	1.64
59.1	-34.1	2630	2526	-1.2	0.28	0.54	-9.5	-2.20	-1.55	3.0	4.00	4.01	8.75	2.41	2.19	70.95	2.33	1.98
54.4	-25.9	3299	439	-2.0	-8.65	-6.89	-2.9	3.08	4.24	6.2	11.14	10.94	67.91	70.79	19.77	71.56	42.71	13.59
54.4	-25.9	3299	1040	-1.2	-3.55	-2.99	-1.3	-1.46	-1.16	3.9	6.34	6.33	25.87	8.69	3.12	25.91	8.71	2.27
54.4	-25.9	3300	439	1.4	-8.65	-6.89	5.1	3.08	4.24	5.3	11.14	10.94	51.13	70.79	19.77	35.07	42.71	13.59
54.4	-25.9	3300	1041	1.2	-3.55	-2.99	3.0	-1.46	-1.16	3.6	6.34	6.33	13.71	8.69	3.12	11.79	8.71	2.27
54.4	-25.9	3300	3095	4.5	-0.43	-0.33	1.4	-5.87	-5.98	2.1	3.68	3.64	11.72	4.50	1.93	12.07	6.60	1.62
59.2	-34.0	2850	269	3.2	-4.14	-2.99	4.8	7.32	8.28	4.8	6.90	7.12	215.56	22.79	9.12	218.46	12.49	8.32
59.2	-34.0	2850	882	-.6	-2.30	-1.86	1.1	0.45	1.27	3.4	5.56	5.69	43.05	4.08	2.29	31.71	2.56	3.01
59.2	-34.0	2850	2092	-.6	-0.75	-0.39	1.6	-3.00	-2.38	3.2	4.30	4.32	33.20	2.10	1.96	27.09	1.90	1.64
59.2	-34.0	2850	2551	-1.6	0.28	0.54	1.0	-2.20	-1.55	8.0	3.99	3.99	23.40	2.41	2.19	10.72	2.33	1.98

Table 10.1: Comparison of WOCE current meter statistics with assimilation and reference experiments, respectively.

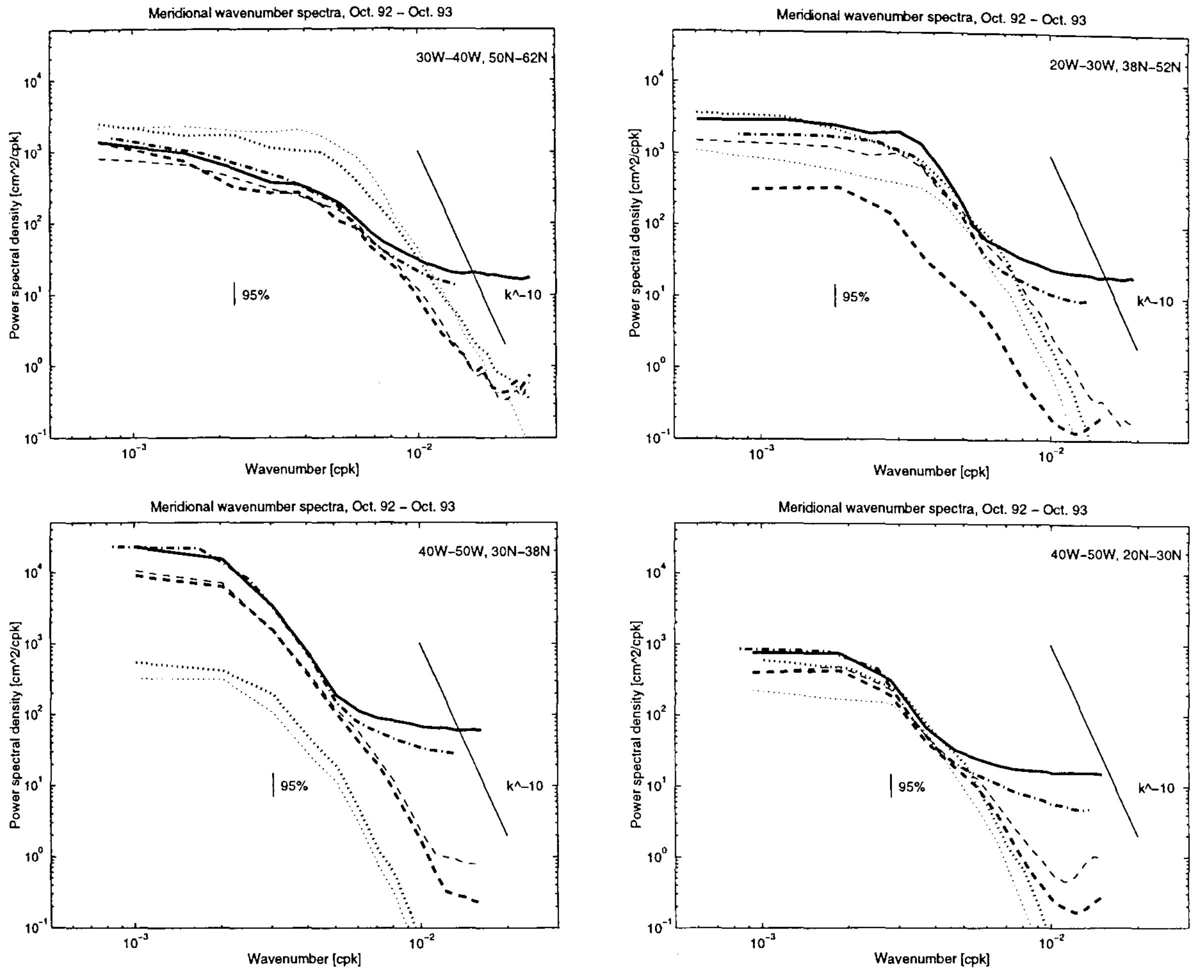

Figure 10.9: Meridional wavenumber spectra of sea surface height anomalies in 10° by 10° boxes. (a) Irminger Sea (50°–62°N, 30°–40°W), (b) northeastern Atlantic (38°–52°N, 20°–30°W), (c) northern boundary of the subtropical gyre (30°–38°N, 40°–50°W), (d) southern part of the subtropical gyre (20°–30°N, 40°–50°W). Spectra shown refer to the mapped ERS-1–TOPEX/Poseidon data (solid line), to the assimilation experiment with daily wind (thick dashed line) and without wind forcing (thin dashed line), and the reference experiment with daily wind (thick pointed line) and without wind forcing (thin pointed line).

probably very similar on the mesoscale and mapping algorithm and autocorrelation function assumed being identical in both cases, the significantly different energy levels may be explained by the much higher data coverage of the combined ERS-1–TOPEX/Poseidon data.

Also included in Figure 10.9 are the spectra of a sensitivity experiment that was run with the wind forcing completely turned off. This was thought to be useful for investigating the origin of mesoscale activity. To find out to what extent the assimilation of altimeter data can make up for errors in the wind forcing of an ocean circulation model, the third year of the "spin down" experiment was also run in assimilation mode.

Figure 10.9(a) shows the meridional wavenumber spectra for the Irminger Sea area. As in the CME model, LEVEL considerably overestimates the eddy variability in this region. Interestingly, turning off the wind forcing does not lower the eddy activity, consistent with the suggestion that the mainly buoyancy driven subpolar gyre – and hence the associated eddy fluxes – is much less sensitive to changes in the wind forcing than the mostly wind driven subtropical gyre. This is supported further by the very different ratio between wind forced and spin down spectra of the NAC region shown in Figure 10.9(b).

Assimilation generally brings the energy level for all wavelengths in closer agreement with the observed spectra. However, the assimilation cannot prevent the model spectra from dropping rapidly for wavelengths shorter than about 120 km (in the Irminger Sea area, Fig. 10.9(a)) to 180 km (in the central subtropical gyre, Fig. 10.9(d)), where biharmonic friction (consistent with the k^{-10} spectral slope) effectively dissipates small scale energy. Although better than the results of the 1/3° CME model with an overall spectral cut-off at 150–200 km, the spectra presented here indicate the still too low horizontal resolution for a simulation of the mesoscale energy flow.

10.6 The seasonal cycle in the assimilation

10.6.1 Description of seasonal cycle

Figure 10.10 shows four seasonal averages of surface temperature, from Levitus, the control and assimilation runs. Several features are apparent. First, the three fields look very similar (there are minor differences between model and data near the equator, probably due to the lack of a mixed layer in the model, and in small areas of midlatitudes of up to 2°C). Second, the assimilated and control runs are again similar, with the former being somewhat less smooth. However, it is clear that the combined surface heating and relaxation to data has functioned well in maintaining the models close to reality at the surface. As an example of the effect the awssimilation has on the temporal evolution of the near-surface temperature field, Figure (10.11) displays the one-year time series of potential temperature at 30°N, 30°W in the upper 400 m. Clearly, the smooth evolution of the reference run's temperature is modified by the assimilation. Positive SSH anomalies are associated with warm-core temperature anomalies, visible around days 75, 160, 200, 310, and 340. Pronounced cold anomalies occured at days 150, 170, and 250. The main effect of the assimilation is seen not at the surface, where

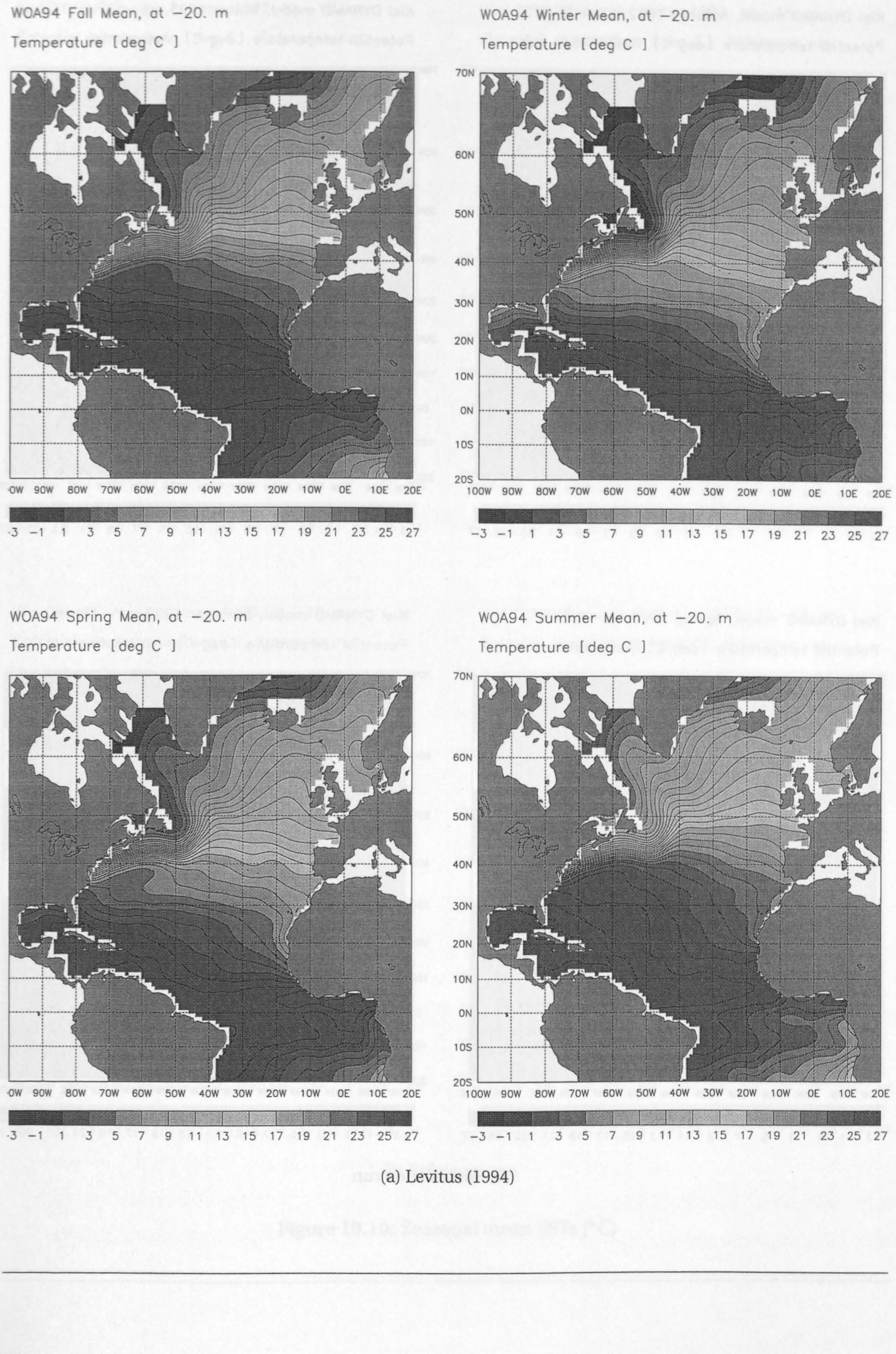
WOA94 Fall Mean, at −20. m
Temperature [deg C]
WOA94 Winter Mean, at −20. m
Temperature [deg C]
WOA94 Spring Mean, at −20. m
Temperature [deg C]
WOA94 Summer Mean, at −20. m
Temperature [deg C]
70N
60N
50N
40N
30N
20N
10N
0N
10S
20S
100W 90W 80W 70W 60W 50W 40W 30W 20W 10W 0E 10E 20E
-3 −1 1 3 5 7 9 11 13 15 17 19 21 23 25 27

(a) Levitus (1994)

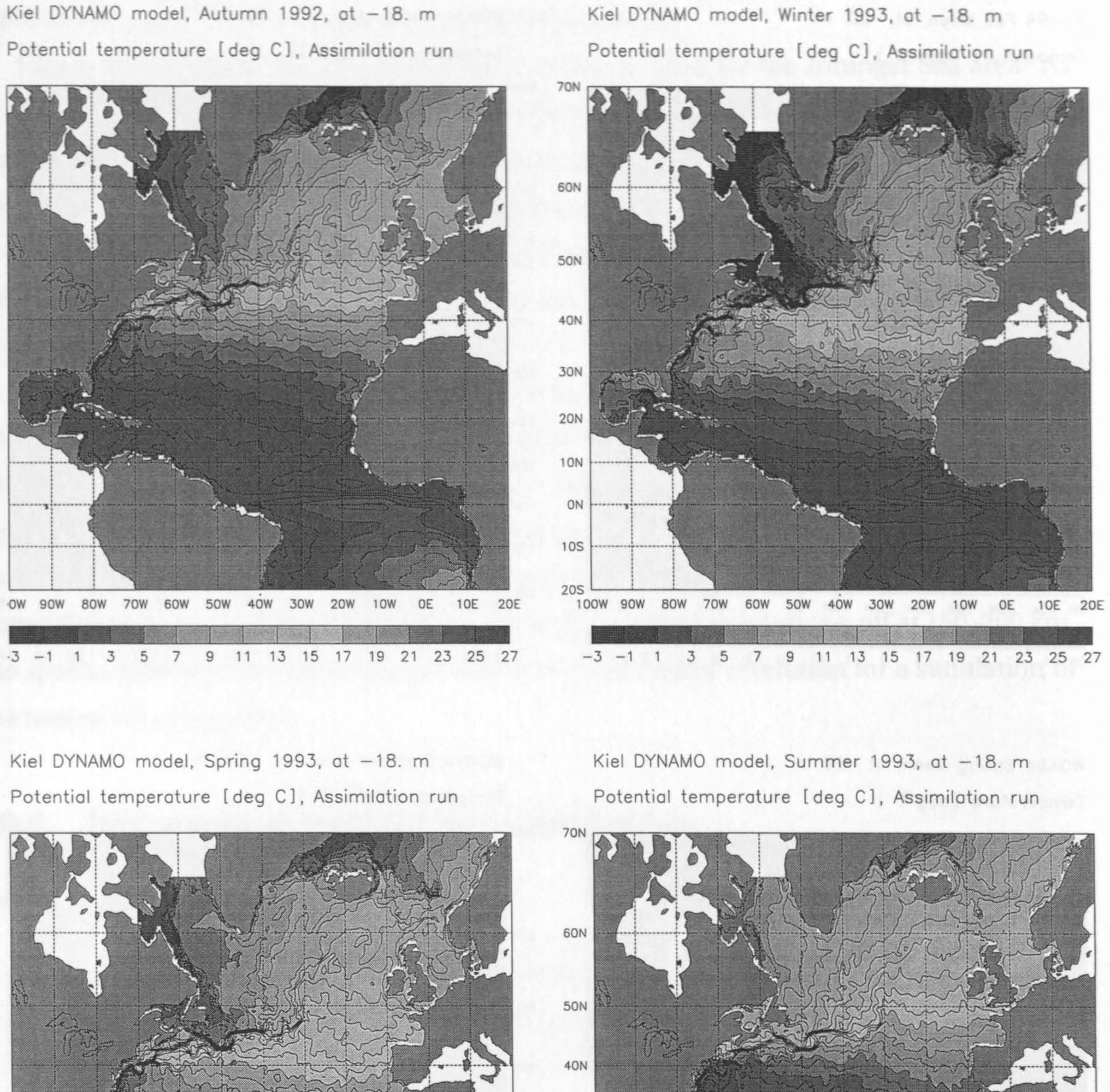

Kiel DYNAMO model, Autumn 1992, at −18. m

Potential temperature [deg C], Assimilation run

Kiel DYNAMO model, Winter 1993, at −18. m

Potential temperature [deg C], Assimilation run

Kiel DYNAMO model, Spring 1993, at −18. m

Potential temperature [deg C], Assimilation run

Kiel DYNAMO model, Summer 1993, at −18. m

Potential temperature [deg C], Assimilation run

70N
60N
50N
40N
30N
20N
10N
0N
10S
20S
100W 90W 80W 70W 60W 50W 40W 30W 20W 10W 0E 10E 20E
-3 -1 1 3 5 7 9 11 13 15 17 19 21 23 25 27

(b) Assimilation run

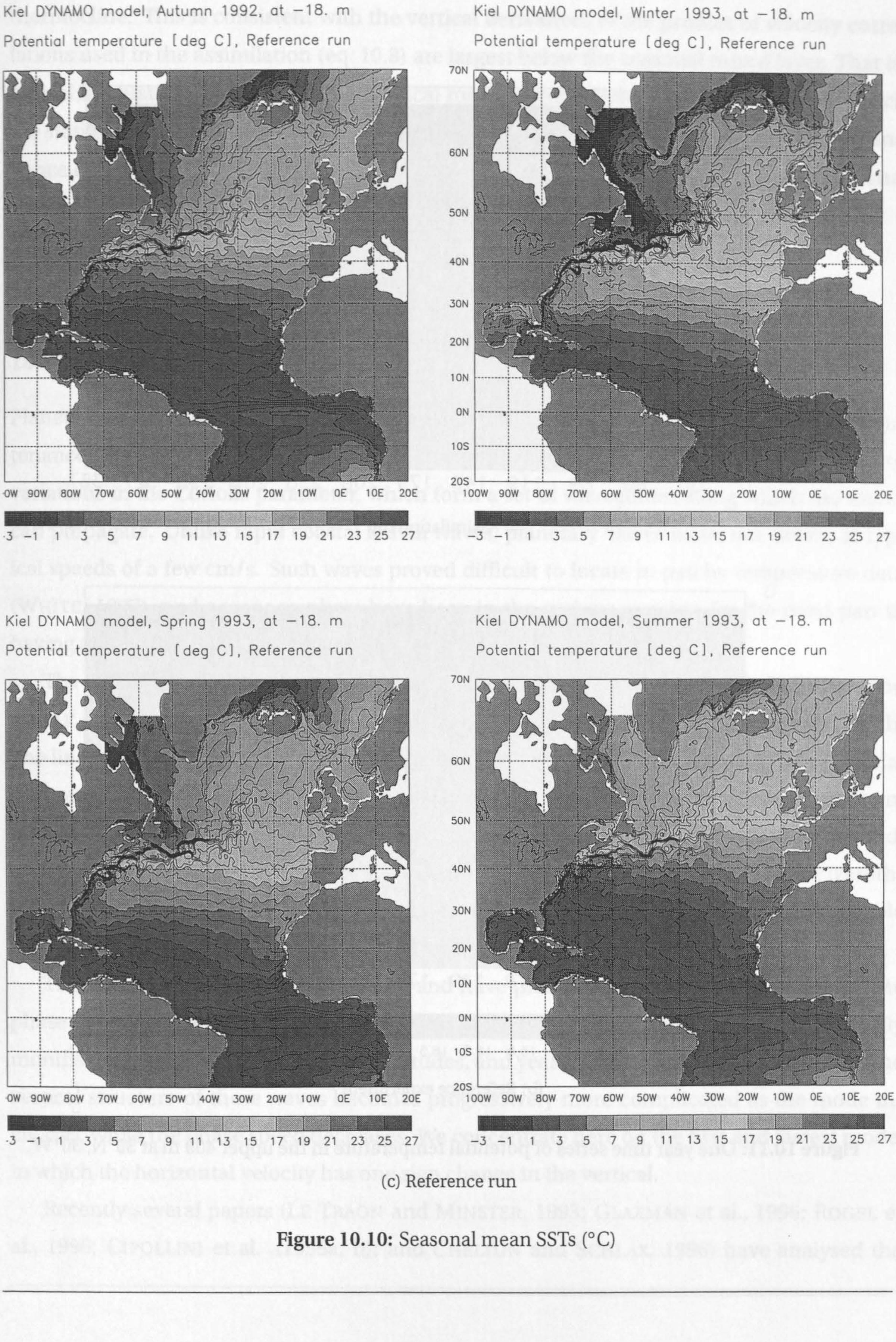
Kiel DYNAMO model, Autumn 1992, at −18. m
Potential temperature [deg C], Reference run
Kiel DYNAMO model, Winter 1993, at −18. m
Potential temperature [deg C], Reference run
Kiel DYNAMO model, Spring 1993, at −18. m
Potential temperature [deg C], Reference run
Kiel DYNAMO model, Summer 1993, at −18. m
Potential temperature [deg C], Reference run
70N
60N
50N
40N
30N
20N
10N
0N
10S
20S
0W 90W 80W 70W 60W 50W 40W 30W 20W 10W 0E 10E 20E
100W 90W 80W 70W 60W 50W 40W 30W 20W 10W 0E 10E 20E
-3 -1 1 3 5 7 9 11 13 15 17 19 21 23 25 27

(c) Reference run

Figure 10.10: Seasonal mean SSTs (°C)

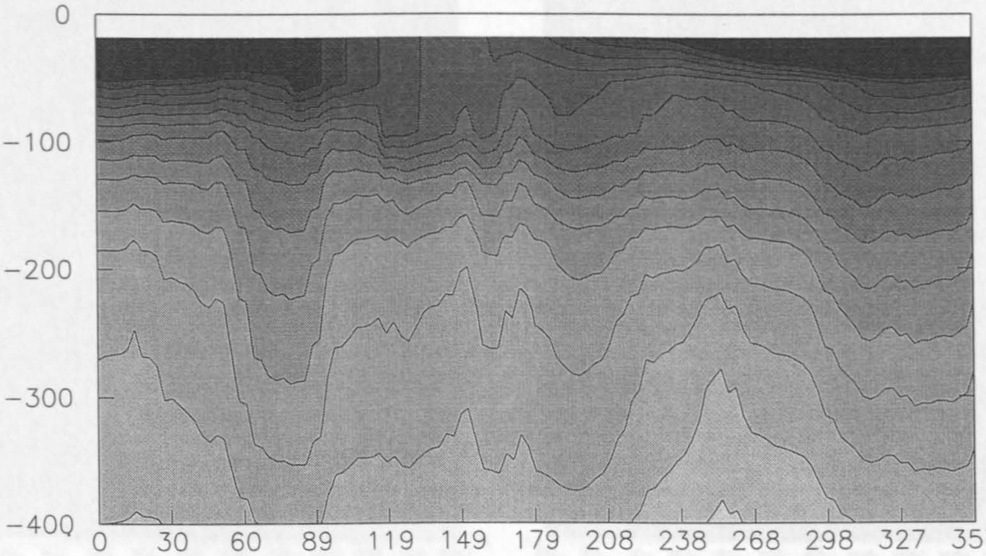

(a) Assimilation run

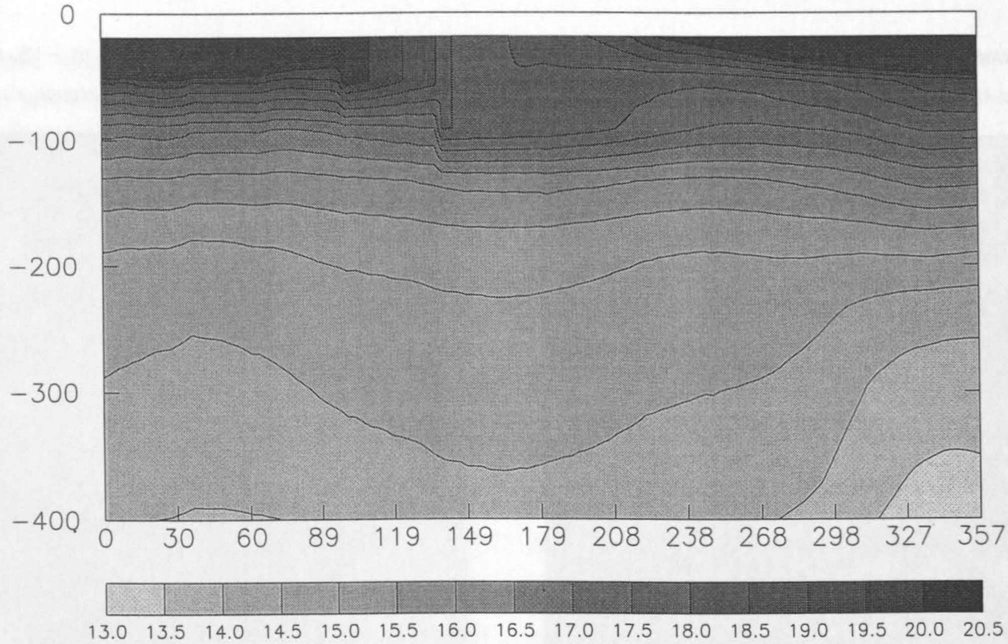

(b) Reference experiment

Figure 10.11: One year time series of potential temperature in the upper 400 m at 30°N, 30°W.

the seasonal cycle is still dominated by the local heat fluxes, but is found below the seasonal thermocline. This is consistent with the vertical derivatives of the profiles of velocity correlations used in the assimilation (eq. 10.8) are largest below the seasonal mixed layer. That is, typical fluctuations about the climatological mean of the reference experiment (from which the statistics are taken) have only little velocity shear in the mixed layer and largest shear (and hence largest vertical excursion of the geostrophically balancing isopycnals) in the seasonal thermocline.

10.7 Planetary waves in the North Atlantic

10.7.1 Background

Planetary, or Rossby, waves play a fundamental part in the spin-up of the ocean, the maintenance of western boundary layers, and many other features. They owe their existence to variations in the Coriolis parameter, which form a set of waveguides along which the waves can propagate. Unlike rapid coastal Kelvin waves, planetary waves move but slowly, at typical speeds of a few cm/s. Such waves proved difficult to locate in patchy temperature data (WHITE, 1977), and oceanographers have been in the curious position for the most part in having a theory before it could receive unequivocal confirmation.

The theory for such waves is well known (DICKINSON, 1978; GILL, 1982; LEBLOND and MYSAK, 1978), and holds for an ocean whose background state is at rest, with a uniform depth. The linearised three-dimensional equations are cast onto an infinite, complete set of vertical normal modes. For each mode, the resulting free horizontal (i.e., two-dimensional) problem, with an equivalent depth and reduced gravity, can be solved. All phase speeds are westward, and waves which are long in all directions are nondispersive. The lowest-order mode (zeroth) is barotropic, and almost uniform vertically for a free surface, and is probably unobservable (CHELTON and SCHLAX, 1996) and is not of interest here.

The remaining modes are baroclinic, and have phase speeds of order a few cm/s. The phase speeds depends inversely on the square of the Coriolis parameter, and waves take only months to cross an ocean basin at low latitudes, and years to decades at higher latitudes. The vertical structure of these waves becomes progressively more complicated as the mode increases, while the phase speed decreases. We concentrate here on the first and fastest mode, in which the horizontal velocity has one sign change in the vertical.

Recently several papers (LE TRAON and MINSTER, 1993; GLAZMAN et al., 1996; ROGEL et al., 1996; CIPOLLINI et al. (1996a, b); and CHELTON and SCHLAX, 1996) have analysed the

TOPEX/Poseidon data used in our assimilation, and found clear evidence of westward propagation of long waves throughout the North Atlantic. Surprisingly, away from the tropics the westward phase velocity shows values inconsistent with theory, being higher by a factor of 1.5 to 2. Estimates vary slightly between authors, depending on the method used and the precise region analysed, but the estimates are generally consistent within themselves. CHELTON and SCHLAX (1996) were forced to conclude that 'the standard theory for freely propagating, linear, baroclinic Rossby waves is deficient in predicting the observed phase speeds'.

Linear theory has been modified by KILLWORTH et al. (1997) to include a baroclinic east-west flow, and they were able to reproduce most of the observed wave speed changes in the world ocean, with especial success in the North Atlantic[4]. DÖÖS (priv. comm.) has examined TOPEX/Poseidon data, and output from a hierarchy of models, and found strong differences both between models and data, and between models within 20° of the equator in the Atlantic. These models, however, were forced by climatological winds, and so may lack some of the forcing which would be present in models forced by actual wind stress.

Our assimilation provides a valuable opportunity to compare the behaviour of the control run and the assimilated run insofar as Rossby wave propagation is concerned. We are interested to know whether the control run itself reproduces the wave features in the altimeter data, or whether some measure of assimilation is necessary to observe the features.

10.7.2 Planetary wave observations

Fig. 10.12 shows longitude-time contours of SSH anomaly (known as HOVMULLER diagrams) at 35°N, for the control, assimilation, and TOPEX/Poseidon, with the same contour colouring. Not surprisingly, the altimetry shows the strongest signal, the assimilation the next strongest, and the control case the weakest. The levels vary by a factor of two between satellite and control. Despite the lower variability, all three datasets demonstrate clear evidence of westward wave propagation[5]. Wave propagation is even visible in runs without wind forcing (both control and assimilation), which suggests that buoyancy effects, perhaps at coasts, are producing much of the wave signal.

The phase speeds of this propagation vary both between longitudes (all cases show an increase in phase speed with position westward) and between datasets. The control run shows evidence of a 3.7 cm/s propagation in the latter half of the simulation at 30–40°W; something that may be eastward propagation around 60–70°W, again in the second half of the simulation, and a more rapid propagation, around 4.6 cm/s at 70–80°W in the early part. The assimilation run is much clearer, and shows wave crests at almost all longitudes, with phase speed increasing monotonically westward. At 20–30°W, the speed is about 2.36 cm/s at 50–70°W, the speed is 5.74 cm/s; and there is evidence of as much as 8.2 cm/s yet further west in the early half of the run. The strongest signals, the altimeter data, show the same pattern, with speeds varying from 2.8 (20–30°W), through 5.6 (40–60°W) to 6.4 cm/s (60–80°W). Given the uncertainties in estimating phase lines in Fig. 10.12, the differences between altimeter and assimilation phase speeds are not believed significant.

---

[4] Other candidates for explaining the wave speed increase exist, such as topographic slopes.

[5] These data do not prove that the propagation is purely westward; however, the other analyses in the literature already cited demonstrate clearly that westwards is overwhelmingly preferred to other orientations.

For comparison, CHELTON and SCHLAX (1996) found a propagation speed of 4.9 cm/s at the same latitude, between 10 and 70°W. This was found using a Fourier approach, and represents a smoothing between the different figures cited above for TOPEX/Poseidon.

These speeds are all reasonably well fitted by the KILLWORTH et al. (1997) theory.

Similar results hold at other latitudes. At 20°N, for example (not shown) there is again clear evidence of propagation, at speeds of 8–10 cm/s with TOPEX/Poseidon data showing slightly slower values. However, these differences are probably within the errors of the estimation, as spectral density plots show. However, there is no obvious amplitude difference between control and assimilation at this latitude, though both are somewhat smaller than the observations.

10.8 Conclusion/Discussion

Evaluating the success of an assimilation is difficult, since oceanographers lack sufficient data of either quality or quantity to permit a statistically relevant comparison of prediction and data. We have had to recourse to proxies for adequate data sources here: single sections, current meters, etc. are not ideal units for comparison. A small deviation of assimilated solution from data is enough to make results look erroneous, for example.

There are several indicators that the assimilation technique is providing better solutions than the control run, especially near-surface where the method should work best. There are also many cases, noted above, where the assimilated and control runs look similar, so that the act of assimilation is *not* modifying the solution when it should *not* do so. For example, assimilation can require a lighter water mass to appear at the surface than is present in the simulation. If this were to occur frequently, a signal would be visible in the surface heating. Yet there is no overall indication that this has occurred. The method is careful to conserve water mass properties, and it is evident that it has been successful in this.

Where the assimilation and control runs differ, this is usually on the side of additional realism for the assimilation: planetary wave propagation amplitudes, surface EKE, the path of the Gulf Stream extension, and so on.

There is, however, only so much any scheme to assimilate the time-varying part of the surface height field can achieve. We argued that mean fields were unlikely to be changed dramatically by assimilation, and indeed – for example – the erroneous deep water mass structure persists from control to assimilation run. Signals associated with this are presumably in the null space of the assimilation. These errors in turn provide false estimates of mean available potential energy, the dominant source of eddy energy. Whether assimilation over time periods much longer than one year can improve this is unknown.

As far as we are aware, no method of assimilating only surface values has been able to adjust the time-mean fields. If the model used for assimilation possesses some poor aspects, as all extant models do, then continuing with methods such as those used here – which, as noted, act to maintain water mass structures – is unlikely to yield significantly better results in the future. Instead, it will be necessary to assimilate *in situ* deep temperature and salinity data so as to constrain the mean flow fields, in addition to surface values; this will require an extensive observational campaign, or other forms of remote or autonomous sensing. At the very least, part of the mean ocean structure must be assimilated if the mean flow in the models is to be improved.

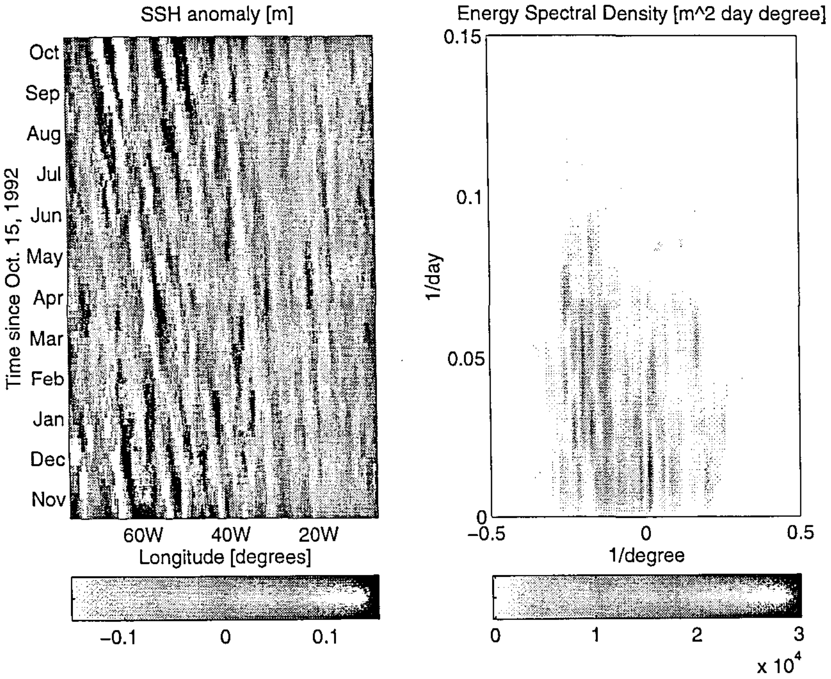

(a) Mapped ERS-1–TOPEX/Poseidon data

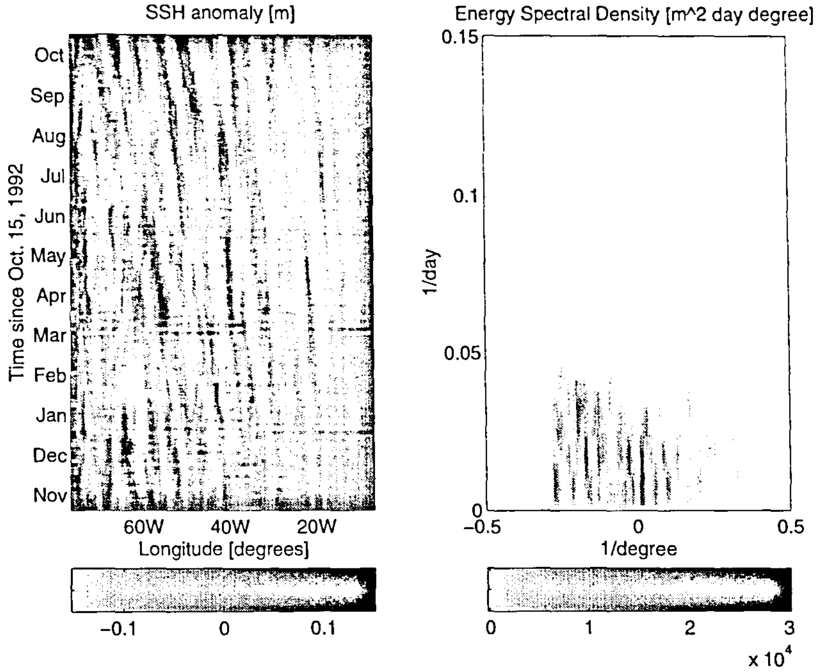

(b) assimilation experiment with daily wind forcing

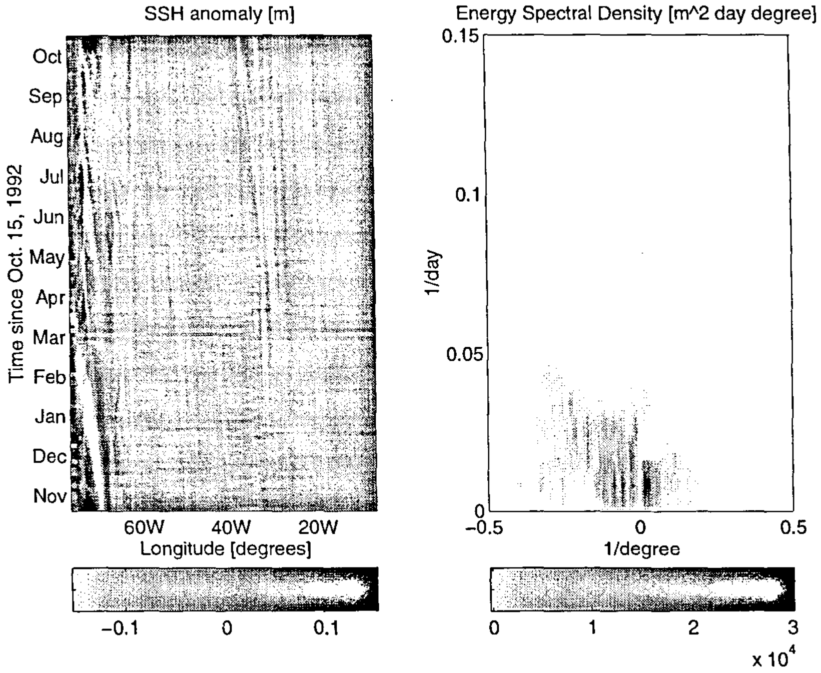

(c) reference run with daily wind forcing

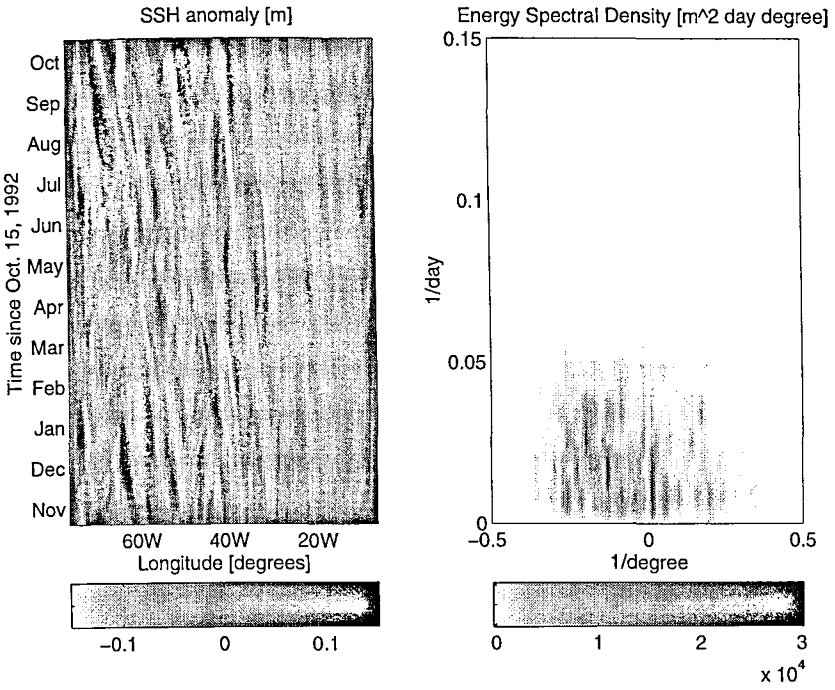

(d) assimilation experiment without wind forcing

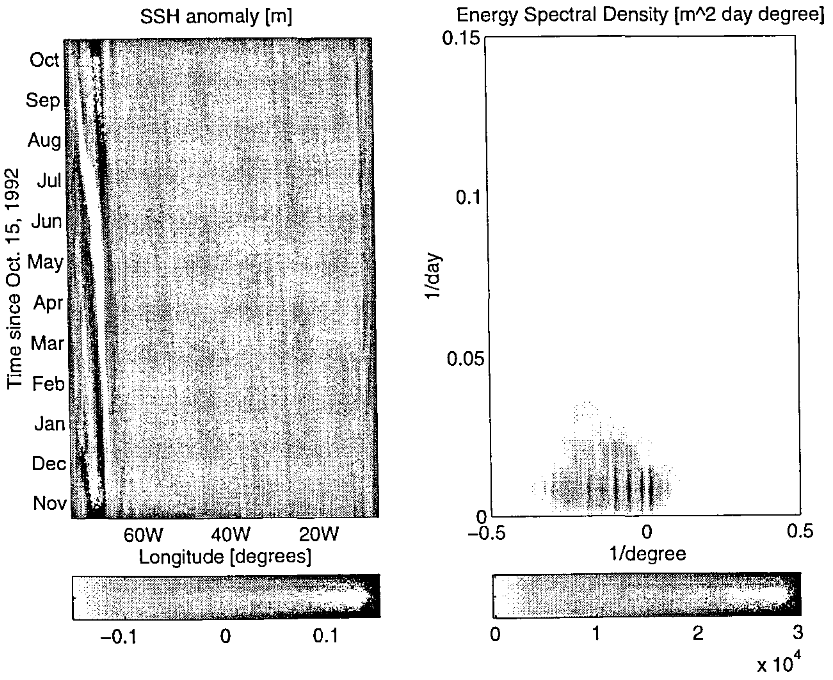

(e) reference run without wind forcing

Figure 10.12: Longitude-time contours of SSH anomaly at 35°N, together with the corresponding energy spectral density. (a) mapped ERS-1–TOPEX/Poseidon data, (b) assimilation experiment with daily wind forcing, (c) reference run with daily wind forcing, (d) assimilation experiment without wind forcing, (e) reference run without wind forcing.